NTNU

Norwegian University of
Science and Technology

Microstructure and Mechanical Properties of Welded AA6082 Aluminium Alloys

Jonas Vestfjell Jakobsen

Materials Science and Engineering
Submission date: June 2016
Supervisor: Trond Furu, IMTE
Co-supervisor: Ole Runar Myhr, IMT

Norwegian University of Science and Technology
Department of Materials Science and Engineering

Abstract

The present work have investigated variants of an AA6082 aluminium alloy. Five different alloys with various amounts of Mn, Cr and Zr have been subjected to three homogenization procedures. After homogenization, the aluminium billets were extruded into plates that were artificially aged to T6-temper. Further, the profiles were MIG welded to obtain a heat affected zone. The effect of these parameters on microstructure and mechanical properties of the various alloys in welded state have been studied. The microstructure after extrusion and welding were investigated by optical microscope and hardness measurements. In addition, subsequent heat treatments have been performed in an attempt to further increase the density of dispersoids for one specific alloy.

Welding of age-hardened aluminium alloys change the microstructural hardening phase that can be a challenge for the mechanical properties in the heat affected zone (HAZ) and lead to a reduction of the yield strength. The strength of the ageing effect is crucial for the load-bearing capacity of welded structure. The degree of work hardening in the HAZ is important to achieve the same yield strength level as the base material. Introduction of dispersoids in the alloys can affect the microstructure and strength of the aluminium alloys, and in the present work, an attempt to increase the strength by the introduction of dispersoids is carried out.

Results from this study show that chemical composition, homogenization procedure, artificial ageing and welding influence the grain structure and mechanical properties of these AA6082-alloys. Density of dispersoids increases with increasing amount of Mn, Cr and Zr, low homogenization temperature and short holding time. Dispersoids retard recrystallization effectively after extrusion and welding. A typical welding profile were obtained for all of the tested alloys and the different levels of dispersoids formed during this work have not improved the welding properties significantly.

Sammendrag

Denne avhandlingen undersøker varianter av AA6082 aluminiumslegering. Fem ulike legeringer med ulike nivå av Mn, Cr og Zr har blitt utsatt for tre homogeniserings prosedyrer. Etter homogeniseringen, ble boltene ekstrudert til plater som ble utherdet til maksimal styrke (T6). Videre ble profilene sveist for å oppnå en varmepåvirket sone. Effekten av disse parameterne på mikrostruktur og mekaniske egenskaper av de forskjellige legeringene i sveist tilstand har blitt studert. Mikrostrukturen etter ekstrudering og sveising ble undersøkt ved lysmikroskop og hardhetsmålinger. I tillegg er det blitt utført etterfølgende varmebehandlinger for å øke tettheten av dispersoider av en utvalgt legering.

Sveising av utherdet aluminiumslegeringer endrer mikrostrukturen til herdefasen som kan være en utfordring for de mekaniske egenskaper i den varmepåvirkede sonen (HAZ) og fører til en reduksjon av flytespenningen. Styrken som oppnås ved utherdingen er avgjørende for bæreevnen av sveiste strukturer. Graden av arbeidsherding i HAZ er viktig for å oppnå samme strekkfasthet som grunnmaterialet. Introduksjon av dispersoider i legeringene kan ha en effekt på mikrostrukturen og mekaniske egenskaper av aluminiumslegeringene, og i dette arbeidet, er det blitt gjort forsøk på å øke styrken ved å introdusere dispersoider.

Resultatene viser at kjemisk sammensetning, homogeniseringsprosess, utherding og sveising påvirker kornstrukturen og mekaniske egenskaper til AA6082-legeringene. Tettheten av dispersoider øker med økt mengde Mn, Cr and Zr, lav homogeniseringstemperatur og kort holdetid. Dispersoidene hemmer rekrystallisering effektivt etter ekstrudering og sveising. Typiske sveiseprofiler er oppnådd for alle testede legeringer og de ulike nivåene av dispersoider dannet i dette arbeidet har ikke forbedret sveiseegenskapene signifikant.

Preface

This project has been a part of collaboration between the Norwegian University of Science and Technology (NTNU) and Hydro Aluminium. It was carried out at the Department of Materials Science and Technology at NTNU, during the final semester of the 5 year Master's Degree Program in Material Science and Engineering.

This study is a part of a larger collaboration project involving Hydro, Reinertsen and Snøhetta where the focus is to project a floating bridge with underwater tunnel and where various aluminium alloys are included in the solution. The components must be joined together and the problems of welding aluminium alloys must be enhanced. In this study, various variations of alloy AA6082 are welded and investigated considering mechanical properties in the heat affected zone and the base material.

The main aim of this study has been to contribute to a better understanding of which effects the alloying elements Mn, Cr and Zr and dispersoids have on the microstructure and mechanical properties of the welded aluminium alloys.

Jonas Vestfjell Jakobsen

Trondheim, June 2016

Aknowledgement

I would like to offer special thanks to my supervisors, Adjunct Professor Dr. Trond Furu[1] and Dr. Ole Runar Myhr[2] for their guidance and encouragement about aluminium and throughout this study. Their commitment and knowledge provided me with necessary input to carry out this thesis.

My appreciation goes to Chief Engineer Trygve Schanche[3] for his help with various needs and difficulties encountered in the metallurgical laboratory and optical microscope. I would like to thank Senior Research Scientist Martin Lefstad[4] and Senior Technician Arne Gellein[4] for help with the extrusion and artificial ageing of the specimens. Thanks to Research Scientist Hans Fostervoll[4] for help with the welding of the samples. Further, I would like to thank Research Fellow Magnus Remøe[3] for conversations regarding measurements of dispersoids. Finally thanks to Senior Engineer Yingda Yu[3] for instructions and education concerning use of the Scanning Electron Microscope.

[1] Hydro Aluminium, Sunndalsøra.

[2] Hydro Aluminium, Raufoss.

[3] Norwegian University of Science and Technology (NTNU), Trondheim.

[4] SINTEF Materials and Chemistry, Trondheim.

Table of Contents

List of Abbreviations

H1	=	homogenization procedure H1
H2	=	homogenization procedure H2
H3	=	homogenization procedure H3
GP-zones	=	metastable Guinier-Preston zones
β	=	equilibrium phase (Mg_2Si)
β’	=	hardening precipitate (semi-coherent needles/bonds)
β’’	=	hardening precipitate (semi-coherent needles)
σ_i	=	intrinsic yield strength of pure aluminium
σ_p	=	contribution from hardening precipitates to the yield strength
σ_d	=	contribution from dispersoids to the yield strength
σ_{ss}	=	contribution from alloying elements in solid solution to the overall yield strength
T4	=	solution heat treated and naturally aged
T6	=	solution heat treated and artificial peak-aged
wt. %	=	weight percent
P_Z	=	Zener-Drag effect
P_D	=	sum of contributions to the stored energy from dislocations located at the sub-grain boundaries, and statically stored dislocations within the sub-grains
γ_{GB}	=	Grain boundary energy
f	=	Particle volume fraction
r	=	Particle radius
HAZ	=	Heat Affected Zone
HV1	=	Vickers hardness, load 1 Kg

1 Introduction

Aluminium and its alloys are extensively used in industries where light weighted materials is appreciated for its ability to reduce the self-weight while maintain the acquired strength of large components. For industries where design and detailed shaped components are of interest, aluminium alloys have the advantage of infinite ranges of possible section shapes due to extrusion techniques and ease of fabrication. Aluminium in its pure form is relatively soft and weak and thus, alloying it with a range of different elements to achieve required mechanical properties is necessary to match the mechanical properties of competitive materials such as conventional steels.[1]

In this study, the microstructure and mechanical properties of welded AA6082-aluminium alloys are studied. The alloy is designates as a 6xxx-series of aluminium which have Mg and Si as the main alloying elements. The 6xxx-series aluminium alloys are, due to their good physical- and chemical properties which includes low density, high strength, good weldability and corrosion resistance, widely used in structural industries.[2] Aspects that affect the mechanical behavior of the components are important when designing alloys for structural uses. Knowledge of the combination of chemical compositions and thermo-mechanical history of the alloys and their effect are essential.

The mechanical properties of 6xxx-aluminium alloys are to a large extent, determined by natural or artificial ageing.[3] Small, hard, and fine dispersed particles precipitates during the ageing stage, where the shape and coherency with the aluminium matrix determines the strengthening effect. When the alloy is exposed for a weld thermal cycle, as in welding, the hardening precipitates may dissolve at the same time as coarse non-hardening phases form, leading to a reduction of the yield stress. Due to localization of stresses in the HAZ when subjected to load, large structures can collapse with relatively small global shifts even if the local fracture is ductile. In the industry, the thickness of the aluminium components is increased to compensate for the poorer strength in the HAZ.

The degree of work hardening in the HAZ is a decisive factor for the behavior of the structure when subjected to loads that result in localized flow. If the work hardening and the flow stress in the HAZ are sufficient enough to achieve the same yield strength level as the parent material, the structure could withstand a larger degree of deformation before eventually fracture in the HAZ. Alloys that have optimal balance of strength in the parent material and in

the HAZ are desirable in the aluminium industries due to predictable behavior of welded aluminium elements. A possibility to achieve increased work hardening of the HAZ and level out the mechanical properties between the parent metal and the HAZ can be provided by designing an alloy with high levels of small dispersoids. The dispersoids prevent recrystallization of the material after heat exposure providing a micro structural advantage of welded structures as well as increasing the ductility. High levels of dispersoids can lead to increased strength and thus reduced components sizes and weight reduction.

The investigation is a continuation of a smaller specialization project where AA6082 aluminium alloys with various Mn contents ranging from 0-1,2 wt.%. These alloys were welded and tensile tested and the results showed promising tensile properties with increasing dispersoid content.

In this study, the main objective is to achieve a sufficient density of dispersoid phases based on Mn, Cr, and Zr and a homogenization method that promotes the formation of small dispersoids that can provide a significant increase in the strength in HAZ.

2 Theoretical background

The theoretical aspects considering the principles and mechanisms for the various aluminium alloys in this project are presented in this chapter. This covers aluminium and AlMgSi-alloys in general, casting, homogenisation, extrusion, dispersoid precipitation, strengthening mechanisms and welding.

2.1 Aluminium

Aluminium is one of the most abundant elements on the earth after oxygen and silicon. Compared to weight aluminium components is relatively strong, which reduces energy consumptions in transportation and gives advantages during structural applications. The density is 2.7 g/cm^3 which is 1/3 the weight of steel. Aluminium is easy to form due to ductility and low melting point which allows a widely flexibility in design and integration in several industries. It has a long life and low need for maintenance. The formation of protective oxide coating makes it highly corrosion resistant and it is easy to recycle.[4]
In nature, aluminium only exists in the form of aluminium hydroxide in a mineral denoted bauxite. The production of the aluminium starts with crushing, drying and grinding of the bauxite in mills. A mix of water and the crushed bauxite produce a thick paste that is further treated and alumina (Al_2O_3) is extracted. Primary aluminium in pure form is gained by melting the alumina with electrical current that breaks the bonds between the aluminium and oxygen atoms. This is casted into various forms and can be processed into different products.[5] The pure aluminium is relatively soft and weak, and must be alloyed to achieve good mechanical properties to match tensile strengths of competitive metals.[1] The lifecycle of aluminium is shown in Figure 2.1.

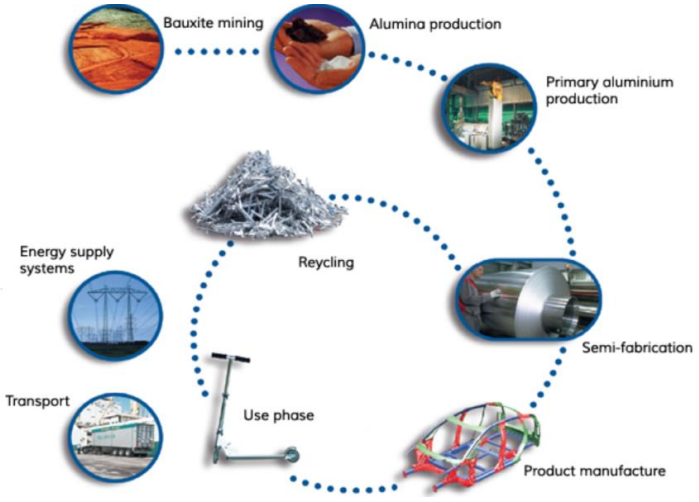

Figure 2.1: Life cycle of aluminium, from bauxite mining to recycling. [6]

2.2 AlMgSi-Alloys

6xxx-series aluminium alloys are by far the most widely used alloys in extrusion. The AlMgSi-alloys provides excellent combination of mechanical properties, solution heat treatability at extrusion temperature, good weldability, good corrosion resistance, high extrudability and formability.[7] The 6xxx-series main alloying elements are Mg and Si, but the alloys usually contain several other elements that affect the properties of the alloy. Some of the mechanical properties and other alloying elements for these types of alloys are presented in Table 2.1 and Table 2.2 respectively.

Table 2.1: General mechanical properties for AlMgSi-alloys.[8]

Mechanical properties for AlMgSi-alloys	
Yield strength (σ_y)	190-360 MPa
Tensile strength (σ_u)	220-390 MPa
Elongation	17-12%

Table 2.2: General effect of several alloying elements in AlMgSi-alloys.[9],[8]

Element	**Effect**
Mg	Increase strength and hardness. Good corrosion resistance, increased weldability.
Si	Gives heat treatable alloys when combined to Mg. Corrosion resistance.
Mn	Grain refiner, inhibit recrystallization. Increase yield and tensile strength. Corrosion resistance.
Zn	Increase strength and hardness. Gives heat treatable alloys when combined with Mg.
Fe	Contamination.
Cr	Grain refiner, inhibit recrystallization.
Cu	Increased strength and hardness. Reduces corrosion resistance.

2.3 Processing and thermal history of aluminium

Processing of the primary aluminium includes casting, homogenisation, extrusion and artificial ageing. The thermal history of these steps is presented in Figure 2.2.

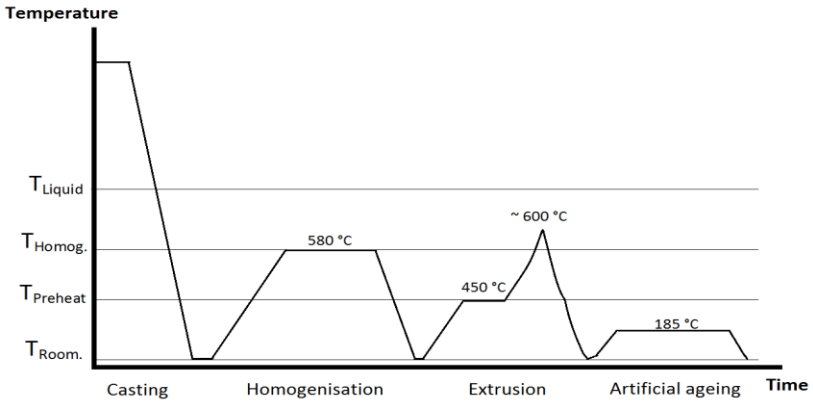

Figure 2.2: Thermal history of AlMgSi aluminium alloy. [10]

2.4 Casting and homogenization

Before production of aluminium products and mechanical working such as extrusion, virgin aluminium, scrap and the desired addition of alloying elements are casted into ingots. To achieve good products, ingots of high quality are of importance and are achieved by mixing of the components together with effective fluxing, degassing and filtering of the melt before casting it. The main goals are to remove slag, oxides, gases and non-metallic impurities. The casted blocs of aluminium (also denoted billets) that are to be extruded can vary in diameters and lengths. A uniform ingot structure is achieved by a direct-chill (DC), semi-continuous process.[3]

After casting and cooling of the alloy, evenly distribution of the alloying elements, removal of micro segregations, and improved workability by removing non-equilibrium, low melting point eutectics that can cause cracking of the billets are vital. These effects are achieved in the homogenization procedure.[3] In addition, control of the precipitation of dispersoid particles from dispersoid forming elements such as Mn and Cr can be achieved in the homogenization procedure as well as spheriodizing of insoluble phase particles.[11]

During solidification of the casting, formation of intermetallic phases occurs. These intermetallic phases often consist of Fe due to the low solubility of iron in aluminium.

In AlMgSi-alloys, α-AlFeSi, β-AlFeSi intermetallic particles and non-equilibrium phases including Mg_2Si are formed. During the homogenization, these intermetallic particles and the non-equilibrium phases change to stable equilibrium phases. For the 6xxx-alloys, a critical change is the transformation from β-AlFeSi to α-AlFeSi along with dissolution of Mg_2Si particles. The β-AlFeSi reduces the ductility of the alloy during extrusion due to plate shaped particles that can lead to local crack propagation, which again can lead to surface defects during extrusion. The α-AlFeSi, which are round shaped, provides better extrusion conditions.[12], [13] In addition, β-AlFeSi and Mg_2Si particles in grain boundaries are locally melting during extrusion, which weakens the structure. The α-AlFeSi particles are thermally stable during temperatures reached in the extrusion stage and are less likely to melt locally. Another benefit of the α-phase is that the ratio between Si and Fe are lower than the β-phase which leaves more Si to contribute in strengthening of the alloy.[12]

In AlMgSi-alloys that contains Mn and/or Cr, dispersoids are formed in the temperature range during the homogenization process. Dispersoids are very small particles with diameters in the range 10-500 nm.[14] The dispersoids have high density and high thermal stability which have a strong effect to prevent recovery, recrystallization and grain growth.[15] The size and distribution of the dispersoids are dependent on the homogenization parameters. At high homogenization temperature and long holding time, the dispersoids gets coarse, while lower temperature and less holding time leads to fine, densely dispersed dispersoids.[14] For 6xxx-alloys, the formation of these dispersoids are encouraged by the presence of Mn and Cr.[12]

During the soaking stage in the homogenization process, the rate of diffusion is influenced by the temperature and holding time. The minimum holding time accepted in the industry is about 2 hours. Some elements such as Mn diffuse slowly, and to remove all of the micro-segregations, longer holding time is necessary. The holding time is also dependent on the size of the billet, where a large billet needs longer holding time. The cooling stage should be rapid but if it is quenched, the flow stress of the material is raised which will affect further processing. A controlled cooling rate of 300-500 °C/h is sufficient for most billets.[12]

2.5 Extrusion

Extrusion is a metal forming process where a block (also called billet) of metal are forced through a die. This reduces the cross section of the block to match the geometry of the die. It requires large forces to push the metal through the die, and to reduce this force, it is common to heat the billet to a temperature where the deformation resistance of the metal is reduced.[16] During the extrusion process, the grain structure of the alloy is changed due to the changed cross section from billet to extruded product. This is imaged in Figure 2.3, which shows how the grains deform, and stretches out when being pressed through the die. Directly after the extrusion, the microstructure consists of fibrous elongated grains.

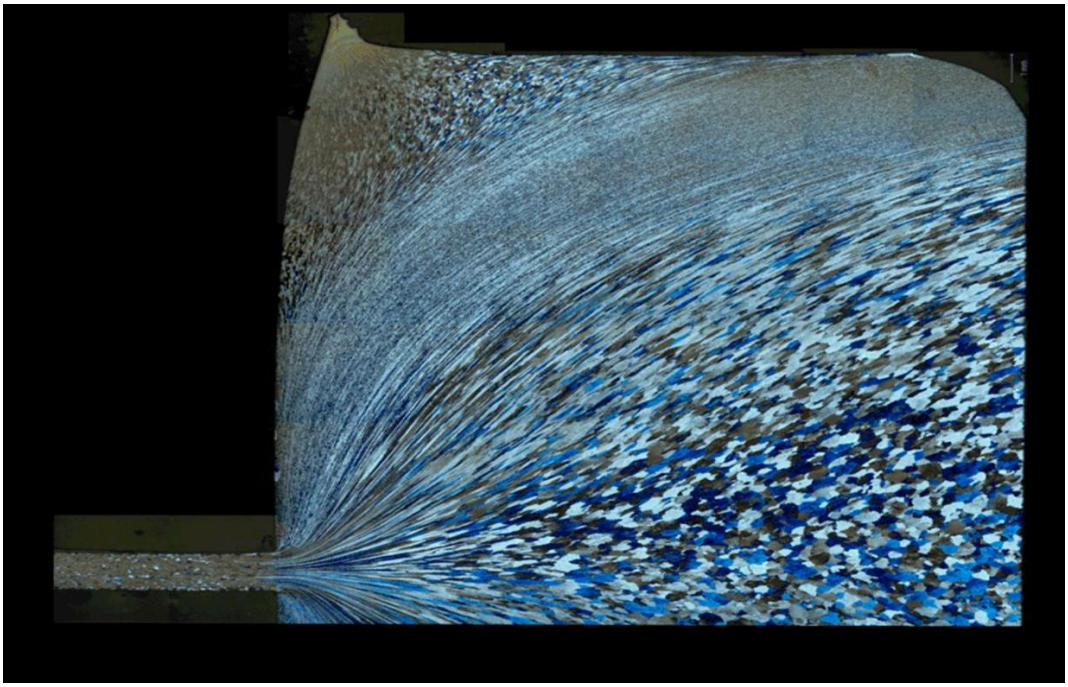

Figure 2.3: In situ microstructure of aluminium during extrusion. (Printed with permission from Dr. Trond Furu)

Until close to the entrance of the die, the deformation of the billet is relatively uniform. When the friction is increased due to pressing against the container-wall, a dead zone of stagnant metal is produced. At the surface layer of the extrusion, the billet undergoes extensive shear deformation compared to the center, which is essentially pure elongation. The high friction and temperatures reached during the extrusion causes recrystallization of the grain structure.[16] The conditions for recrystallization are better for the surfaces of the extrusion compared to the center. This is due to the higher strain rates reached of the billet at the surface

where the die and billet are in contact.[17] The coarse grains on the surface of the extrusion can cause problems such as; bending failure, orange peel finish, streaking and surface brighten variations. By modifying process variables such as billet conditions, die design and extrusion parameters which can promote a non-recrystallized or close to non-recrystallized structure, eliminates these problems.[18] Other ways to avoid coarse grain formations are controlling the exit temperature during extrusion, increasing the recrystallization temperature by adding recrystallization-inhibiting elements such as Mn and Cr, which works as grain refiners and will retard grain growth after extrusion. Various homogenization procedures are also a factor that affects the recrystallization conditions of the extruded alloys.[19]

2.6 Recrystallization and effect of dispersoids on grain structure

The dispersoid phases favour retention of a non-recrystallize structure in a number of semiproducts after heat treatment such as extrusion, ageing and welding. The nonrecrystallized microstructure has great effect on the strength of the alloy. The degree of influence the various dispersoids have on a structure and properties are different, however, all dispersoids increase the recrystallization temperature of the alloys and thus preventing recrystallization of the alloys in normal heat treatment ranges.[20] The recrystallization is retarded due to pinning of the moving reaction front by the particles. The time before cooling after extrusion influences the recrystallization and water quenching gives a considerable thinner recrystallization surface layer compared to air-cooling.[11]

Figure 2.4 show the most effective antirecrystallization element in aluminium alloys where the recrystallization temperature (50% recrystallization) of cold-rolled binary Al-TM alloy sheets are plotted with transmission metal content (TM). From this, it is determined that Sc has the highest influence on preventing recrystallization i.e. increase the recrystallization temperature of the alloy.[20]

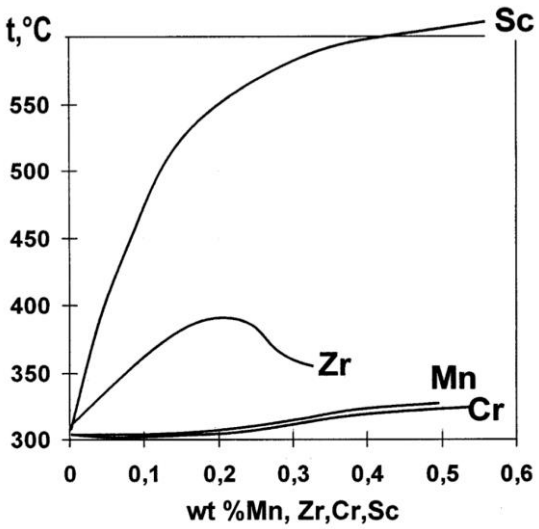

Figure 2.4: Recrystallization temperature (50% recrystallization) of cold-rolled binary Al-TM alloy sheets vs. TM content.[20]

Production parameters and alloying elements affects the grain structure during and after the extrusion process. The degree of deformation, temperature and the speed rate of the extrusion affects the recrystallization process that takes place. Addition of Mn in the aluminium alloy leads to increased formation of dispersoids. High density of these small precipitates can inhibit grain growth and retard the recrystallization after extrusion. [15] A comparison of two different AA6082 alloys with 0,006 wt% Mn and 1,172 wt% Mn are shown in Figure 2.5. The effect of Mn on the grain structure where the high Mn content alloy (b) has retarded recrystallization in a larger degree compared to the alloy with low content of Mn (a).[21]

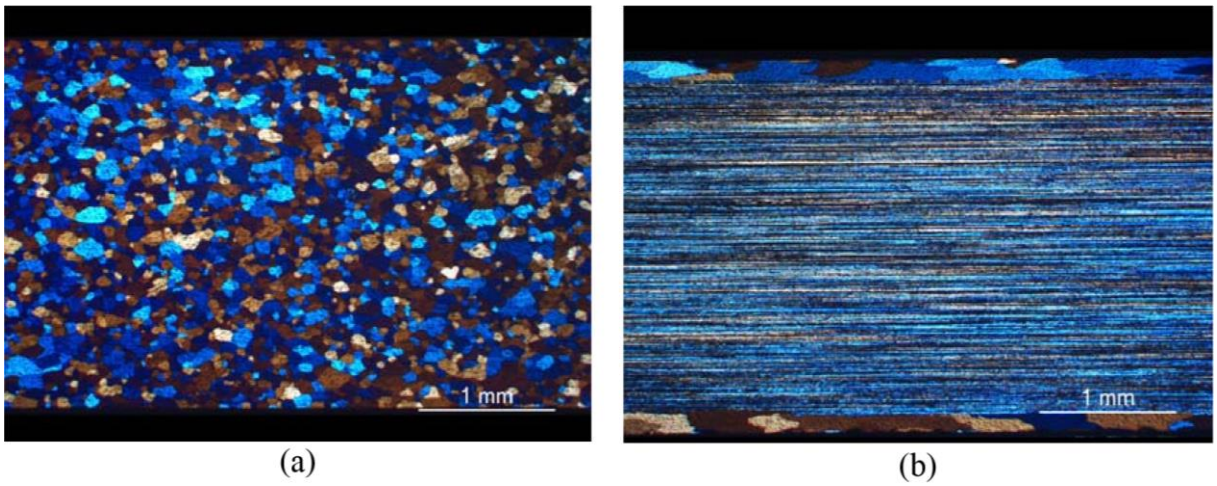

Figure 2.5: Micrographs of the grain structure of AA6082 alloys with different Mn content. (a) 0,006 wt% Mn and (b) 1,172 wt% Mn. The degree of recrystallization increases with amount of Mn.[21]

The materials grain structure has great influence on the mechanical properties of metals. For aluminium, the grain structure is not directly related to strength properties but the fibrous structure indicates that the alloy contains high levels of small particles that contribute to the strength. Important mechanism of controlling strength of aluminium alloys is thus solution hardening, precipitation hardening and strain hardening. Generally, strength and ductility is highly influenced by the size and density of grains where high density of small grains ensures good strength. Large grains accumulate a higher degree of dislocations pile up at the grain boundaries that increase the stress level locally. The larger the grain size, the more dislocations are piling up at each grain boundaries, and thus making large stresses. The stresses produced allow plastic deformation to propagate to the neighboring grain that leads to a lower resistance to yielding and fracture of the material. Compared to a material with high density of small grains, the large locally pile-ups of dislocations in a grain decreases due to more evenly distribution of dislocations in the material which reduces the local stresses at each grain. [22]

Dispersion of small particles like dispersoids tend to oppose recrystallization through the Zener drag pressure (P_Z), which describes the relationship between size, fraction and driving force for recrystallization.[23]

$$\boldsymbol{P_z = \frac{3\gamma_{GB} f}{2r}} \quad \textbf{(1)}$$

$\gamma_{GB} = Grain\ Boundary\ Energy$

$f = Particle\ Volume\ Fraction$

$r = Particle\ Radius$

The total driving pressure for recrystallization can be expressed by equation 2. P_D is the sum of the contributions to the stored energy from dislocations located at the sub-grain boundaries, and statically stored dislocations within the subgrains.[24] Both the particle fraction (f) and the particle size (r) will influence the Zener drag effect.[23]

$$\boldsymbol{P = P_D - P_Z} \quad \textbf{(2)}$$

$P_D = Driving\ pressure\ for\ recrystallization$

2.7 Mn-, Cr- and Zr- dispersoids

Chromium and manganese are classified among the 1. series 3d transition metals (TM). Zirconium is classified as a 2. series 4d transition metal. Figure 2.6 shows the metallic radius of the respective elements. As can be seen, the metallic radius of Cr and Mn are similar, and relatively small, while the metallic radius of Zr are larger.[25]

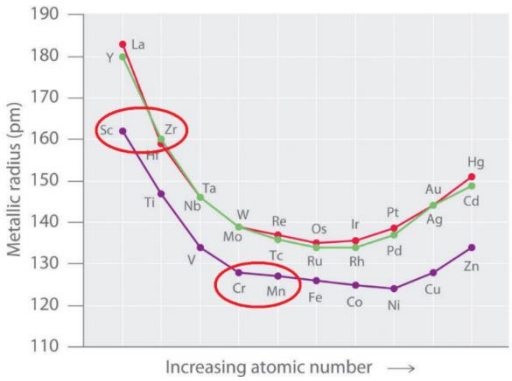

Figure 2.6: Metallic radius and atomic number of various transition elements.[25]

For the Al-TM systems, a temperature of both eutectic and peritectic invariant transformations, is close to that of aluminium melting. This is represented in Figure 2.7 which shows the Al-rich side of the Al-Mn,-Cr and-Zr binary equilibrium diagrams. The phase diagrams also show that solid solution has a narrow solidification range and the solidus- and liquidus-lines come up closer to each other. These features in combination with low diffusion coefficient of TM in liquid and solid aluminium create supersaturated solid solution of TM in aluminium during ingot solidification which decompose and form dispersoids when subsequent heat treatment of the ingots (usually homogenisation) are performed. These are secondary precipitates of dispersed intemetallic Al_6Mn, Al_7Cr, and Al_3Zr phases.[20]

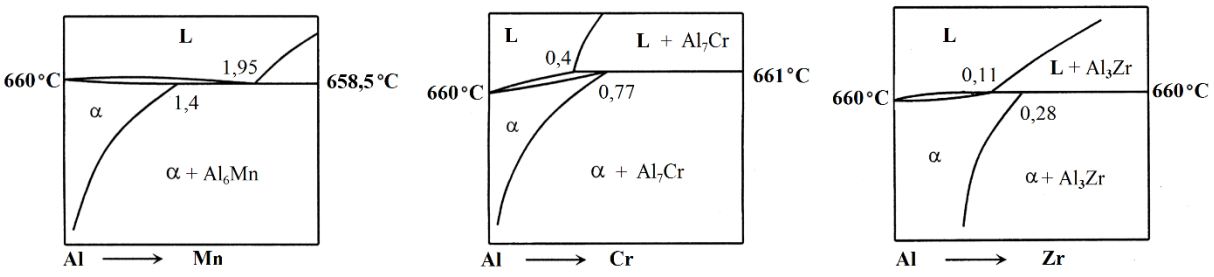

Figure 2.7: Binary equilibrium diagrams for Al-Mn, Al-Cr and Al-Zr systems. [20] (Al-Zr modified from [26])

Modification of the microstructure and thus enhancement of the alloys properties has for a long time been used by addition of small amount of Mn and/or Cr.[15] Dispersoids containing Sc and Zr has also been used to an extent, however, Sc is a very rare and expensive element and thus increase the cost of the aluminium alloys.

Different types of precipitates containing Mn and/or Cr forms during high temperature heat treatment (400-580 °C). The precipitates forms in a variety of crystallographic structures and chemical compositions.[11] These dispersoids are found to be either α-Al(MnCrFe)Si phase or α-AlCrSi phase. The structure of the dispersoids is complex and the interface between the dispersoids and the Al matrix is incoherent. Through many years of research, several suggestions of nucleation sites for the dispersoids have been developed. Hirasawa [1975] found evidence that the nucleation site for Mn containing dispersoids are on the β- and β-Mg_2Si needles which forms during the heat up period. Westengen et al [1980] investigated using electrical resistivity measurement and TEM-metallography, the formation of both Mn- and Cr-containing dispersoids in AlMgSi-alloys. The alloy containing Mn-dispersoids were found to have a large variety in the electrical resistivity during high temperature annealing, while the alloy containing Cr-dispersoids were found to have much less variety in resistivity. The TEM examination showed dispersoids in both alloys after the heat treatment. Both Westengen et al [1980] and Conte [1996] has found the dispersoids to arrange relatively nonuniformly in the alloys. Observations by Westengen et al indicates that uniform distribution of dispersoids are promoted by slow heating rates. Kolby et al [1994] found indications that the nonuniform distribution of dispersoids are caused by nonuniform distribution of Si after solidification.[11]

2.7.1 Precipitation of Mn and/or Cr containing dispersoids [15]

Lodgaard and Ryum investigated the formation of dispersoids in AlMgSi-alloys containing Mn and/or Cr focusing on nucleation mechanisms and the reason for the tendency of nonuniform dispersoid distribution. The nucleation mechanisms of the dispersoids were investigated more accurately by adding an additional and continuous heat treatment to the alloys (slow heating (200 °C/h) up to 580 °C hold for 6 hours). The microstructure of an alloy containing 0,5 wt.% Mn after this additional heat treatment are shown in Figure 2.8. Figure 2.8 (a) shows a very inhomogeneous distribution of dispersoids. This alloy were up-quenched to T_x = 580 °C in salt bath before transferred directly to a furnace and hold at this temperature for 6 hours. As shown in Figure 2.8 (b) the dispersoid distribution is nearly uniform when the alloy is first up-quenched to T_x = 250 °C before continuous increase in temperature at a rate of

3 °C/min up to 580 °C and hold for 6 hours. The same result were observed in other alloys containing Mn and/or Cr which demonstrate that the nucleation of dispersoids is strongly affected by slow heating from $T_x \approx 250$ °C to homogenization temperature, 580°C.

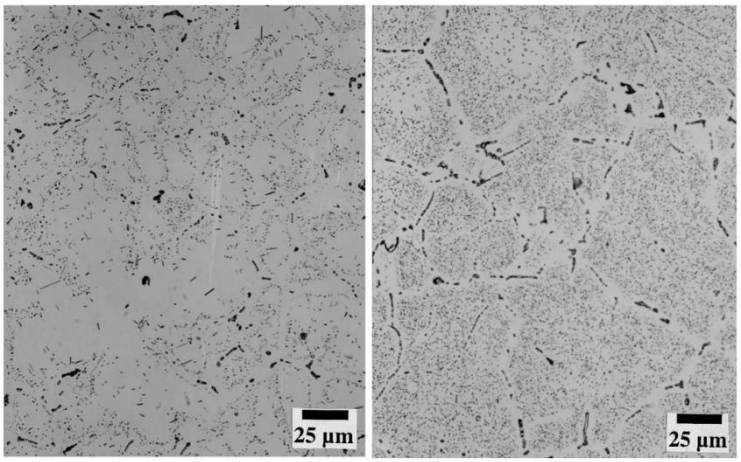

Figure 2.8: (a) Dispersoid distribution in AlMgSi-0,5Mn alloy when T_x = 580 °C. (b) Dispersoid distribution in AlMgSi-0,5Mn alloy when T_x = 250 °C.[15]

The reactions, which take place during heating from room temperature to 580 °C were further investigated by electrical resistivity measurements. The main results from the electrical resistivity measurements done by Lodgaard are reprinted in Figure 2.9. In alloy B (0,3 wt.% Mn) and alloy C (0,5 wt.% Mn) it can be seen that the precipitation of Mn-containing dispersoids starts in temperature ranges from 400 – 460 °C, and at ~ 550 °C, most of the Mn has precipitated away. As can be seen for alloy E (0,5 wt.% Mn – 0,15 wt.% Cr) and alloy F (0,3 wt.% Mn – 0,15 wt.% Cr), the precipitation starts and finishes at the same temperature as for the alloys B and C, which contains only Mn. The electrical resistivity drop reflects the total amount of elements. The total drop increases with increasing Mn and/or Cr. For alloy D (0,15 wt.% Cr) the precipitation starts at ~ 490 °C and is not completed until ~ 580 °C. The resistivity measurements indicate that the precipitation of particles containing only Cr is more sluggish than particles containing only Mn or Mn and Cr.

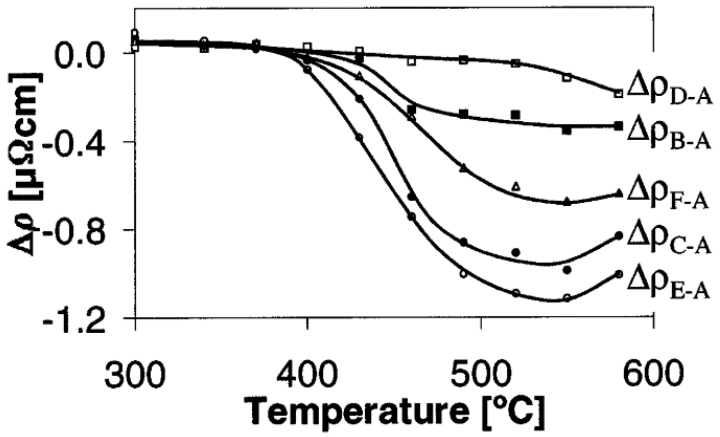

Figure 2.9: Electrical resistivity change in the alloys. The change is only due to the precipitation and dissolution of dispersoid-forming elements.[15]

The precipitates formed during the continuously heating were also examined by TEM. In alloy C (0,5 wt.% Mn) only β'-precipitates were observed after continuous heating to 340 and 370 °C. By further heating to 400 °C, small dispersoids (5-10 nm) were observed as shown in Figure 2.10. In addition to the dispersoids an additional type of precipitation was observed which is also indicated in Figure 2.10. This type of precipitate is referred to as the 'u-phase' precipitate, which is rod shaped. After heating to 430 °C the dispersoids had grown to 10-20 nm and was found to be α-Al(MnFe)Si phase. To investigate if there was a relationship between the β' precipitates, the α-dispersoids and the 'u-phase' precipitates, one specimen was continuously heated to 350 °C and hold at this temperature for 2 hours before quenched. After this heat treatment, all of the three types of particles were found to be present. In addition, a composite particle consisting of β' precipitate and the 'u-phase' precipitate were frequently observed shown in Figure 2.11. Nucleation of dispersoids were only observed at the surface of the 'u-phase' which indicates that only the 'u-phase' act as a nucleation site for the dispersoids and not the β'- precipitates. This is shown in Figure 2.12.

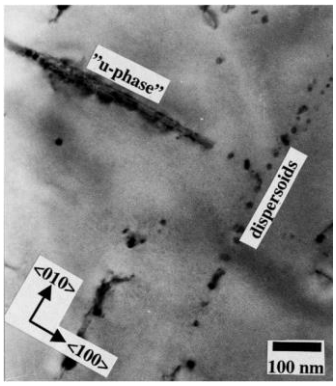

Figure 2.10: TEM bright-field micrograph of a 'u-phase' particle and dispersoids after continuously heating to 400 °C of alloy C (0,5 wt.% Mn).[15]

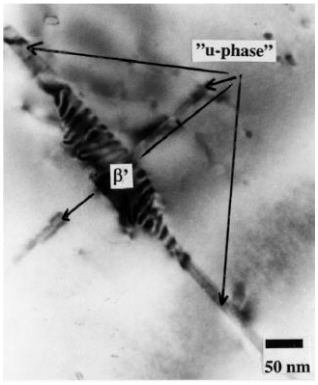

Figure 2.11: TEM bright-field micrograph of alloy C (0,5 wt.% Mn) after continuously heating to 350 °C and subsequent annealing at this temperature for 2 hours showing composite particle composed of the β'- and the 'u-phase'-particle.[15]

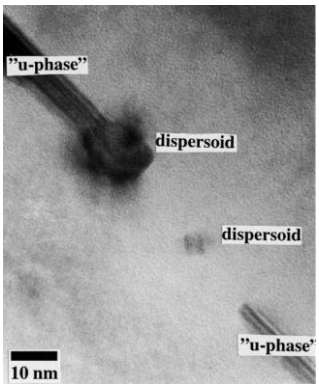

Figure 2.12: TEM bright-field micrograph of dispersoids nucleated on the surface of the 'u-phase' precipitate in alloy C (0,5 wt.% Mn) after continuous heating to 350 °C and subsequent annealing at this temperature for 2 hours.[15]

A model of the precipitation sequence of the β'-precipitates, the 'u-phase'-precipitates and finally the formation of dispersoids are shown in Figure 2.13. During continuous heating, the β'-precipitates nucleate with subsequent growth, coarsening and partial dissolution with increasing temperatures from 100 – 350 °C. By further increase of the temperature, the β'-

precipitates dissolve completely as the ‘u-phase’ develops and act as a nucleation site for the dispersoids, which will consume the ‘u-phase’ completely. The final result is a breaking up of the original β’ into chains of dispersoids. The model is valid for alloys containing Mn and Mn + Cr. For the Alloy containing only Cr, the ‘u-phase’ precipitates is not found and the nucleation site for the dispersoids have not been identified.

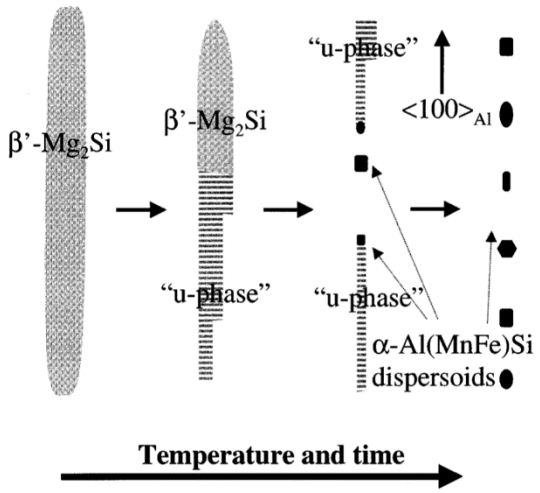

Figure 2.13: A model of the precipitation of the dispersoids.[15]

Zirconium is one of the most important micro alloying elements in aluminium alloys. It forms fine and metastable Al_3Zr-particles in the $L1_2$ ordered structure shown in Figure 2.14 (a). Their pinning effect can have a huge impact of improving the microstructural properties of aluminium alloys. In 6xxx aluminium alloys with high content of Si, the $(Al, Si)_3Zr$ phase which have DO_{22} ordered structure is formed shown in Figure 2.14 (b). It is reported by Reiso et al that the coarse $(Al, Si)^3Zr$ phase is promoted by the combination of high Si content and high homogenization temperatures.[27]

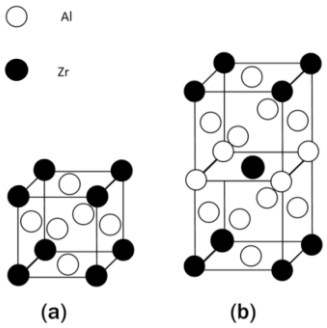

Figure 2.14: The L_{12} –structure (a) and $D0_{22}$ –structure (b).[28]

Himuro et al studied the precipitation state changes of an AlMgSi-Zr alloy with finely dispersed $L1_2$-type of Al_3Zr particles accompanying recrystallization. From the results, it is assumed that the $L1_2$-type of Al_3Zr precipitates dissolve on a grain boundary and the DO_{22}-type of $(Al, Si)_3Zr$ reprecipitates and drastically grows owing to enhanced diffusivity associated with the grain boundary. The presence of Si further enhances the stability of the DO_{22}-type of $(Al, Si)_3Zr$-precipitates.[27]

2.8 Strengthening mechanisms for AlMgSi-alloys

In the case of AlMgSi-alloys, precipitates have great influence on the strength (σ_p,). Other strength contributions come from intrinsic yield strength from pure aluminium matrix (σ_i, typical 10 MPa)[24] and solid solution hardening (σ_{ss}). In addition there is strength contribution from dipsersoid phases which are included in the σ_p. The optimal strength of the alloy is obtained by a combination of these.[29] The strengthening contributions can be presented as Equation 3.

$$\boldsymbol{\sigma_y = \sigma_i + \sigma_{ss} + \sigma_p} \quad \textbf{(3)}$$

$\sigma_y = overall\ macroscopic\ yield\ strength$

$\sigma_i = intrinsic\ yield\ strength\ pure\ aluminium$

$\sigma_{ss} = effect\ from\ solid\ solution$

$\sigma_p = contribution\ form\ precipitates\ and\ dispersoids$

2.8.1 Strengthening from elements in solid solution

The pure aluminium is strengthened by introduction of solute atoms in solid solution in the solvent-atom lattice. The solid solution and precipitate phases hardens the material due to elastic interactions between the solute atoms and dislocations. Figure 2.15 (a) shows the influence of a larger atom in a lattice. Elastic stress fields arise around the dissolved particles which makes dislocation movement harder. There are two distinct mechanisms for retarding dislocation motion with second phase particles. For small and/or soft particles, the particles may be cut by the dislocations. For large particles that resist cutting, the dislocations are forced to bypass the particles. Figure 2.15 (b) shows sketches of dislocation cutting and

bypassing. Both of these ways act as dislocation barrier.[16] An increase in the nominal Mn concentration leads to a corresponding increase in the solid solution concentration of Mn. This is expected to give an significant increase in solid solution strengthening σ_{ss} in Equation 3.[24]

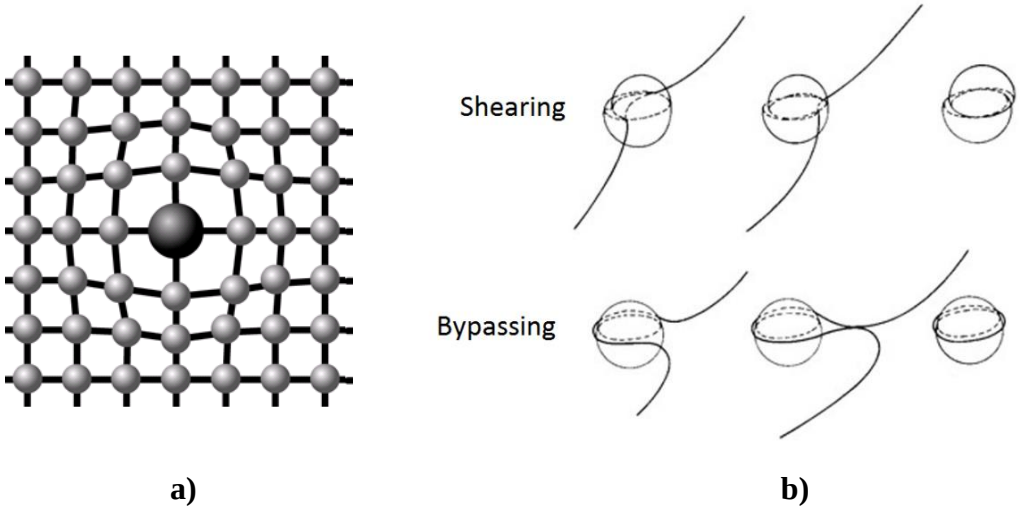

Figure 2.15: a) Solid solution hardening, b) Shearing and bypassing of particles/dispersoids. [30], [31]

2.8.2 Precipitation strengthening

Precipitation hardening is the most important mechanism in strengthening of the AlMgSi-alloys. The small particles are distributed in the relatively ductile matrix which increases the overall mechanical properties. Precipitation hardening or age hardening is formed by solution treating and quenching where second phases is in solid solution at elevated temperature. The second phase particles precipitate upon quenching and aging at a lower temperature. This phase must be soluble at an elevated temperature and it must exhibit decreasing solubility with decreasing temperature for the precipitation hardening to occur.[16] In the case of AlMgSi-alloys, the second phases consist of the main alloying elements Mg and Si. A phase diagram showing the solubility of Mg and Si as a function of temperature represented by the Mg_2Si phase are presented in Figure 2.16.

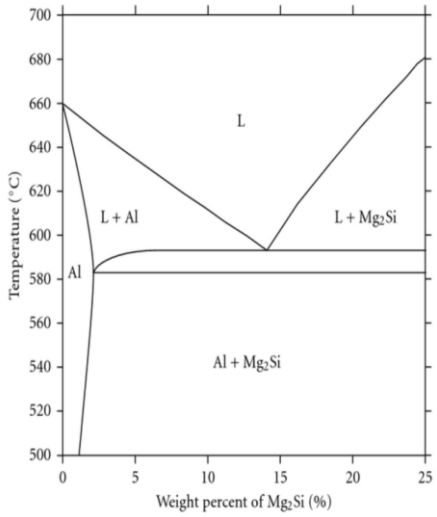

Figure 2.16: Phase diagram showing the solubility of Mg and Si as a function of temperature represented by the phase Mg_2Si. [32]

The precipitation hardening process is carried out in several steps. First the alloy is heated to temperature above the solvus temperature. This is to produce a homogenous solid solution α. The solving of the alloying elements enables dissolution of the second phase and eliminates segregations such as dislocations and grains in the alloy. After the alloy is set in the solublization temperature, quenching of the alloy by air or water limits diffusion of atoms toward potential nucleation sites, and an unstable supersaturated solid solution α_{ss} is formed due to decreased solubility with decreasing temperature. The supersaturated alloy can then be subjected to artificial ageing. In this stage, the alloy is heated below the solvus line usually in the temperature range from 160-200 °C. This allows atoms to diffuse at short distances. Due to the unstable α_{ss} phase, the second phase atoms diffuse at several nucleation sites that lead to controlled dispersion of particles. Typical precipitation sequence for AlMgSi-alloys is given in Equation 4 while Table 2.3 shows the composition and the shape of the precipitates. The strengthening effect of the precipitates depends on the particles resistant to dislocation movement.[33] The hardest phase for the aluminium 6xxx series is the β'' and Figure 2.17 shows the strength evolution with ageing time of 6xxx-alloys.[34]

The precipitation stages of the α_{ss} basis are described in several stages:

$$\alpha_{ss} \rightarrow \text{atomic clusters} \rightarrow \text{GP zones} \rightarrow \beta'' \rightarrow \beta' \rightarrow \beta\ (\text{stable}) \quad (4)$$

Table 2.3: Precipitate composition and shape.[35]

Phase	Composition	Shape	Size	Crystal system
GP	Si/Mg>1	Almost spherical	1-2 nm	Unknown
β''	Mg_5Si_6	Needles	Up to 40x40x350 Å	Monoclinic
β'	$Mg_{1,7}Si$	Ribbons	Several µm long	Hexagonal
β	Mg_2Si	Plates or cubes	10-20 µm	Hexagonal

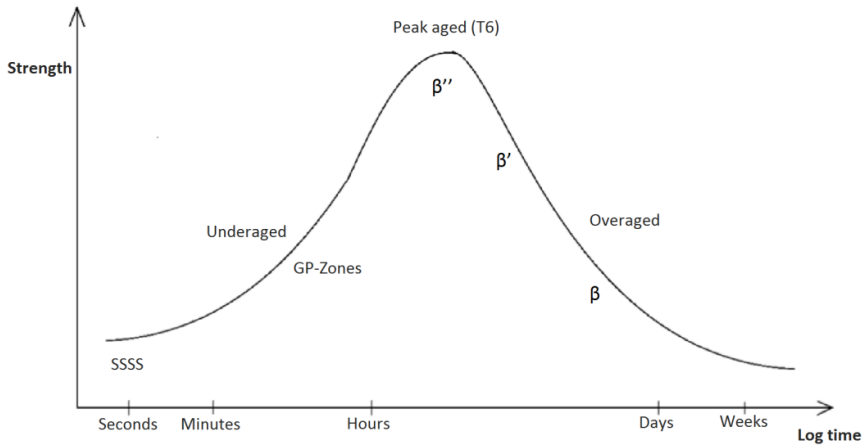

Figure 2.17: Modified sketch of strength evolution during artificial ageing of an AlMgSi-alloy.[16]

2.8.3 Strengthening from dispersoids

The strength of a mechanically alloyed material is in addition to precipitation hardening and solid solution hardening, dependent on the distribution of fine dispersoids.[36] The dispersoids formed during the homogenization affect the yield stress in different ways.[24] The dispersoids contribute to an increase in σ_p in Equation 3. The yield strength is related to dispersoids and interactions of dislocations according to the Orowan bowing mechanism. Strengthening takes place when the dislocations cannot cut the dispersoids due to the dispersoids incoherency with the aluminium matrix (non-shearable). The degree of

strengthening from dispersoids depends on the distribution of the dispersoids in the matrix, the interparticle spacing between the dispersoids, the size and the shape of the dispersoids.[36] Equation 5 is based on classical analytical solutions for particle-dislocation interactions which are derived for non-shearable particles.[24]

$$\boldsymbol{\sigma_p = k_4\sqrt{nr}} \quad \textbf{(5)}$$

Here, k_4 can be approximated as $\sqrt{8}\beta MGb$, where β is a constant in the range of 0,3-0,5 and M, G, and b are the Taylor factor, the shear modulus, and the magnitude of the Burgers vector, respectively, and n and r are the number density and average radius of the dispersions. For precipitation strengthening alloys like 6xxx-series alloys, the strength contribution from dispersoids is relatively small compared to the contribution from hardening precipitates like the β''-particles. The combined effect of precipitates and dispersoids can be expressed by the following equation which verifies the small contribution from dispersoids:

$$\boldsymbol{\sigma_p = \sqrt{\sigma_{p1}^2 + \sigma_{p2}^2}} \quad \textbf{(6)}$$

σ^2_{p1} and σ^2_{p2} are the individual particle strength contributions from precipitates and dispersoids, respectively. From this equation, it is evident that the strength contribution from dispersoids is negligible at peak strength for a typical precipitation strengthening AlMgSi-alloy. By using Equation 5 for typical values of the number density and mean radius of dispersoids the strength contribution σ_{p2} (dispersoids) is found to be about 20 MPa. This gives σ_p=151,3 MPa in Equation 6. The contribution from dispersoids is thus 1,3 MPa which is a negligible strength contribution from dispersoids when precipitation hardening dominates as in peak-aged condition. This is in contrast to the situation at the start of the aging, when σ_{p1} from precipitates is close to zero, and the σ_p contribution therefore will be solely given from the dispersoid contribution σ_{p2}.[24]

Figure 2.18 shows the strengthening effect at a constant volume fraction of dispersoids with different dispersoid sizes. It can be seen that the strengthening efficiency is highly dependent on the size of the dispersoids where small dispersoids give superior strength contribution compared to larger dispersoids. It is also shown that the strength contribution increases with higher density of dispersoids.[36]

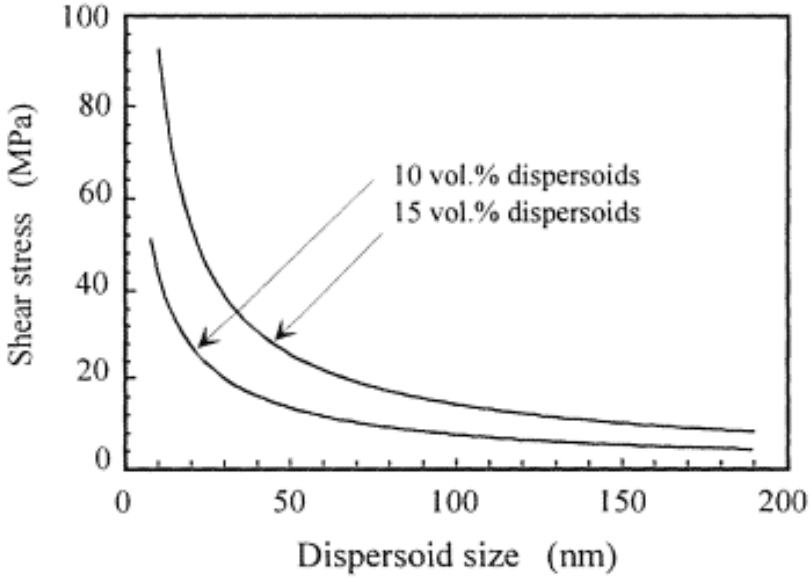

Figure 2.18: Orowan strengthening effect showing the shear stress with size of dispersoids. Increased strength with increasing dispersoid density and decreasing dispersoid size.[36]

Dispersoids have also an indirect effect on the yield stress in the way they affect the grain structure. It is well known that dispersoids impede recrystallization through the so-called Zener drag pressure Since sub-grains are smaller than recrystallized grains, it could be reasoned that the dispersoids lead to an increase in the yield strength due to grain boundary hardening if they contribute to a fine-grained structure consisting of sub-grains, rather than a coarse-grained recrystallized grain structure. However, it has been shown that grain boundary hardening or "Hall-Petch" strengthening, is relatively small for aluminum alloys, with a typical yield strength contribution of 10MPa - 20MPa for sub-grains in the range 4μm - 10μm.[24]

2.8.4 Effect of dispersoids on Si in solid solution

The increase in the nominal Mn concentration gives a corresponding increase in the solid solution concentration of Mn. A significant increase in solid solution strengthening σ_{ss} in Equation 3 is expected with increasing levels of preferably Mn and Cr. The strengthening mechanisms above should all contribute to an increase in the yield strength with increasing content of Mn and/or Cr. However, the hardness of the age-hardened alloys may decrease with increasing levels of Mn and Cr.[24]

The concentration of Si may change after casting of the alloys. Fractions of Si will be tied up during casting and homogenization in coarse non-hardening phases. Essentially Fe and Mn

will influence the effective Si content which influences the precipitation potential by leading to shortage in Si to form hardening β''-precipitates. This can be extended with other dispersoid forming phases which combines to Si such as Cr and possible Zr. The effective Si-concentration in the matrix after casting can be approximated by Equation 7 where the concentrations are in wt%:[37]

$$[Si]_{eff} = [Si]_{nom} - \frac{[Fe]+[Mn]+[Cr]}{3} \quad (7)$$

2.8.5 Effect from dislocation interactions

In addition to the negative effects from Mn on resulting yield strength after ageing, Mn additions will also have a positive contribution to the strength, i.e., from particle-dislocation interactions (particle hardening) from solid solution hardening, and from grain boundary hardening, since the dislocation promotes the formation of a fibrous grain structure, with smaller grains than a recrystallizaed structure.[24]

2.9 Welding of aluminium

Welding is merging of two components surfaces. This coalescence of the surfaces can be achieved by melting the two parts together which forms metallic bonds across the interface.[38] Cold welding of aluminium where the temperature is below the melting point of the alloy can also be executed. For these methods, there is no melting of the components.[39] This project accounts for the welding method Metal Inert Gas Welding (MIG) also known as Gas Metal Arc Welding (GMAW), which is a high temperature fusion welding method.

When choosing materials for industrial structure applications, the weldability of the material is a key feature.[40] Welding is a widely used fabrication method for joining large components with relatively ease and is a worldwide used method of joining components.[41] One difficulty to overcome with welding of aluminium is that the mechanical properties of the weld joint have a general reduction compared to the parent material. This is due to the thermal cycles during the welding procedure which affects the initial precipitation structure of the aluminium and alloys.[40] The strength contribution from the precipitates reduces in the heat affected zone due to over-ageing of the precipitates which coarsen and change shape. The

reduced strength is also associated with an increase in the interparticle spacing between precipitates which leads to an easier dislocation bowing.[41]

2.9.1 MIG-Welding

In MIG-welding, the arc burns from a feeding wire that is continuously feeding through a die in the welding gun. The wire acts as both the electrode and the filler metal. The arc is formed when the wire is in connection with the metal to be welded. The wire is continuously melting with the parent metal and the welding bead is formed through the welding. On the welding gun, around the feeding wire, there is a gas supply which prevents oxidation of the welding pool. The shielding gas usually consists of Ar +1-2% O_2, CO_2 Or a mixture of these two. Factors that are affected by the shielding gas are the size of the droplet due to the current and the shape of the welding pool. Ar gas is an inert gas and addition of O_2 is to get a more stable transition of the droplet. CO_2 is not an inert gas and therefore can react with the weld pool and oxidize. The quality of the weld is dependent on several factors such as; welding speed, feeding speed, wire dimensions, welding distance, shielding gas, and current.[39]

The weld metal in a fusion weld consist of a mixture of the parent metal and if added, the filler metal. The structure of the weld metal is an as cast structure, and the properties of the weld depends on the composition, the quality, the grain size of the deposit and solidification rate. Most filler wires do not have the ability to be age hardened, but dilution with the parent metal will activate some degree of age hardening. Small weld beads will generally give better properties than large weld beads due to faster solidification which leads to finer grain sizes.[42]

2.9.2 Heat Affected Zone (HAZ)

Alloys in the as-cast or annealed conditions will not experience loss of strength in the HAZ if the strength of the weldment matching that of the parent metal. Alloys that have had its strength enhanced by cold work or precipitation hardening may however experience substantial loss of strength in the HAZ.[42]

The loss of strength in heat-treatable alloys is caused by coarsening or over-ageing of the precipitates in the 6xxx alloys. Schematic representation of the change in microstructure during welding of aluminium alloys at ambient temperature is shown in Figure 2.19. A typical hardness curve across the weld of a 6xxx-alloy is shown in Figure 2.20. There are also a potential for loss of alloying elements from the weld pool that may result in a reduction in strength. Magnesium has a low boiling point and may be lost or oxidized during welding. Loss of magnesium is worst when MIG welding, but careful attention to shielding gas will minimize the problem.[42]

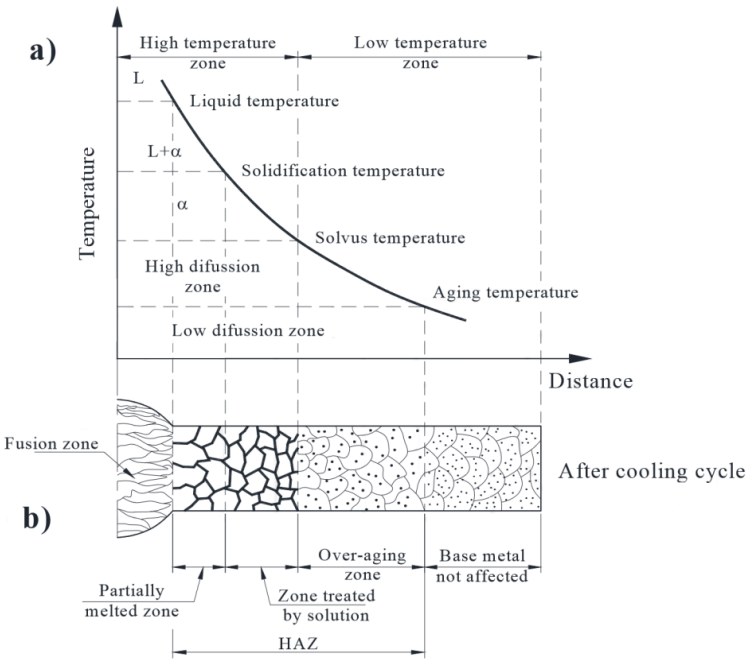

Figure 2.19: Schematic evolution of microstructure changes during welding of heat treatable aluminium alloys. a) thermal cycle. b) microstructure at respective temperatures.[33]

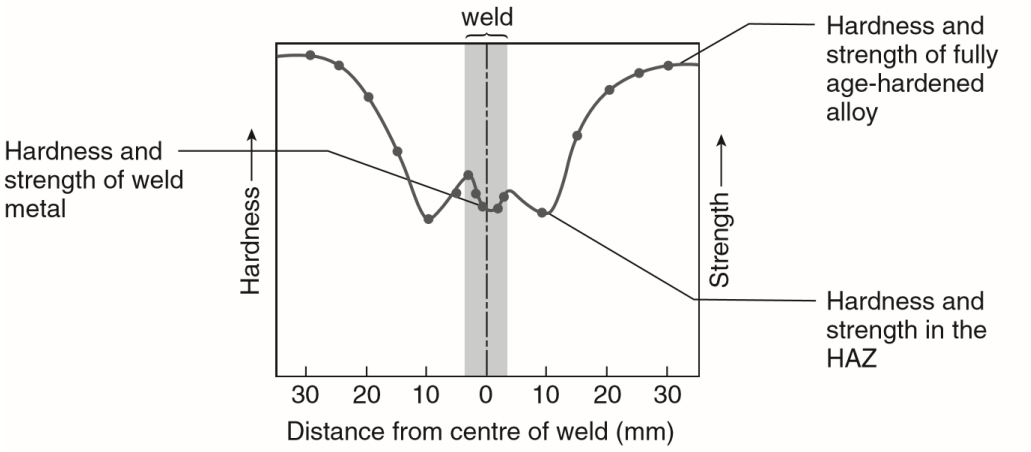

Figure 2.20: Typical strength of welded age-hardened AlMgSi-alloy. In this case a 6061 T6 age-hardened alloy.[42]

2.9.3 Particle coarsening and dissolution

Several competitive processes operate when commercial alloys are subjected to welding or heat treatment. These processes may contribute to a change in the volume fraction and size distribution of the base metal precipitates. Particle coarsening (Ostwald ripening) and particle dissolution (reversion) are the two most important processes.[43]

Seen from Figure 2.21 the particle coarsening occurs at temperature below the equilibrium solvus $T_{eq.}$ of the precipitates. At higher temperatures, particle dissolution becomes the dominating process. In an undefined area between these two mechanisms, a zone where both particle dissolution and particle coarsening can take place simultaneous in parts of the weld where the temperature falls in the "grey zone". Small particles tend to dissolve and precipitate on larger particles (coarsening). In a welding procedure, the thermal pulse experienced by the heat affected zone adjacent to the fusion boundary can result in dissolution of the precipitates in the base metal.[43]

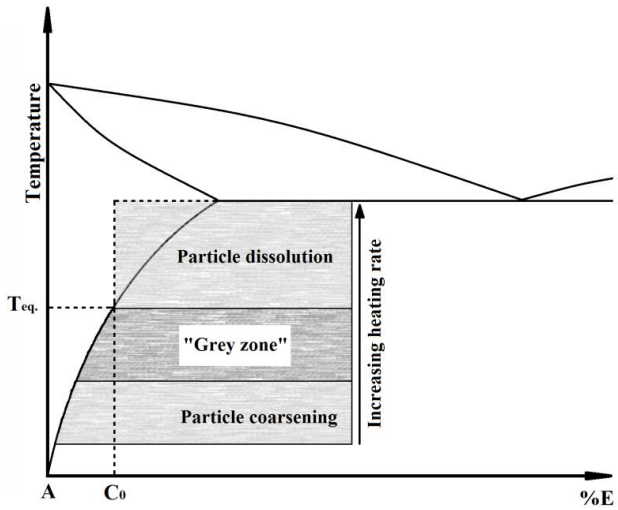

Figure 2.21: Schematic diagram showing the characteristic temperature ranges where specific physical reactions occur during reheating of grain size-controlled and dispersion-hardened materials.[43]

2.9.4 Microstructure evolution during welding

The precipitate dissolving and coarsening showing the microstructure evolution during the thermal processing involving heat treatment and welding is schematically shown in Figure 2.22. Figure 2.22 a) shows that when the alloy is artificial aged, the microstructure consist of fine needle-shaped β'' particles and are uniformly dispersed in the matrix. This is the dominating hardening phase in T6 heat-treated 6xxx-alloys. However, in the temperature range between 250 – 480 °C, the precipitates which are thermodynamically unstable are

affected. The smallest precipitates will start to dissolve in part of the HAZ experiencing temperatures above 250 °C, while the larger precipitates continue to grow. These precipitates do not contribute to the strengthening as much as the needle shaped precipitates and in combination with increased interparticle spacing, the HAZ softens. Closest to the fusion line the β'' particles are fully reverted and at the same time, coarse rod shaped β' precipitates may form. The dissolving β'' particles act as a supply to the rapidly growing β' particles. The microstructure correspond to the schematically image in Figure 2.22 b).[44]

In the highest reached temperatures closest to the fusion line, a large fraction of alloying elements will remain in solid solution at the end of the thermal cycle. This enables conditions for extensive ageing at room temperature over a period of a week.[45] If the welding is followed by post-weld heat treatment (PWHT) the hardening β'' particles can reprecipitate to an extent depending on matrix vacancy and level of Mg and Si in solid solution. The reprecipitation would be expected to be most extensively in the fully reverted region due to high solute content and high consentration of quenched-in vacancies. However, in parts of the HAZ where the peak temperature is lower, these particles will be suppressed due to the matrix is depleted with respect to vacancies and solute. This leads to development of a permanent soft region within the weld HAZ after PWHT. Figure 2.22 c) shows how the schematically microstructure of the welded aluminium will be in the HAZ after PWHT or natural ageing over a period of a weeks.[44]

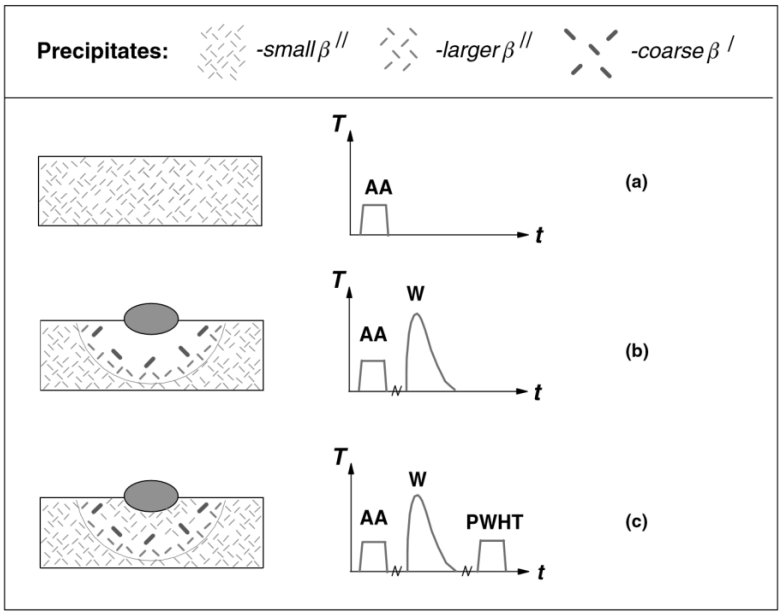

Figure 2.22: Schematic diagram showing the microstructure evolution during multistage thermal processing of AlMgSi alloys involving heat treatment and welding. AA: artificial ageing, W: welding, PWHT: post weld heat treatment. The outer boundary of the HAZ is indicated by the semicircles in the diagrams. [44]

Myhr et al. studied the microstructural evolution during the cooling weld thermal cycle in AlMgSi-alloys. Figure 2.23 (a) shows a TEM micrograph of the hardening precipitates that are present after artificial ageing with the majority being β'' particles. The shadows surrounding the needles are reflections of coherency strains being presence in the aluminium matrix. The smallest particles are most likely to be sheared by dislocations during plastic deformation, while large particles are bypassed in a partly coherent particle/matrix interface. Figure 2.23 (b) shows the microstructure of the alloy consisting of a combination of the fine needle-shaped β'' precipitates and of the coarse rod-shaped β' precipitates. This is after a weld simulation to a local peak temperature of 315 °C during a 10 second holding time. Figure 2.23 (c) shows the same condition with higher magnification and the precipitates are better distinguished. As seen from Figure 2.23 (d) the β'' to β' precipitate transformation occurs to an increasing extent with increasing temperature. From this image it is seen that the β' is the dominating phase for the alloy which has been exposed to peak temperature of 390 °C.[44]

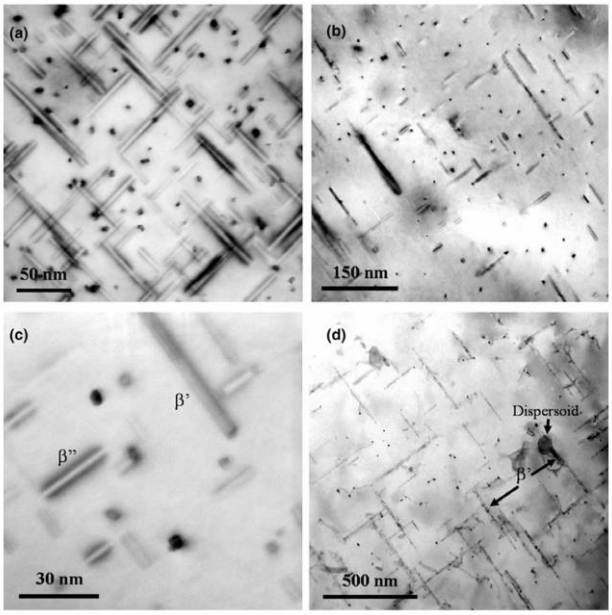

Figure 2.23: TEM bright field images of microstructures observed in the <100> Al zone axis orientation after artificial ageing and Gleeble simulation (Series 1). (a) Needle-shaped β'' precipitates which form after artificial ageing. (b) Mixture of coarse rod-shaped β' particles and fine needle-shaped β'' precipitates which form after subsequent thermal cycling to T_p = 315 °C (10 s holding time). (c) Close up of the same precipitates shown in (b) above. (d) Coarse rod-shaped β' particles which form after thermal cycling to T_p = 390 °C (10 s holding time).[44]

2.9.5 Hardness evolution during welding

Corresponding to the microstructural changes of the alloys during welding, the simultaneous hardness evolution is accounted for. As seen from Figure 2.24 a), the hardness distribution following the β'' dissolution is shown. As the small β'' particles dissolve and the larger grow, the hardness decrease continuously in the HAZ until the dissolution process is complete. The higher experienced temperature, the more β'' particles is affected and in a distance of approximately 1,5 - 2 cm from the fusion center, the temperature is not high enough to affect the precipitates. Figure 2.24 b) shows that during cooling of the weld, some solute may recombine to form the coarse metastable β' precipitates. Figure 2.24 c) shows that the fully reverted region, where Mg and Si are in solid solution, will gain an increase in the hardness. This is achieved by natural ageing or PWHT.

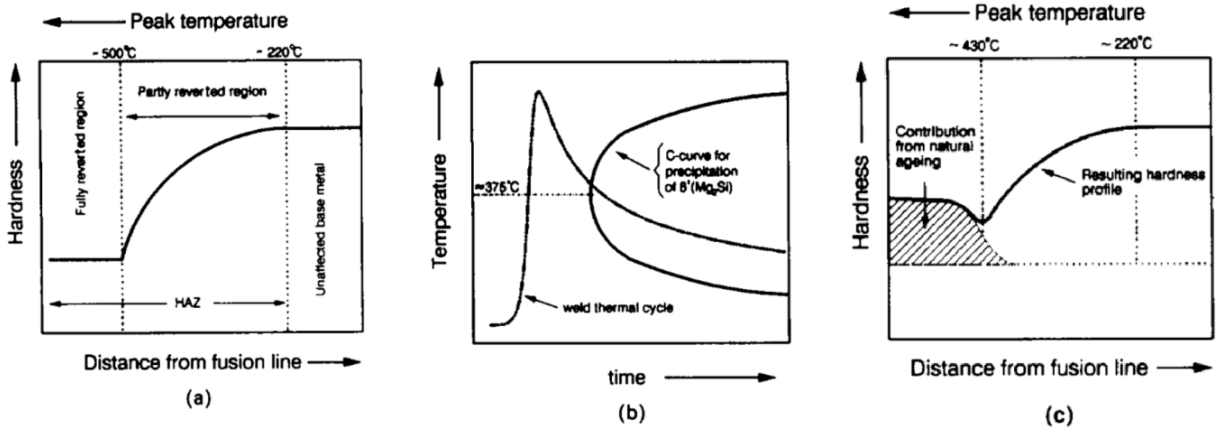

Figure 2.24: Sketches showing the sequence of reactions occurring in the HAZ of AA6082-T6 aluminium weldments: (a) hardness distribution following β'' dissolution. (b) precipitation of β' during the weld cooling cycle. (c) hardness distribution following prolonged room temperature ageing.[45]

3 Materials and experimental procedures

Information of the materials and the various experimental procedures performed in this thesis are listed in the following. Casting and homogenization of the alloys were conducted at Hydro Sunndalsøra. Extrusion, artificial ageing and welding were conducted at SINTEF NTNU Trondheim. Subsequent heat treatments were conducted at NTNU Trondheim.

3.1 Materials

The materials investigated in this thesis were received from Hydro Sunndalsøra in the as-homogenized conditions in the form of casted bolts with a height of 200 mm and 95 mm in diameter. The alloys can be classified, according to international designations, as AA6082. In this study, five different variants of this alloy have been investigated. The chemical compositions of the different alloys are shown in Table 3.1. The composition of the alloys varies where one alloy has a low content of Si while the others have relatively high content of Si. The amount of Mn is approximately the same for all alloys, but some have addition of Cr and in addition one with Zr. A general specification of this alloy is also presented in Table 3.1. The effective Si content ($Si_{eff.}$) is calculated by Equation 5 in Section 2.8.4

Table 3.1: Specific and general composition of the different alloys and calculated $S_{ieffective}$.

Alloy	Si	Fe	Mn	Mg	Cr	Zn	Ti	Zr	Si/Mg	$Si_{eff.}$
1	**0.796**	0.200	**0.601**	**0.639**	0.000	0.010	0.023	0.002	1.25	0.529
2	**1.196**	0.204	**0.601**	**0.655**	0.000	0.010	0.023	0.002	1.83	0.928
3	**1.188**	0.205	**0.603**	**0.649**	**0.251**	0.011	0.022	0.002	1.83	0.835
4	**1.206**	0.206	**0,600**	**0.649**	**0.154**	0.004	0.023	0.001	1,86	0.886
5	**1.130**	0.187	**0.569**	**0.605**	**0.149**	0.007	0.021	**0.131**	1.87	0.785
6082	0.7-1.3	0.0-0.5	0.4-1.4	0.6-1.2	0.0-0.25	0.0-0.25	0.0-0.2			

3.2 Material processing

This section presents the material processing of the profiles during this project. This includes casting, homogenization, extrusion, artificial ageing, welding and subsequent heat treatment. The casting and homogenization were conducted at Hydro Sunndalsøra. The extrusion, artificial ageing and welding were conducted at SINTEF NTNU Trondheim and the subsequent heat treatments were conducted at NTNU Trondheim.

3.2.1 Casting and homogenization

The billets for this study were supplied from Hydro Research and Technology Development Center at Hydro Sunndalsøra. The cylindrical billets were DC casted with a diameter of 95 mm and cut to lengths of 20 cm. After the casting, three different homogenization procedures were conducted to achieve various levels of dispersoids in the alloys considering both size and volume. The goal is to dissolve Mg_2Si-phases and to achieve high levels of small dispersoids in the alloys. The homogenization parameters of the different alloys are given in Figure 3.1.

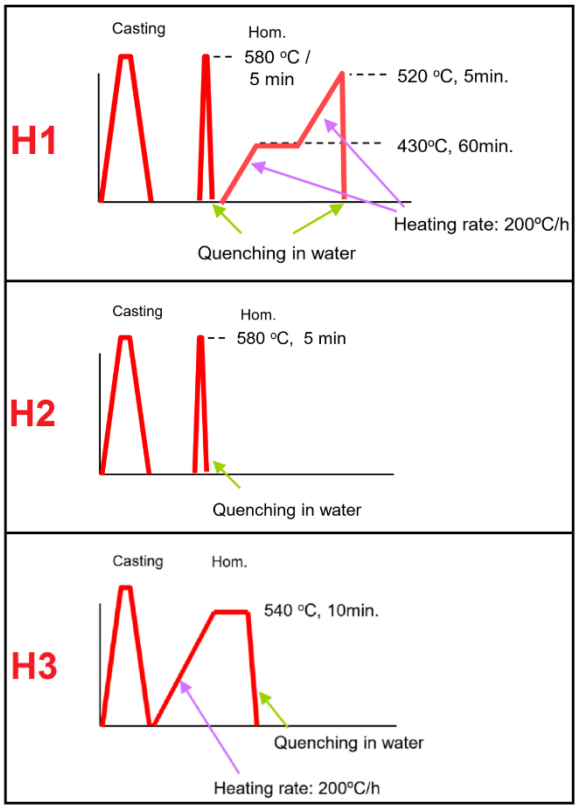

Figure 3.1: Sketches of the three different homogenization procedures.

3.2.2 Extrusion

The billets were extruded into a thin plate at SINTEF Press Laboratory at NTNU in Trondheim. Prior to the extrusion process, the billets were pre-heated to 510 °C at a rate of 100 °C/min by use of induction heating. The dimensions of the applied die were 3 mm x 65 mm. The billets were pressed through the extrusion die and were continously brought to a water bath. The extruded profiles were thus quenched approximately 15 seconds in the process, before each extruded profile was sized to lengths of approximately 50 cm. One billet produced four profiles and they were labeled according to which first came out of the extrusion tool (nr. 1-4, nr. 1 was the beginning of the extrusion and nr. 4 the last). Within 3-5 minutes after the extrusion process, the profiles were preserved in a freezer to prevent natural ageing of the specimens. Some extrusion parameters of each alloy variant are given in Table 3.2. The ram speed of all extrusions were 5,4 mm/s and the container temperature was 430 °C.

Table 3.2: Extrusion parameters.

Alloy	**Breakthrough force F_{max} [kN]**			Die force F_{min} [kN]			**Surface temperature** [°C]		
	H1	**H2**	**H3**	**H1**	**H2**	**H3**	**H1**	**H2**	**H3**
1	3268	3203	3619	2493	2424	2666	534	535	534
2	3241	3187	3555	2393	2392	2593	535	536	534
3	3623	3577	4006	2597	2622	2816	533	536	537
4	3393	3352	3897	2533	2529	2748	534	537	537
5	3419	3479	4058	2585	2582	2852	534	536	535

3.2.3 Artificial ageing

After the extrusion process, four parallels of each alloy variant were obtained. Two of these parallels were artificially aged five days after they were extruded. These were parallel variant 1 and 2 (the start and the middle of the extrusion). The samples were taken out of the freezer 40 minutes before the artificial ageing start. The artificial ageing were conducted at SINTEF (NTNU) where an air-circulating oven was used to heat treat the samples. All alloy variants were conducted to the same artificial ageing treatment. The specimens were placed in the oven at room temperature and the oven was heated up to 185 °C at a rate of 200 °C/h. When the oven reached 185 °C (50 minutes), the samples was hold at this temperature for 5 hours to achieve the highest potential strength, i.e. peak aged to T6. After the heat treatment, the samples were cooled down in room temperature.

In addition to the specimens of interest, a dummy sample was placed in the oven. This sample was used to measure the temperature inside the alloy to confirm the artificial ageing

temperature and time set by the program of the oven. A hole was drilled into the dummy sample at a depth of about 20 mm, and a thermocouple was attached as shown in Figure 3.2

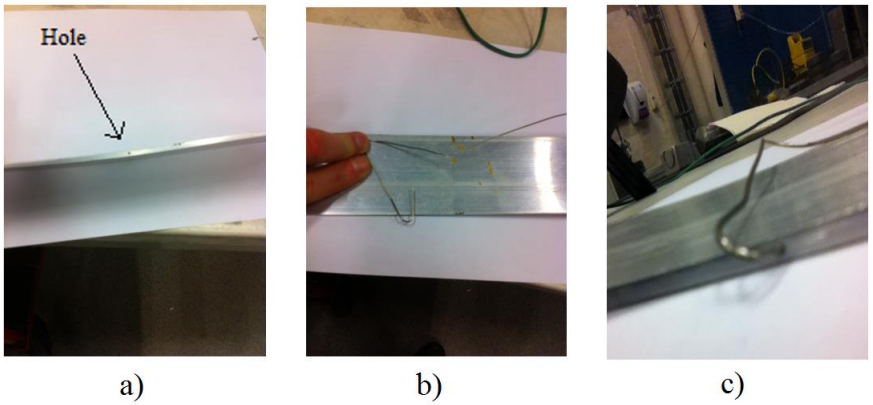

Figure 3.2: Images showing: a) drilled hole in dummy, b) Thermocouple wire and c) thermocouple in dummy specimen.

Figure 3.3 shows a sketch of the temperature and time evolution of both the thermocouple built in the oven, and the externally thermocouple attached to the dummy sample. The temperature of the dummy was approximately 10 °C lower than the oven during the heating to 185 °C. The temperature of the dummy stabilized at 183 °C after 56 minutes while the temperature of the oven showed 185 °C after 50 minutes. To record the cooling rate of the samples, the dummy sample were placed in between the other samples during the room temperature cooling as seen in Figure 3.4 (a). The position of all the samples were frequently switched to get a more uniform cooling as shown in Figure 3.4 (b and c).

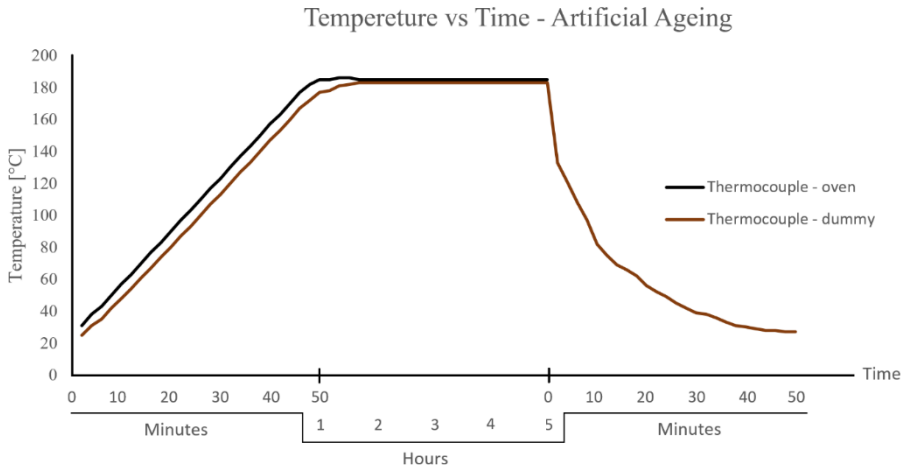

Figure 3.3: Temperature and time evolution of the alloys according to the ovens thermocouple and a thermocouple attached inside a dummy aluminium sample.

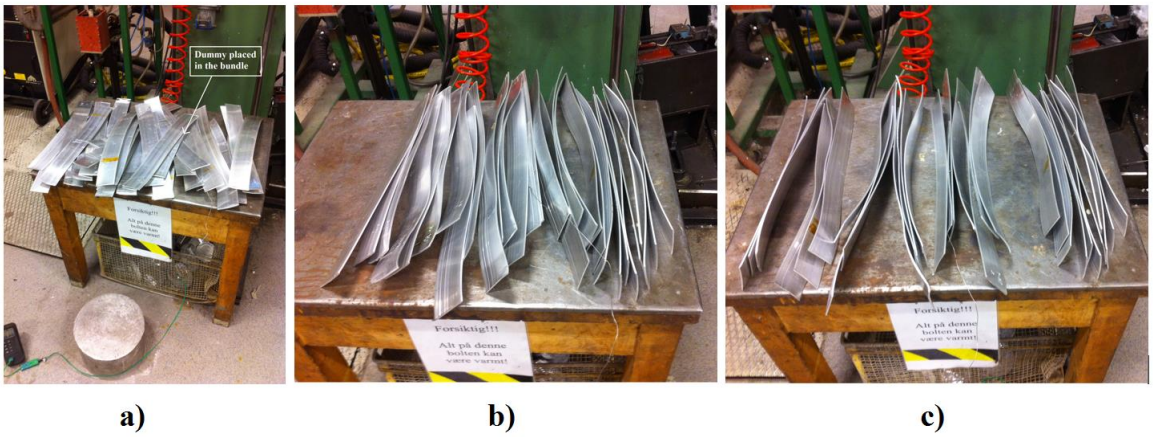

Figure 3.4: Images showing: (a) dummy placed in the bundle, (b) and (c) fanning of the samples to enhance the cooling.

3.2.4 Welding of samples

Fully automatic robotic welding were used to weld the samples. The welding was conducted at SINTEF welding laboratory at NTNU. First, the samples were cleaned with ethanol before positioned and clamped down on the welding table. In addition, the samples were brushed with a steel brush to remove oxide layers. The welding robot was programmed to weld in a straight line from one end to the next. Four samples were welded at a time with two dummy samples at each end. The dummy samples at the start and end ensured making the welding of the samples as even as possible by removing differences at weld start and weld stop. Images showing the sample setup, welding in action and after welding are presented in Figure 3.5. The welding parameters of the procedure are presented in Table 3.3.

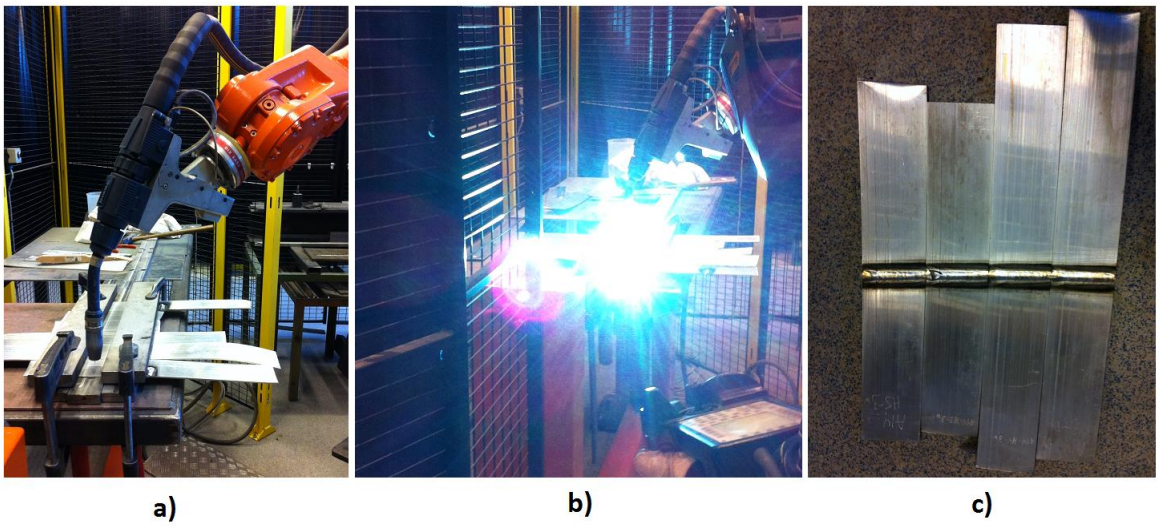

Figure 3.5: Sample setup and alignment of welding gun (a), welding in action (b) and after welding (c).

Table 3.3: Welding parameters.

Process	Voltage [V]	Amperage [A]	Shielding gas	Welding speed [mm/s]
MIG (GMAW)	23	123	Ar	10

The MIG welding wire used for the welding was a solid $AlMg_{4,5}Mn_{0,7}$ wire. This is a 5183 aluminium alloy and is a standard welding wire for MIG welding of Aluminium alloys with high tensile strength requirements. Typical chemical composition of this wire and mechanical properties is shown in Table 3.4 and Table 3.5 respectively.[46]

Table 3.4: General composition for AA5183 aluminium alloy.[46]

	Mg [%]	Mn [%]	Cr [%]	Al [%]
AA5183 filler wire	4,30 – 5,20	0,50 – 1,00	0,05 – 0,25	Remaining

Table 3.5: Mechanical properties for AA5183 aluminium alloy.[46]

Yield strength [N/mm^2]	Tensile strength [N/mm^2]	Elongation [%]
> 125	> 275	> 17

3.3 Optical characterization

The microstructure of both the extruded samples and the welded samples were examined in a microscope. Before the microstructure examination of the alloys, the samples were prepared according to standard metallographic methods.

3.3.1 Sample preparation

The sample preparation was done according to standard metallographic methods, which includes grinding, polishing and anodizing. Samples from the extruded materials and the artificial aged and welded specimens were cut out using a Struers Discotom-2 saw with a cut-off blade suitable for aluminium alloys.

3.3.1.1 Extruded specimens

The extruded specimens were cut to dimensions about 15x3 mm. The specimens were grinded, polished and anodized according to Section 3.3.1.3 (below). The microstructure of the different alloys can be analyzed visually to give an idea of the effect of dispersoids in the material and the best suited homogenization method to gain the most dispersoids to prevent

recrystallization of the extruded specimens. The samples were examined parallel to the extrusion direction as shown in Figure 3.6 (a) (below) with a magnification of 2.5x.

3.3.1.2 Welded specimens

The alloys were artificially aged and welded after the extrusion. The specimens were then cut to dimensions of 60x3 mm to examine the microstructure of the weld metal, heat affected zone as well as the unaffected zone. The same preparation method as below was performed for these samples. The samples were examined parallel to the extrusion direction as shown in Figure 3.6 (b) (below).

3.3.1.3 Grinding, polishing and anodizing

The samples were grinded by using ATM Saphir 330 manual grinding machine with successively finer grinding paper to remove the old deformation layers and the new deformation layers made by the grinding paper. Water was used as lubricant. All samples, which were to be investigated in the microscope, were conducted by the same grinding procedure. The grinding steps was carried out using the following grinding paper; P320, P500, P800, P1200, P2000, P4000. After the grinding steps, the samples were polished using Struers DP-U3 manual polishing machine. The polishing discs used were 6 µm MD Mol, 3 µm MD Mol and 1 µm MD Nap with associated diamond spray. The samples were rinsed in water and ethanol between each polishing steps.

After polishing, the samples were anodized in a solution of 95 % H2O and 5 % HBF4 with a current of 1,0 A and a voltage of 20 V for 90 seconds. The samples were rinsed in water and ethanol before they were dried.

3.3.2 Optical microscope

The microscope used to study the microstructure of the samples was Leica MEF4M. A camera was connected to the computer with the software ProgRes Capture v2.8.8. Polarized light and a sub-parallel lamda plate were used to image the anodized samples. Both the extruded material samples and the welded samples were examined perpendicular to the extrusion direction and in the center of the material as shown in Figure 3.6 and with magnification 2.5x.

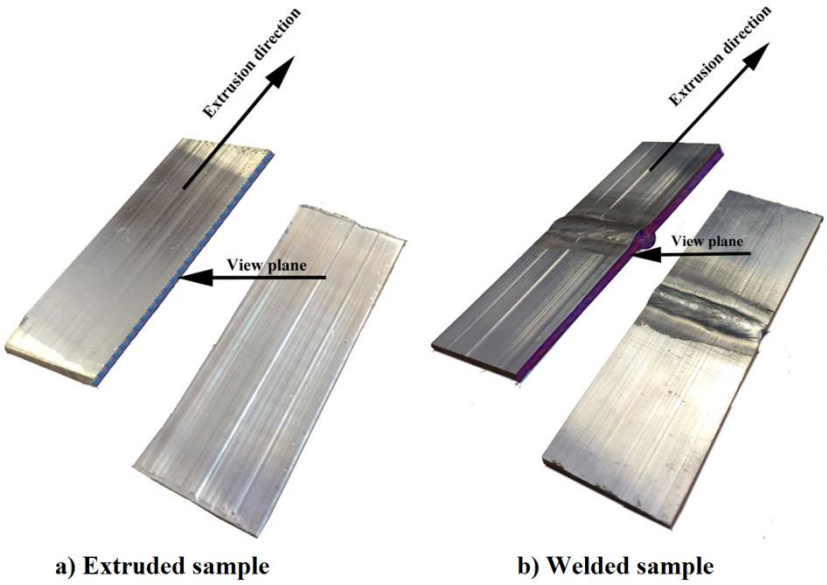

Figure 3.6: The specimens were cut in half along the extrusion direction and the view plane of both the extruded sample a) and welded sample b) is normal to the extrusion direction.

3.4 Hardness measurements of welded samples

The hardness across the weld was measured using Struers Duramin-A2500 hardness tester. The samples were grinded with paper P800 prior to the hardness measurements. The impression force was set to 1 Kg (HV1) and the impression time was about 20-30 seconds. The hardness measurements were taken from the center of the weld and out to both sides of the weld with 1 mm distance between the imprints. The hardness was measured at a distance of 30 mm on both sides from the center of the weld measure the unaffected zones. Figure 3.7 illustrates the hardness imprints.

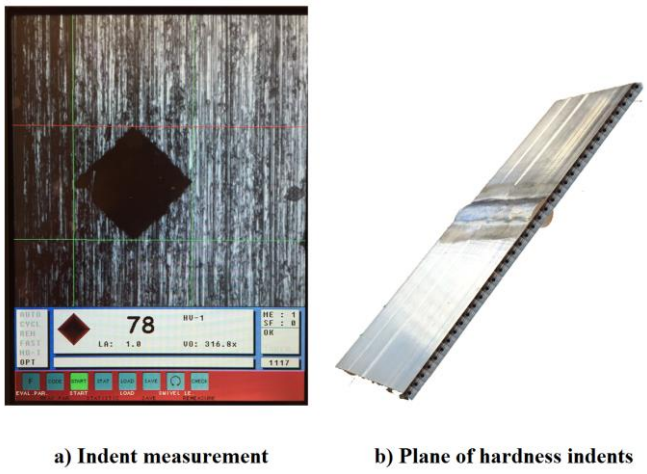

Figure 3.7: Image showing an example of a measured hardness indent a) and the plane of the hardness indents across the welded specimen b). Distance between indents is 1 mm.

3.5 Dispersoid analysis as extruded

To detect the variation in density of the various dispersoids in the samples and the effect of the three different homogenization procedures, a set of 24 images of the alloy variants were taken in a Scanning Electron Microscope (FE-SEM, Zeiss Ultra, 55 Limited addition). The images where further examined in an image processing software (iSolution DT) which uses contrast levels to distinguish and highlight the particles from the matrix.

The dispersoid density and size classification were characterized for alloys 2, 4 and 5, which have approximately the same basis material.

- Alloy 2: AlMgSi – 0,6 wt.% Mn

- Alloy 4: AlMgSi – 0,6 wt.% Mn + 0,15 wt.% Cr

- Alloy 5: AlMgSi – 0,6 wt.% Mn + 0,15 wt.% Cr + 0,13 wt.% Zr

3.5.1 Electron microscope and BSE

By use of optimal metallographic techniques and SEM-parameters, detection and quantification of dispersoids as small as 20 nm in radius can be detected. The samples were prepared as described in Section 3.3.1.3, i.e. grinded and polished to 1 µm. In addition the samples were polished further by OPS suspension due to the 1 µm grinding stripes damage the shape of the dispersoids. The samples where rinsed in distilled water after each polishing steps to avoid contamination of copper. The SEM-parameters are presented in Table 3.6.

Table 3.6: SEM-parameters for images used to analyze dispersoids.

SEM-parameters	Value
Detector	Backscatter
Acc. Voltage	4 kV
Working distance	7,3-7,5 mm
Aperture	60 µm
Magnification	5000x
Pixel resolution	3072x2304

3.5.2 Dispersoid analysis with iSolution DT

The SEM-images were analyzed in iSolution DT. The levels of contrast, brightness and gamma were adjusted to highlight the particles of interest. Noise pixels in the sizes of 1-2 pixels were removed from the image before counting and measurement of size were performed. Dispersoids smaller than 20 nm were removed from the measurements by object

selection in the software. It should be pointed out that for all of the H3 variants and especially the 5-H3 homogenization procedure, many particles below 20 nm that were taken out from the measurements were detected.

Figure 3.8 shows examples of the images taken with SEM (top), further enhanced (middle) and processed in iSolution DT (bottom). Notice the difference in particle size where the H3 homogenization procedure (images on the right) many small dispersoids compared to H2. Blue color in images represents the smallest dispersoids (20 – 40 nm, ECD).

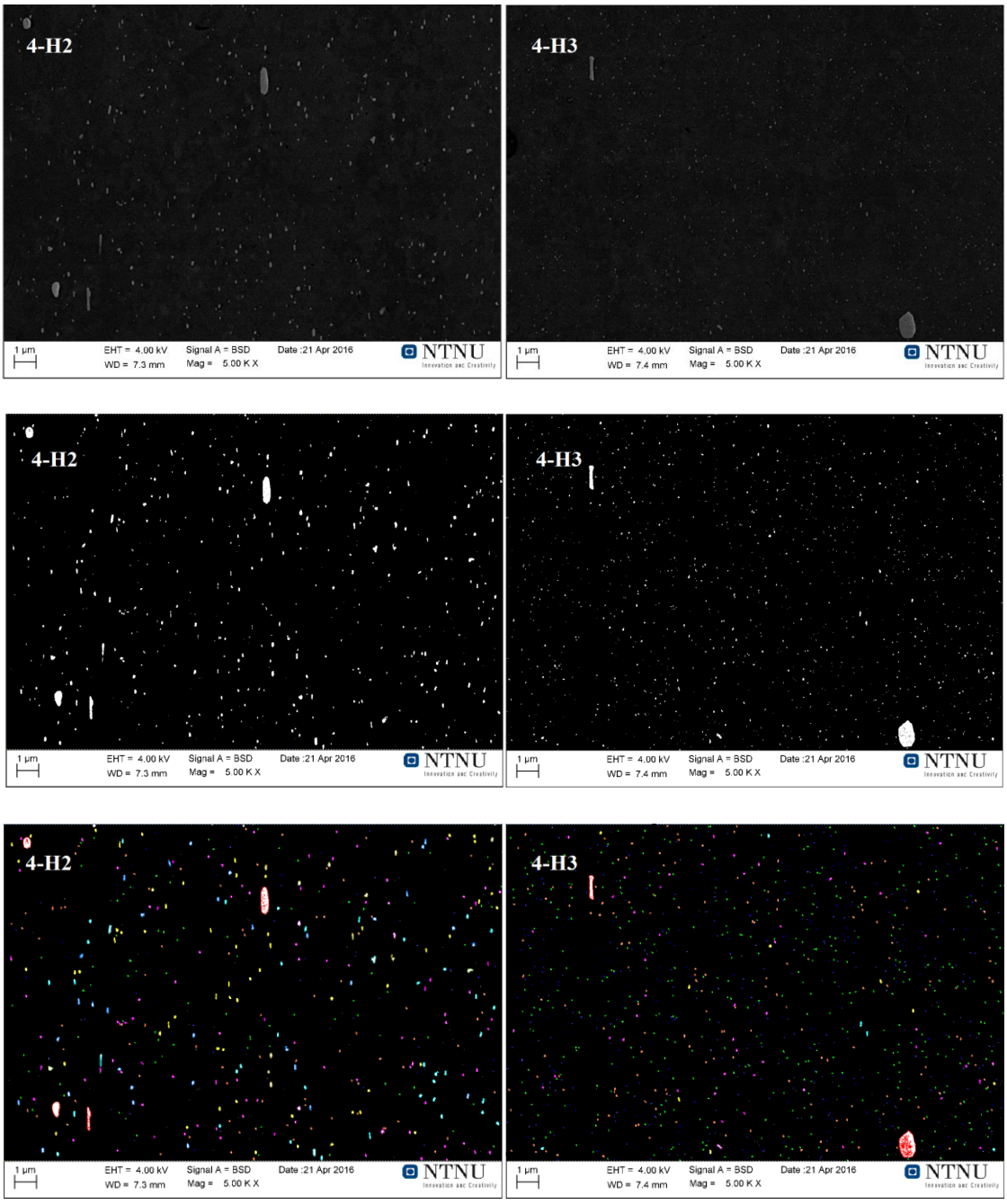

Figure 3.8: Examples of SEM-images, enhanced images (brightness, contrast and gamma) and analysis. In this case the 4-H2 alloy and 4-H3 alloy.

The results from these dispersoid measurements is used to further understand and give information of the best suited homogenization procedure to ensure the highest amount of small dispersoids. These measurements are also used as a control for further investigation of dispersoid phases for the subsequent heat treatments.

3.6 Subsequent heat treatment

From the microstructure analysis, hardness testing and the dispersoid measurements of the various homogenization procedures, the properties of the different alloys have been considered. Alloy 4 (Al-1,20Si-0,65Mg-0,6Mn-0,15Cr) have been chosen to be further investigated. High potential is seen from the hardness measurements in the weld for this alloy in relation to the H2 homogenization method. Various heat treatments are performed in an attempt to further increase the dispersoid density of this alloy. The extruded samples left in the freezer where used as the basis for the subsequent heat treatments. The 4-H2 samples were stored in the freezer for about 2 months after it had been extruded.

3.6.1 Heat treatments procedures

Two different heat treatments have been performed where one was executed in a salt bath and the other in an air-circulated oven. Three samples of this alloy (4-H2) was heat treated in the two procedures but with different number of cycles (1, 2 and 5 cycles). Figure 3.9 shows the heating procedures.

Salt bath cycle: The samples where hold in a salt bath with temperature of 540 °C for 10 minutes and then water quenched.

Air-circulated oven cycle: The samples where continuously heated from room temperature (heating rate 200 °C) up to 540 °C and hold for 10 minutes before water quenched.

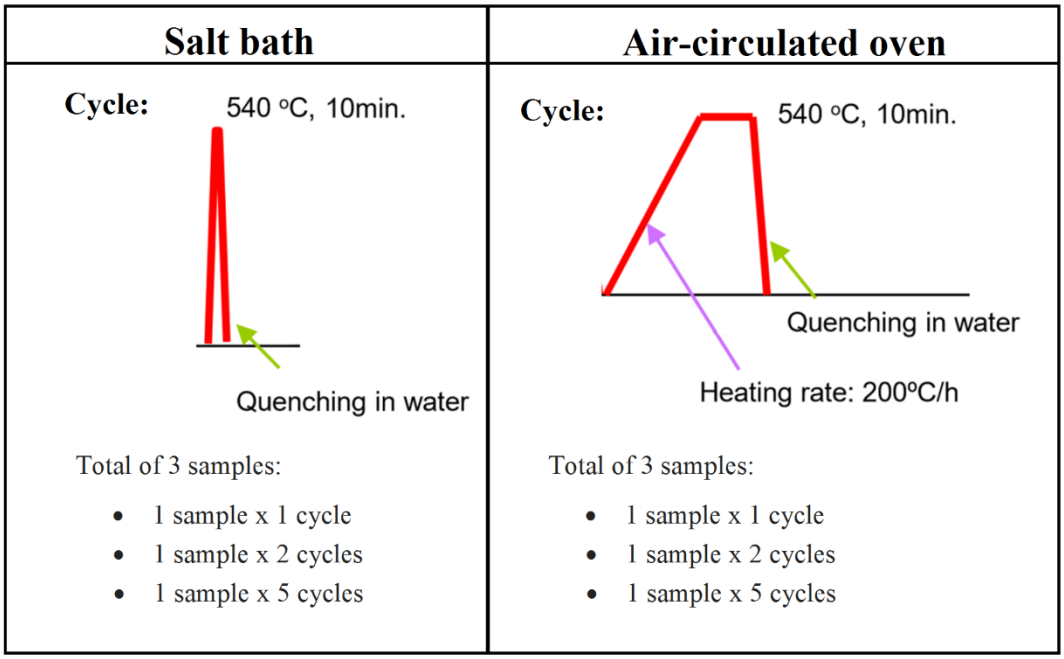

Figure 3.9: Sketches of the two different subsequent heat treatment procedures.

3.6.2 Hardness and electrical conductivity measurements

The hardness and electrical conductivity were measured directly after the respective heating cycle. In addition, the hardness and electrical conductivity were measured 1 and 4 days after the heat treatment to see the effect of natural ageing.

In between the cycles for the air-circulating oven, the samples were hold in room temperature for a day due to cooling of the oven. It is expected that the Mg-Si clusters developed at room temperature quickly dissolve in the up-heating during the next cycle.

The electrical conductivity was measured with a Foerster Sigmascope 2.069. Before testing, the instrument was calibrated with conductivity standards of 58,5 MS/m and 4,415 MS/m. The diameter of the probe was 7 mm and the electrical conductivity was measured with a frequency of 60 kHz. The hardness measurements were measured with 1 Kg force. For both the hardness- and electrical conductivity, the mean value of five measurements is used in the results. The hardness was measured normal to the extrusion direction while the electrical conductivity was measured in the extrusion plane.

3.7 Further investigating after 1 cycle of subsequent heat treatment

The results from the subsequent heat treatment after 1 cycle showed promising behavior. Both the air-circulating sample (x1) and the salt bath sample (x1) were further investigated by means of dispersoid density and size distribution. These variant were also exposed to a new salt bath treatment (400 °C for 5 seconds) to simulate the most destructive temperatures experienced in welding. It should be pointed out that the thermal cycle for conventional MIG welding is different. One sample (x1, air-circulating and x1, salt bath) were cooled in room temperature and one sample (x1, air-circulating and x1, salt bath) were water quenched. The samples are considered T4 and the sample cooled in room temperature are the most comparable to a welding situation, which slowly cools. The hardness and electrical conductivity were measured to determine the effect of the welding on the extruded alloy.

4 Results

The results from the experimental tests are presented below. This involves optical characterization of the samples as-extruded and optical characterization and measurements of hardness of the samples as-welded. Dispersoids measurements for some of the alloys (2, 4 and 5) as-extruded, subsequent heat treatment of a selected alloy (4-H2) and hardness- and electrical conductivity of the respective alloy after the subsequent heat treatment. In addition, dispersoid analysis of the extruded 4-H2 alloy subjected to the subsequent heat treatment for 1 cycle (x1), hardness, and electrical measurements of this sample subjected to salt bath treatment (400 °C, 5 seconds) to simulate temperatures reached in welding.

4.1 Microstructure of material after extrusion

The optical micrographs of the polished and anodized samples in Figure 4.1 show the microstructure of the as-extruded alloys. All images are taken with a magnification of 2.5x, and are taken normal to the extrusion direction as shown in Figure 3.6. These images can indicate the most suitable alloy composition and homogenization procedure to promote a superior microstructure suitable for welding. This is based on the density and size of the dispersoids precipitates in the alloy where a high density of small dispersoids provides the best microstructure by preventing recrystallization (Section 2.4).

The images in Figure 4.1 shows alloys designed with different compositions of Mn, Cr and Zr. The alloys have been homogenized in three different methods (H1, H2 and H3) to examine which method provides the best results considering amount and size of dispersoids, which again leads to an unrecrystallized fibrous structure after extrusion.

The homogenization methods H1, H2 and H3 are presented from left to right respectively, and the alloy compositions from least to most dispersoid elements are presented from the top and down.

In general, it can be determined that the recrystallization of the alloys decreases with increasing amount of dispersoid forming elements, and that the homogenization variant H3 have lower degree of recrystallization compared to H1 and H2 variant.

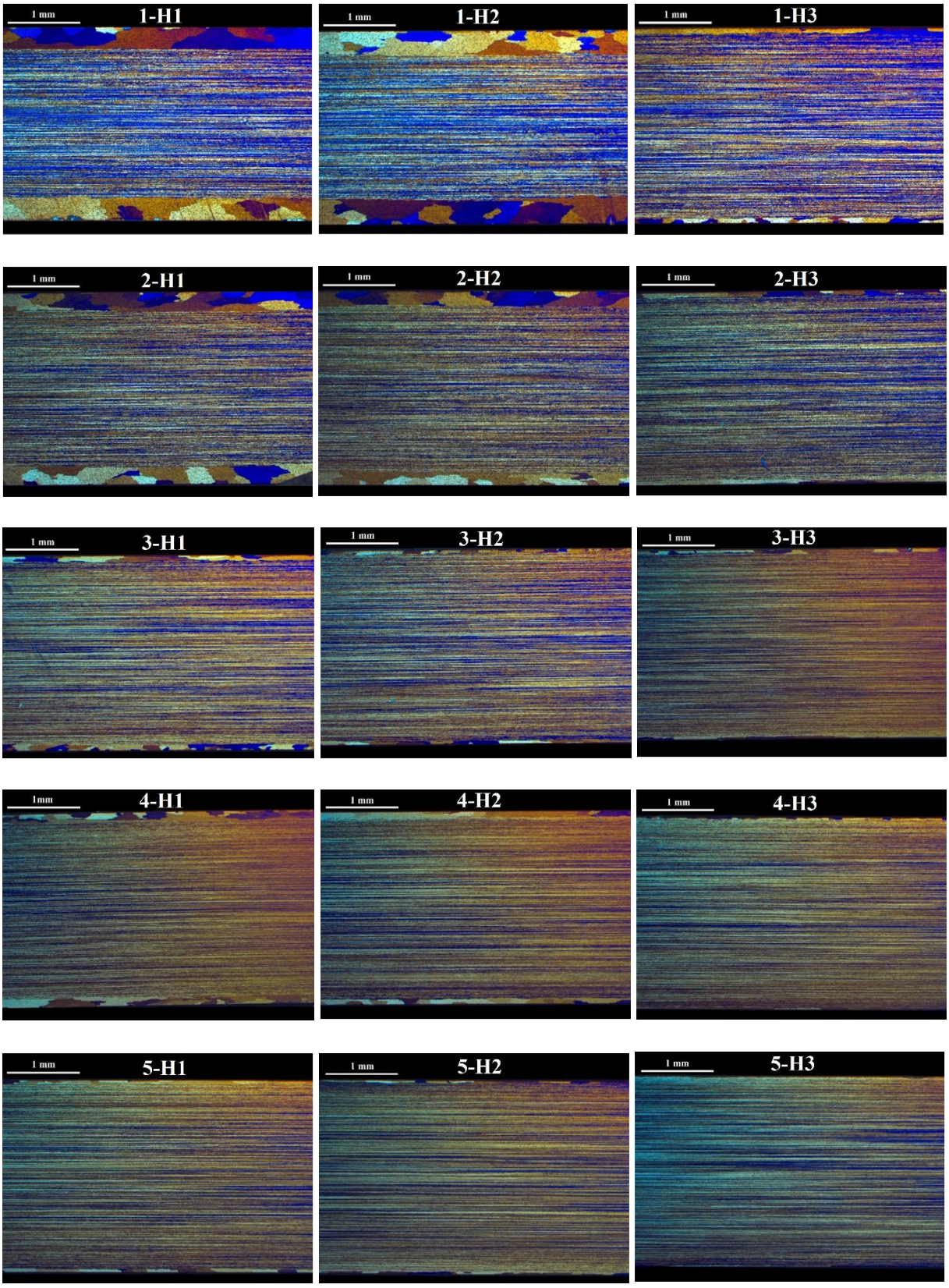

Figure 4.1: Optical images of all samples after extrusion, with magnification 2.5x. The view plane for all samples is normal to the extrusion direction as imaged in Figure 3.6. The images shows that the homogenisation variant H3 has retarded recrystallization after extrusion to a greater extent than the homogenisation variant H1 and H2. It can also be seen that recrystallization are hindered to a greater extent with increasing amount of Mn, Cr and Zr.

4.1.1 Effect of Mn, Cr and Zr and homogenization procedure on the microstructure

The microstructure images in Figure 4.1 can be analyzed regarding amount of Mn, Cr and Zr and homogenization procedures.

4.1.1.1 Alloy 1 Al-0,80Si-0,64Mg-0,60Mn

This alloy variant has relatively low amount of Si. The images show that the grain structure has a relatively large recrystallized area at the surface of the H1 and H2 homogenization method with thickness of recrystallized grains of approximately 0,5 mm. This decreases to approximately 0,2 mm for the H3 homogenization method.

4.1.1.2 Alloy 2 Al-1,20Si-0,66Mg-0,60Mn

This alloy variant has increased amount of Si compared to alloy 1. The recrystallized area at the surface has decreased just slightly for the H1 homogenization method. For the H2 homogenization method the thickness of the recrystallized area is approximately 0,25 mm. and for the H3 method the thickness in approximately 0,1 mm.

4.1.1.3 Alloy 3 Al-1,19Si-0,65Mg-0,60Mn-0,25Cr

This alloy variant is similar to Alloy 2 but in addition Cr has been added. The recrystallized surface areas are very narrow for all homogenization variants where the H1, H2 and H3 variants has approximately 0,2 mm, 0,1 mm and 0,05 mm thick recrystallization grains respectively.

4.1.1.4 Alloy 4 Al-1,20Si-0,65Mg-0,6Mn-0,15Cr

This is a similar alloy as alloy 3 but it has a smaller amount of Cr addition. The recrystallized area for the H1 and H2 variant shows an slight increase in thickness compared to alloy 3 with higher Cr, but for the H3 variant, the recrystallized area are almost completely disappeared.

4.1.1.5 Alloy 5 Al-1,13Si-0,61Mg-0,57Mn-0,15Cr-0,13Zr

This alloy has an addition of Zr compared to the alloy 4. The recrystallized area are almost completely gone for the H1 and H2 homogenization variant, and is completely gone for the H3 homogenization variant.

4.2 Hardness profiles of welded specimens

The hardness across the artificial aged and welded specimens were measured. From the hardness profile, the different zones in the welded alloy are easily distinguished where the zones are usually divided in three. The weld metal (0 - ± 5 mm), the HAZ (± 6 - 20 mm) and the unaffected zone (± 21 – 30 mm). The hardness in the unaffected zone is the hardness of the alloy as-artificial aged. The hardness in the weld center is the hardness of the welding wire used which is alloy AA5183. Near this weld the AA5183 and AA6082 have mixed due to melting and conjunction of the two alloys. The hardness profile of the different alloys variants are presented in Figure 4.2 - Figure 4.9.

4.2.1 Effect of homogenization method on hardness of welded specimens

In this section the hardness curves applies for the alloy compositions separately and the homogenization variants are plotted to see the effect of homogenization procedure on the hardness of the welded specimens.

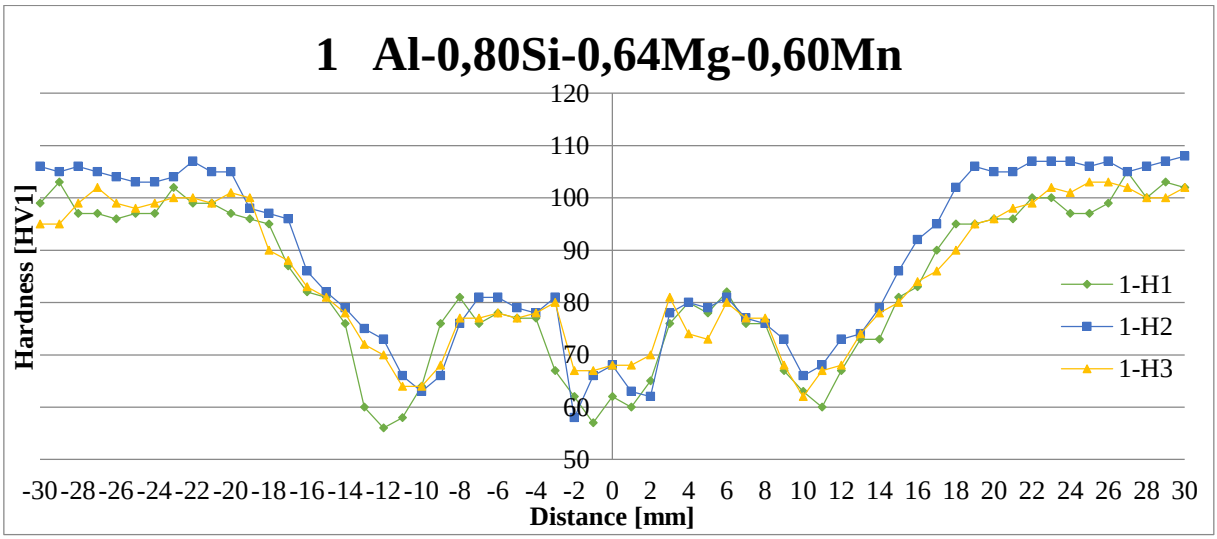

Figure 4.2: Hardness profile of Alloy 1 for all homogenization procedures.

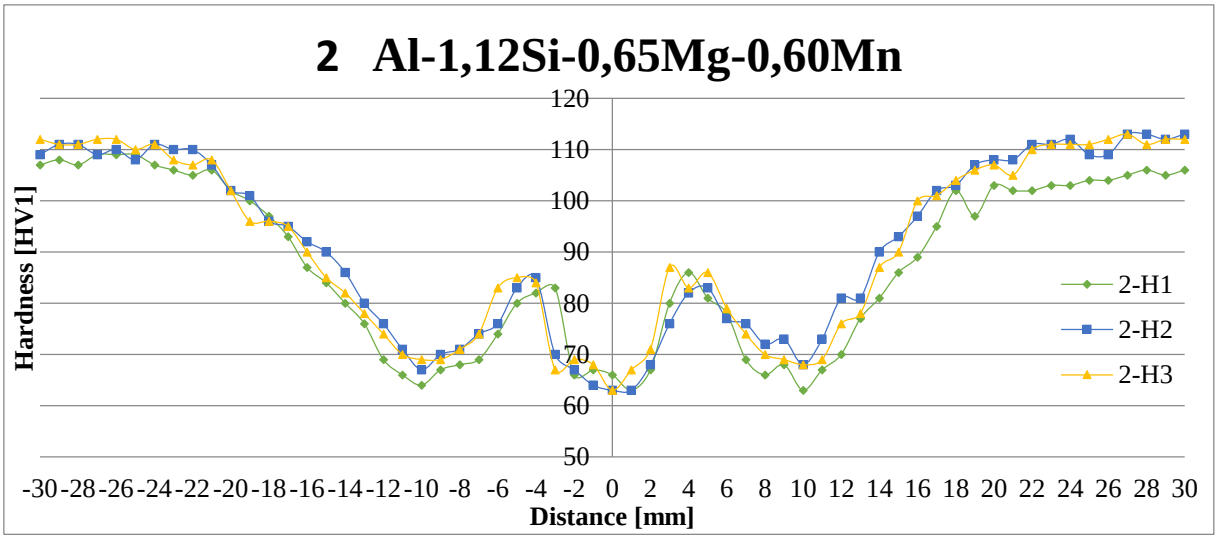

Figure 4.3: Hardness profile of Alloy 2 for all homogenization procedures.

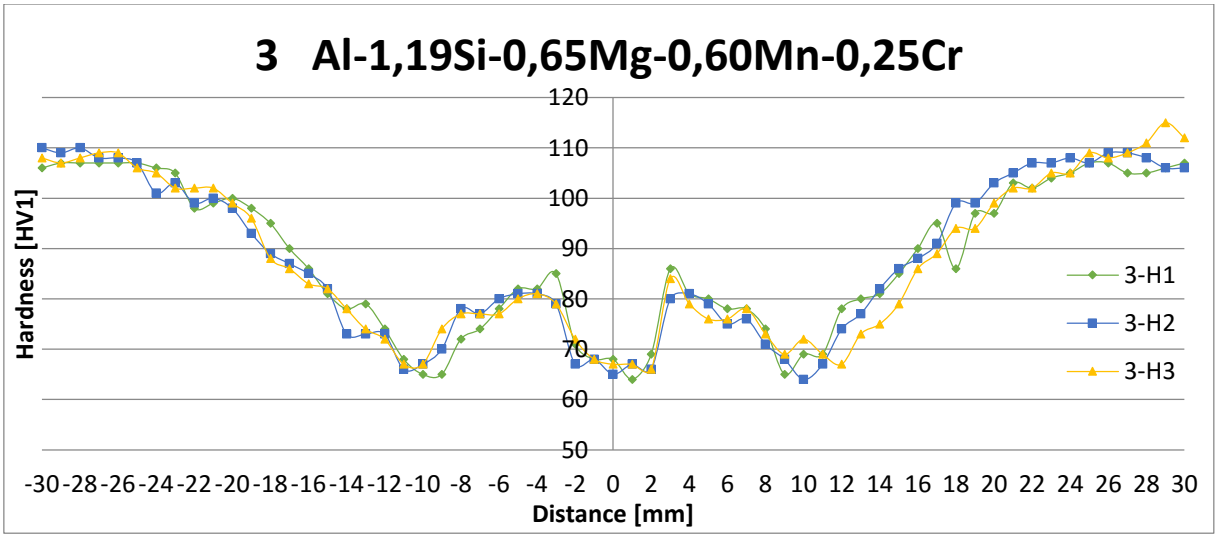

Figure 4.4: Hardness profile of Alloy 3 for all homogenization procedures.

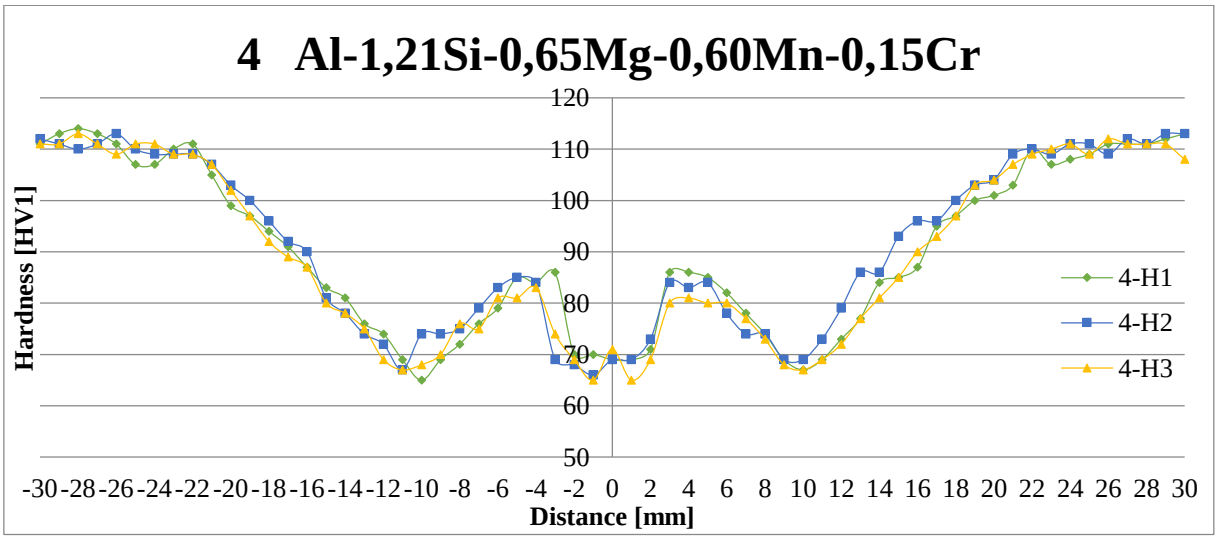

Figure 4.5: Hardness profile of Alloy 4 for all homogenization procedures.

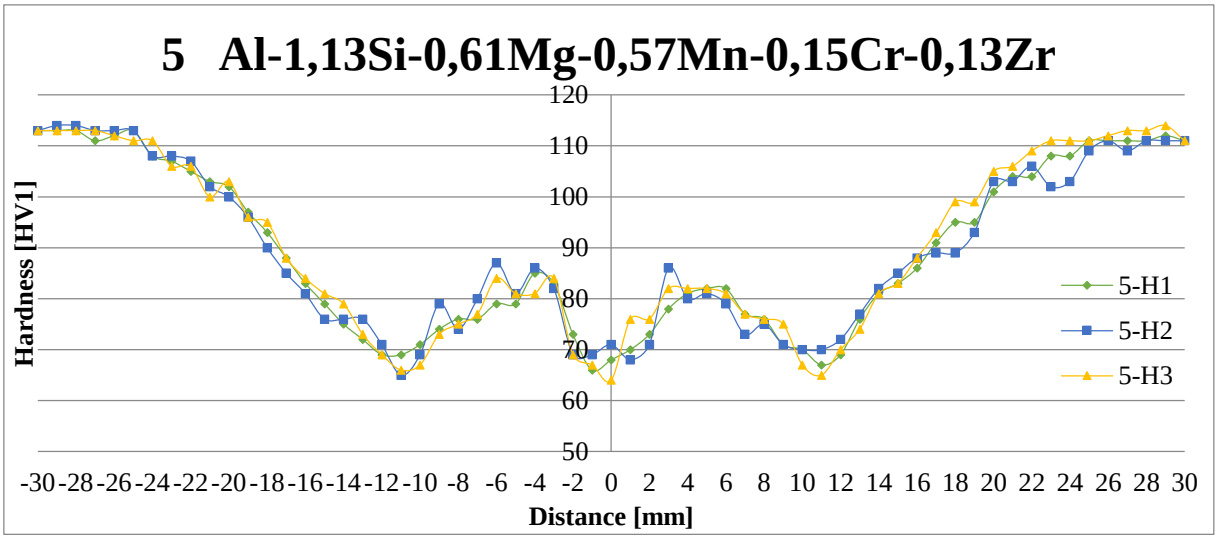

Figure 4.6: Hardness profile of Alloy 5 for all homogenization procedures.

4.2.1.1 Alloy 1 Al-0,80Si-0,64Mg-0,60Mn

From the hardness profiles, it is shown that the H2 procedure has generally a higher strength than the H1 and H3 variant in both the unaffected zone and the entire HAZ. The H1 and H3 procedure are similar, but the H1 procedure has the lowest hardness in both the HAZ and unaffected zone. However, the hardness curve for H1 procedure has a steeper incline compared to the H3 procedure, which indicates that the HAZ is slightly more narrow.

4.2.1.2 Alloy 2 Al-1,20Si-0,66Mg-0,60Mn

From the hardness profile, it is shown that both the H2 and H3 procedure have a similar development in hardness curve and generally highest hardness in both the HAZ and the unaffected zone. The H2 procedure is slightly better. The H1 procedure gives the lowest hardness value in the entire hardness curve.

4.2.1.3 Alloy 3 Al-1,19Si-0,65Mg-0,60Mn-0,25Cr

For this alloy, it is hard to distinguish and determining which homogenization procedure provides the best results due to the curves are overlapping. The H2 and H3 procedure can be decided to be slightly better than the H1 procedure.

4.2.1.4 Alloy 4 Al-1,20Si-0,65Mg-0,6Mn-0,15Cr

The H2 procedure shows a slightly better hardness in general compared to the H1 and H3 procedure. There is however not much difference for the homogenization procedures.

4.2.1.5 Alloy 5 Al-1,13Si-0,61Mg-0,57Mn-0,15Cr-0,13Zr

The last alloy variant with addition of Zr shows small or none difference in the hardness curves. The homogenization procedures have small effect on the hardness for this alloy.

4.2.2 Effect of amount of dispersoids on hardness of welded specimens

In this section the hardness curves applies for the homogenization procedure separately and the different alloy variants are plotted to see the effect of dispersoids on the hardness of the welded specimens.

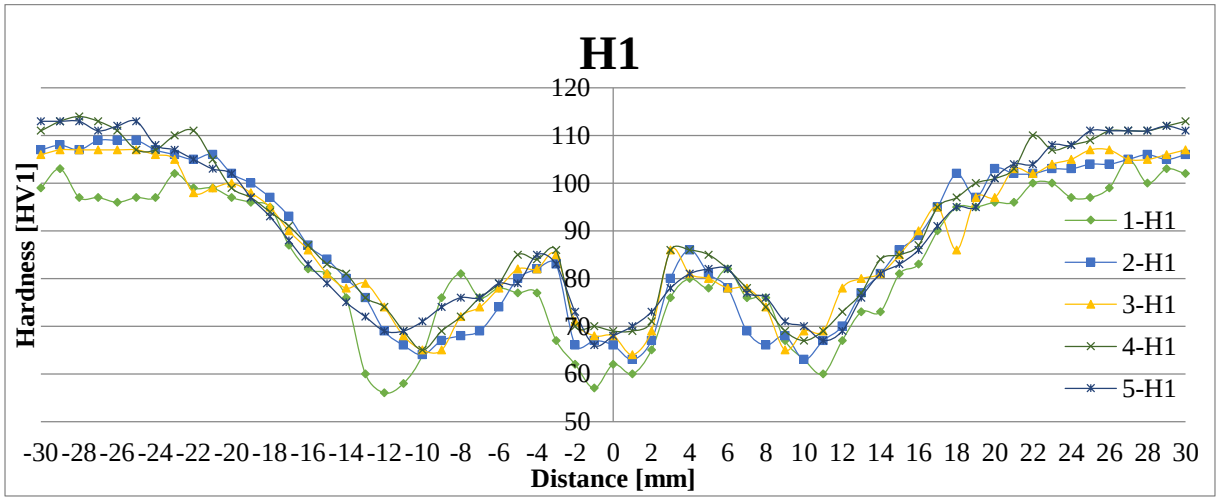

Figure 4.7: Hardness profile of the five different alloy variants homogenized by H1 procedure: Homogenized at 580 °C for 5 minutes and quenched prior to heating to 430 °C hold for 60 minutes (200 °C/h) and additionally heating to 520 °C hold for 5 minutes (200 °C/h) and quenched.

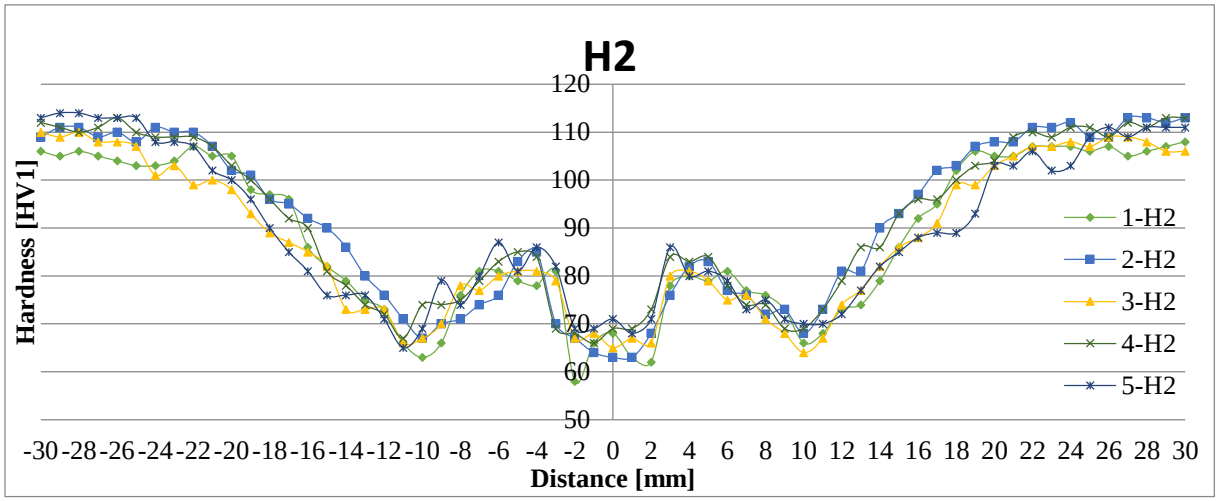

Figure 4.8: Hardness profile of the five different alloy variants homogenized by H2 procedure: Homogenized at 580 °C, hold for 5 minutes, and quenched.

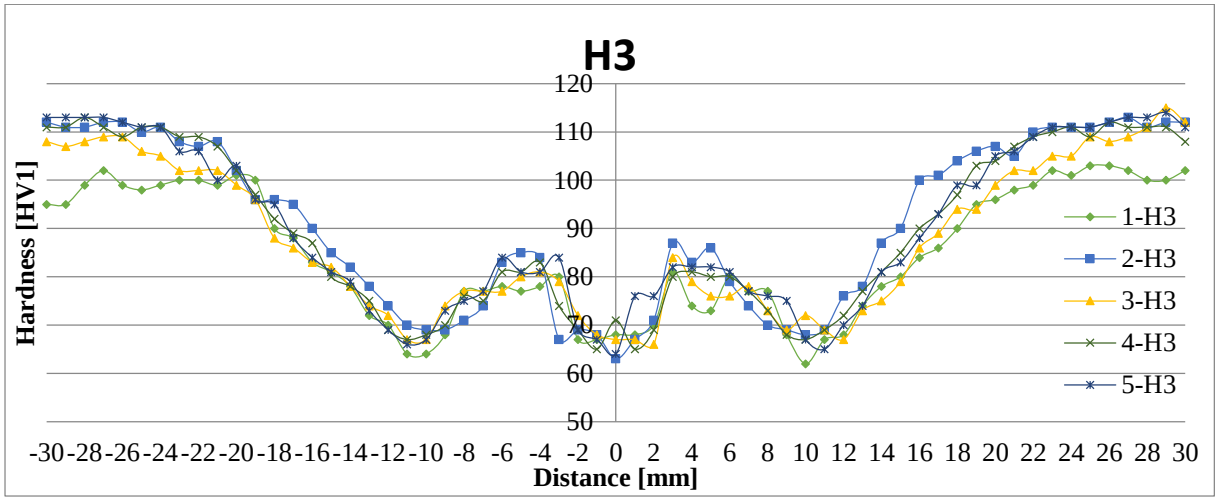

Figure 4.9: Hardness profile of the five different alloy variants homogenized by H3 procedure: Homogenized at 540 °C, hold for 10 minutes (200 °C/h) and quenched.

4.2.2.1 H1 procedure

In general, it can be determined that for the H1 procedure, the hardness in both the HAZ and the unaffected zone increases with increased amount of dispersoids. Alloy 1 with low Si and 0,6 Mn is the weakest in the zones and alloy 5 with high Si, 0,6 Mn, 0,15 Cr and 0,13 Zr has the highest hardness values in the zones.

4.2.2.2 H2 procedure

In general, it can be determined that the alloy 1 and alloy 3 has the lowest hardness in both HAZ and unaffected zone. Alloy 2 and alloy 4 show the best hardness values for this homogenization procedure. Alloy 5 has good properties in the unaffected zone but the lowest peak in HAZ is poor compared to the alloy 2 and 4.

4.2.2.3 H3 procedure

In general, the alloy 1 and 3 shows the poorest properties in the HAZ and unaffected zone. The rest of the alloys shows similar properties with the highest hardness and alloy 2 shows slightly better properties among these three.

4.3 Microstructure of welded specimens

The microstructures of the artificial aged and welded alloys are shown in Figure 4.10 - Figure 4.14. From these images, the effect of dispersoids and homogenization method on the alloys after welding can be determined visually in relation to microstructurally changes from the welding. The images where taken with a series of images with a magnification of 2.5x which were merged together using Adobe Photoshop Elements software.

In general, there is not observed any difference in the microstructure of the samples after welding compared to base material after extrusion. The heat from the welding has not caused recrystallization in the HAZ. The welding wire used is alloy 5183 and this has melted and mixed with the 6082 samples in the weld line.

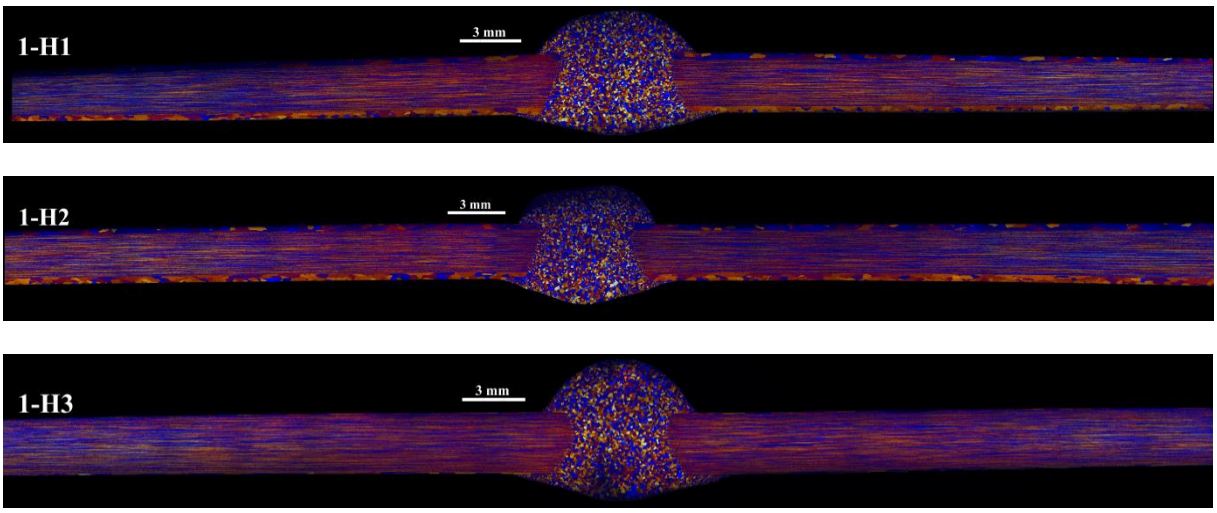

Figure 4.10: Images showing microstructure of the welded specimens for alloy 1 Al-0,80Si-0,64Mg-0,60Mn and the three homogenization procedures. Sharp transition from weld metal to alloy. None micro structural changes compared to as-extruded.

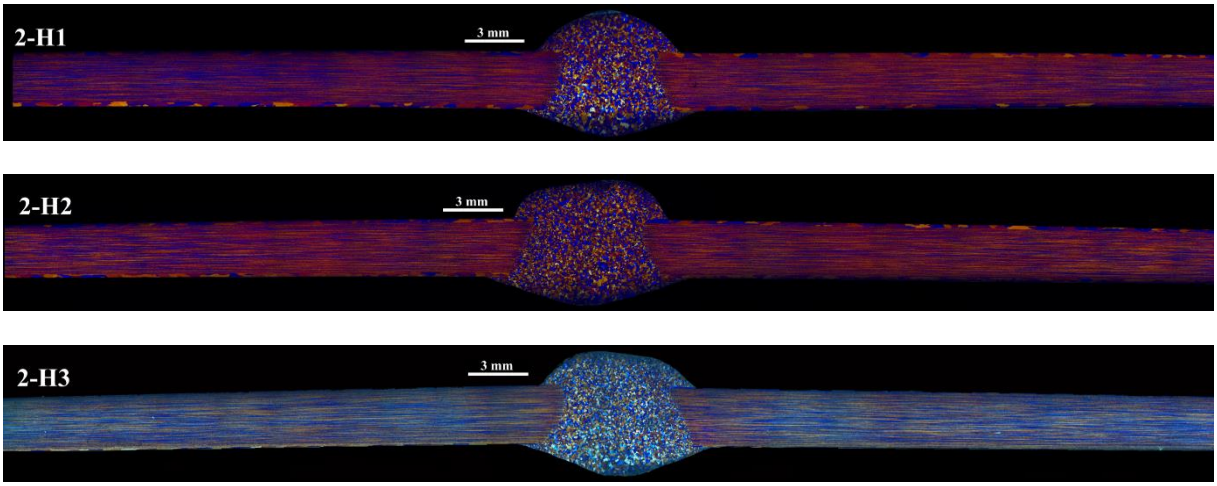

Figure 4.11: Images showing microstructure of the welded specimens for alloy 2 Al-1,20Si-0,66Mg-0,60Mn and the three homogenization procedures. Sharp transition from weld metal to alloy. None micro structural changes compared to as-extruded.

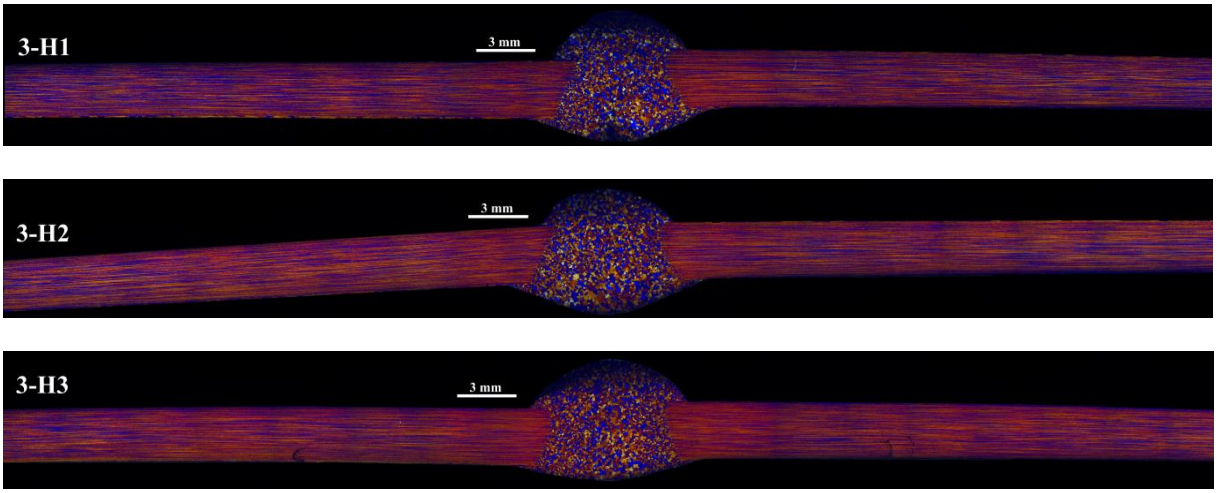

Figure 4.12: Images showing microstructure of the welded specimens for alloy 3 Al-1,19Si-0,65Mg-0,60Mn 0,25 Cr and the three homogenization procedures. Sharp transition from weld metal to alloy. None micro structural changes compared to as-extruded.

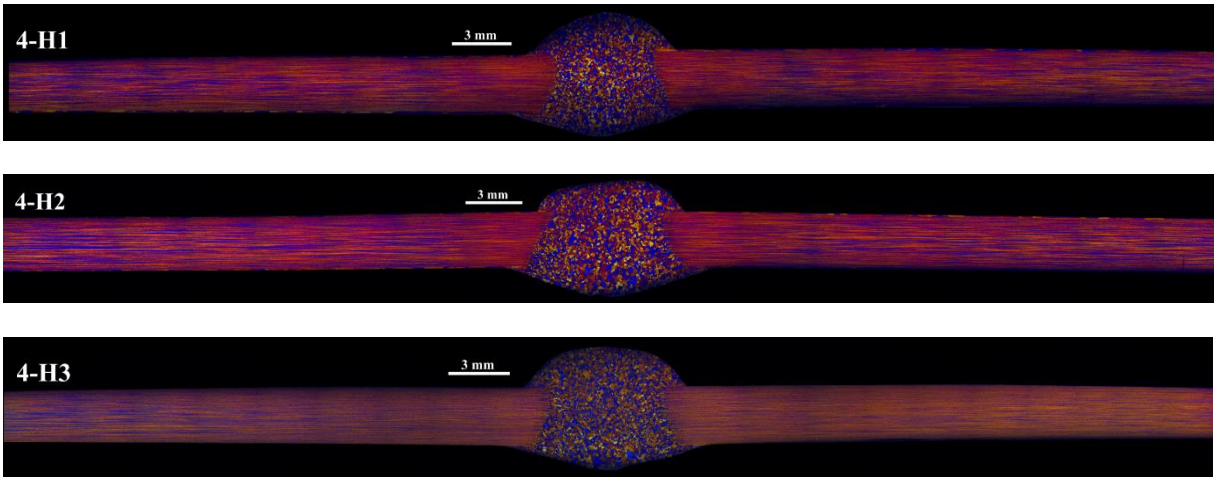

Figure 4.13: Images showing microstructure of the welded specimens for alloy 4 Al-1,21Si-0,65Mg-0,60Mn 0,15 Cr and the three homogenization procedures. Sharp transition from weld metal to alloy. None micro structural changes compared to as-extruded.

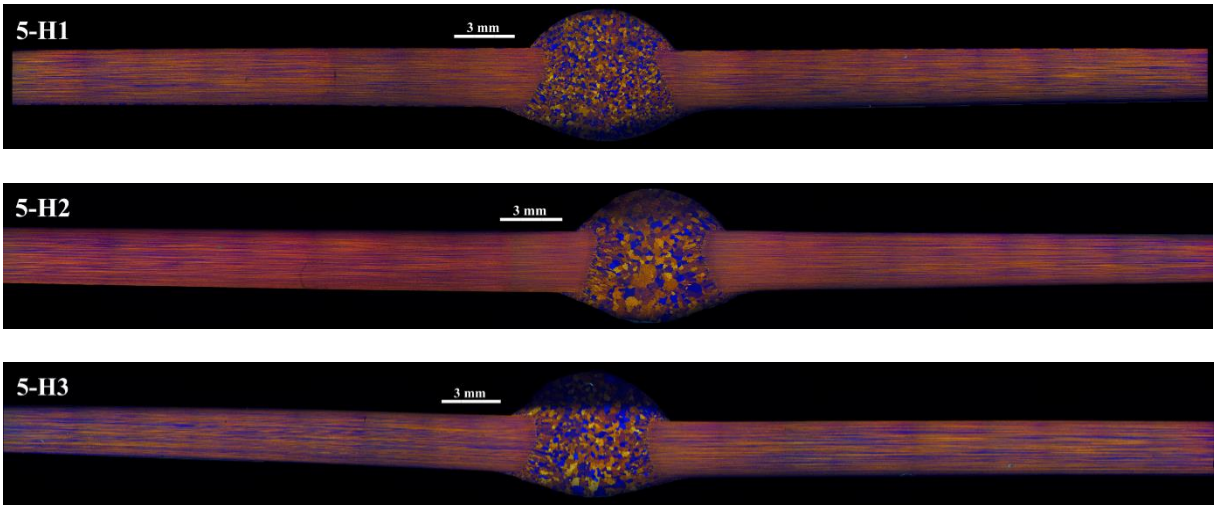

Figure 4.14: Images showing microstructure of the welded specimens for alloy 5 Al-1,13Si-0,61Mg-0,57Mn-0,15Cr-0,13Zr and the three homogenization procedures. Sharp transition from weld metal to alloy. None micro structural changes compared to as-extruded.

4.4 Dispersoid measurements of extruded alloys

The dispersoid measurements of the extruded alloys are shown in Figure 4.15 - Figure 4.20. The figures represent the total count and size distribution of 24 images provided by SEM with a magnification of 5000x. The images were examined in iSolution DT, which is an image processing software that detect phases and particles. Alloy 2, 4 and 5 were chosen to be examined.

It is shown that the dispersoid density increases with increasing amount of Mn, Cr and Zr elements. The H3 homogenization procedure is found to be superior compared to H1 and H2 regarding density of small dispersoids. It is not observed considerable variation in dispersoid distribution between the H1 and H2 homogenization procedure.

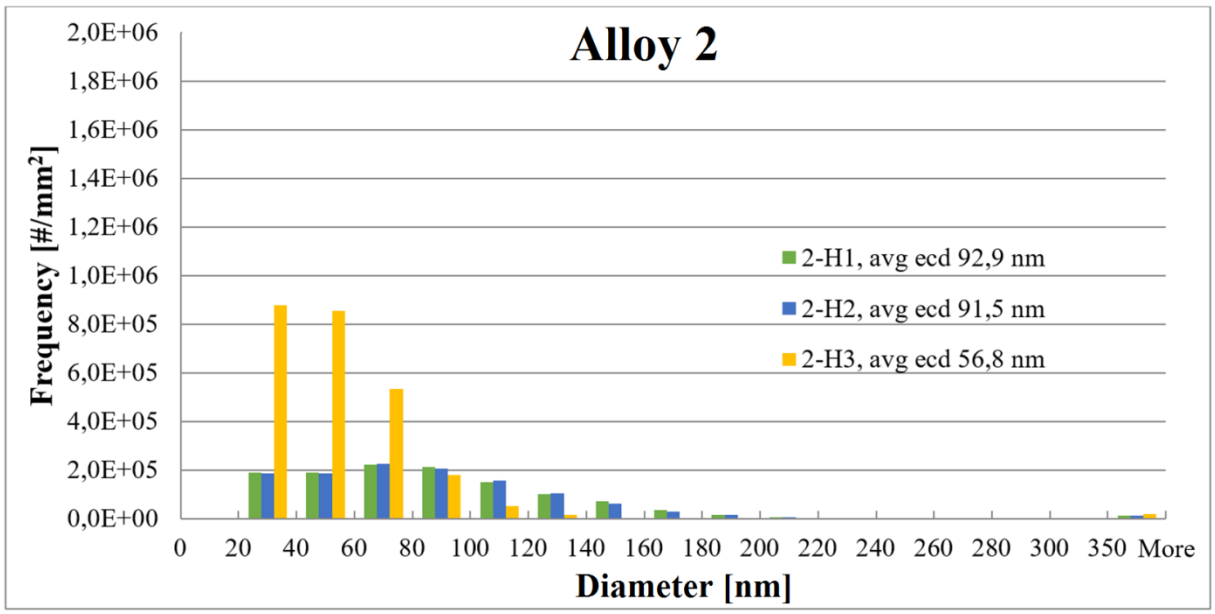

Figure 4.15: Experimental data from dispersoid measurements in SEM and iSolution DT for alloy 2 (AlMgSi-0,6Mn) and homogenization cycles H1, H2 and H3. Lower detection limit for the dispersoid measurements was set to 20 nm.

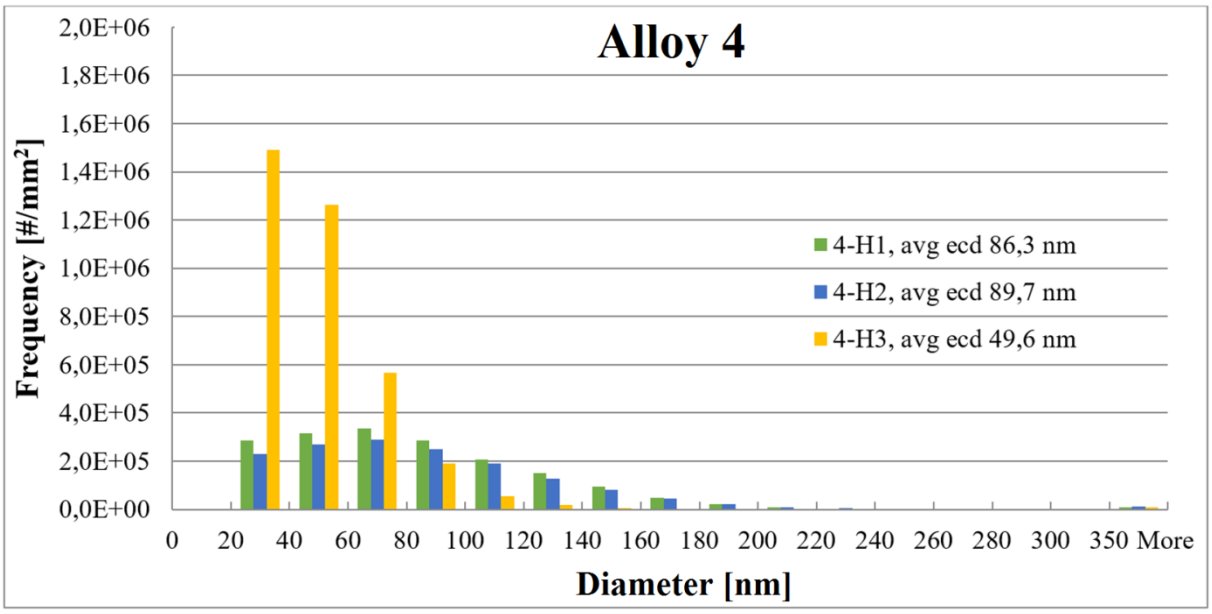

Figure 4.16: Experimental data from dispersoid measurements in SEM and iSolution DT for alloy 4 (AlMgSi-0,6Mn-0,15Cr) and homogenization cycles H1, H2 and H3. Lower detection limit for the dispersoid measurements was set to 20 nm.

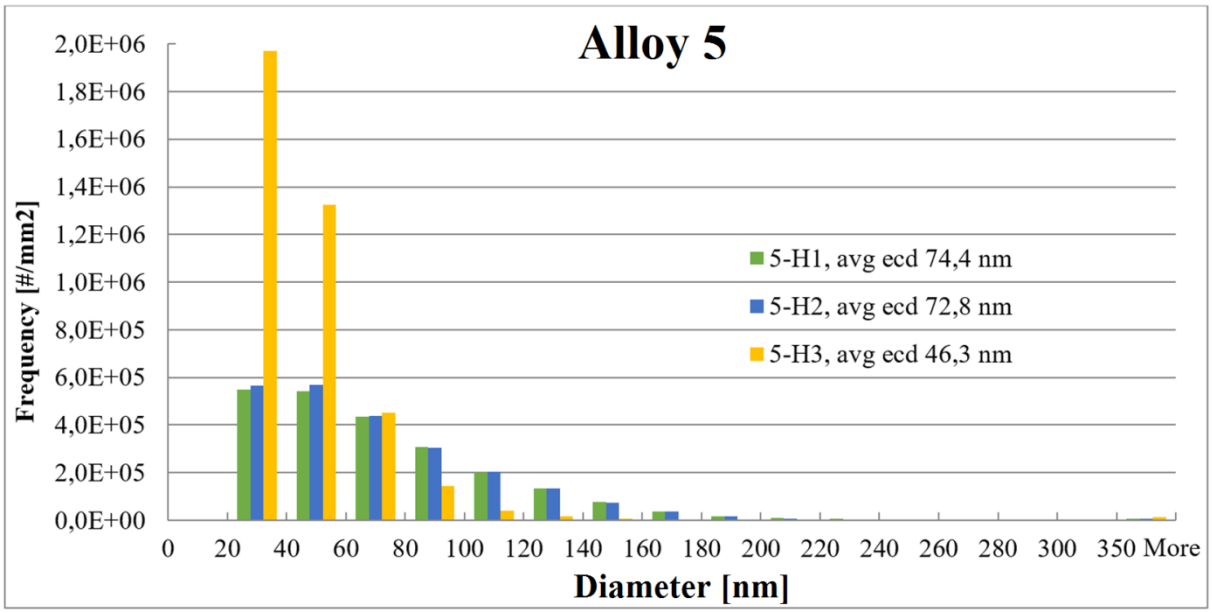

Figure 4.17: Experimental data from dispersoid measurements in SEM and iSolution DT for alloy 5 (AlMgSi-0,6Mn-0,15Cr-0,13Zr) and homogenization cycles H1, H2 and H3. Lower detection limit for the dispersoid measurements was set to 20 nm.

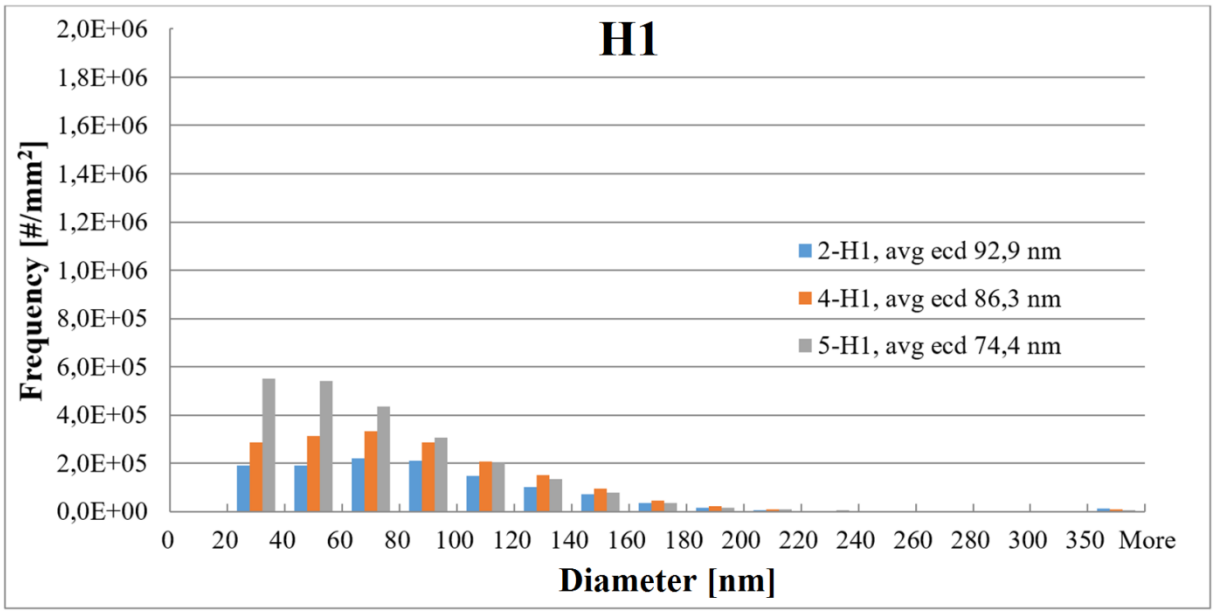

Figure 4.18: Experimental data from dispersoid measurements in SEM and iSolution DT for alloys 2, 4 and 5 and homogenization cycle H1. Lower detection limit for the dispersoid measurements was set to 20 nm.

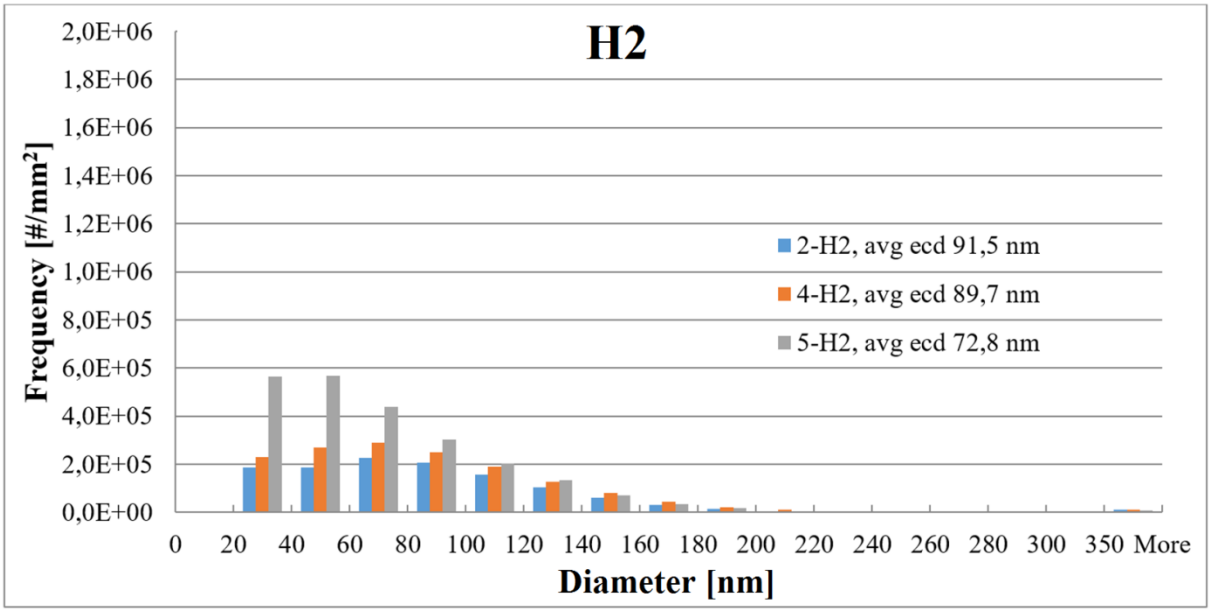

Figure 4.19: Experimental data from dispersoid measurements in SEM and iSolution DT for alloys 2, 4 and 5 and homogenization cycle H2. Lower detection limit for the dispersoid measurements was set to 20 nm.

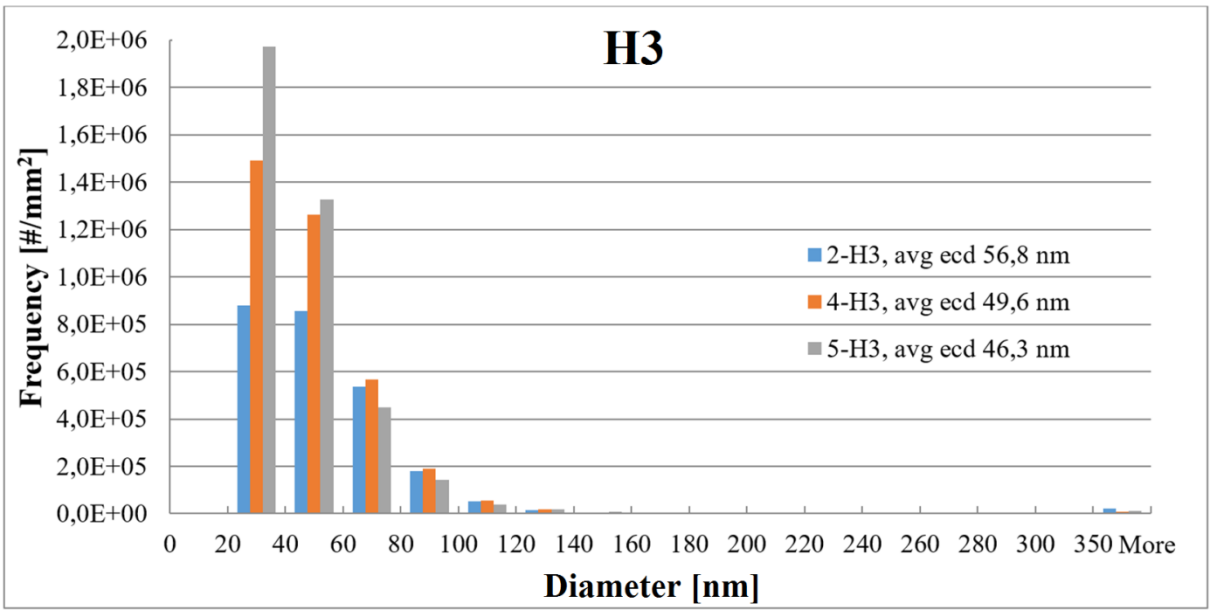

Figure 4.20: Experimental data from dispersoid measurements in SEM and iSolution DT for alloys 2, 4 and 5 and homogenization cycle H3. Lower detection limit for the dispersoid measurements was set to 20 nm.

4.5 Subsequent heating treatment

Alloy 4 (AlMgSi-0,6 wt.% Mn + 0,15 wt.% Cr) is chosen to be further processed with respect to increasing the density of dispersoids. The two different heat treatments (air-circulating oven and salt bath) where used to increase the dispersoid density. The samples were heat treated with various amount of cycles (x1, x2 and x5). The hardness and the electrical conductivity were measured directly after the two heat treatments and 1 and 4 days after the heat treatment. The results are presented in Figure 4.21 - Figure 4.24. In general, the hardness of the air-circulating samples increases with number of cycles and natural ageing. The hardness of the salt bath samples is different were the hardness decreases with number of cycles and increases with natural ageing.

4.5.1 Measurements after number of cycles

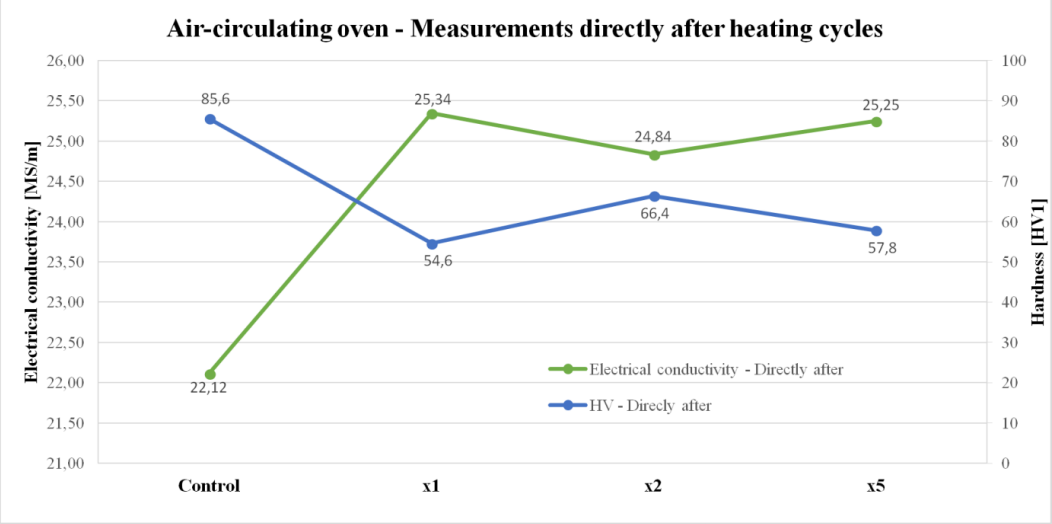

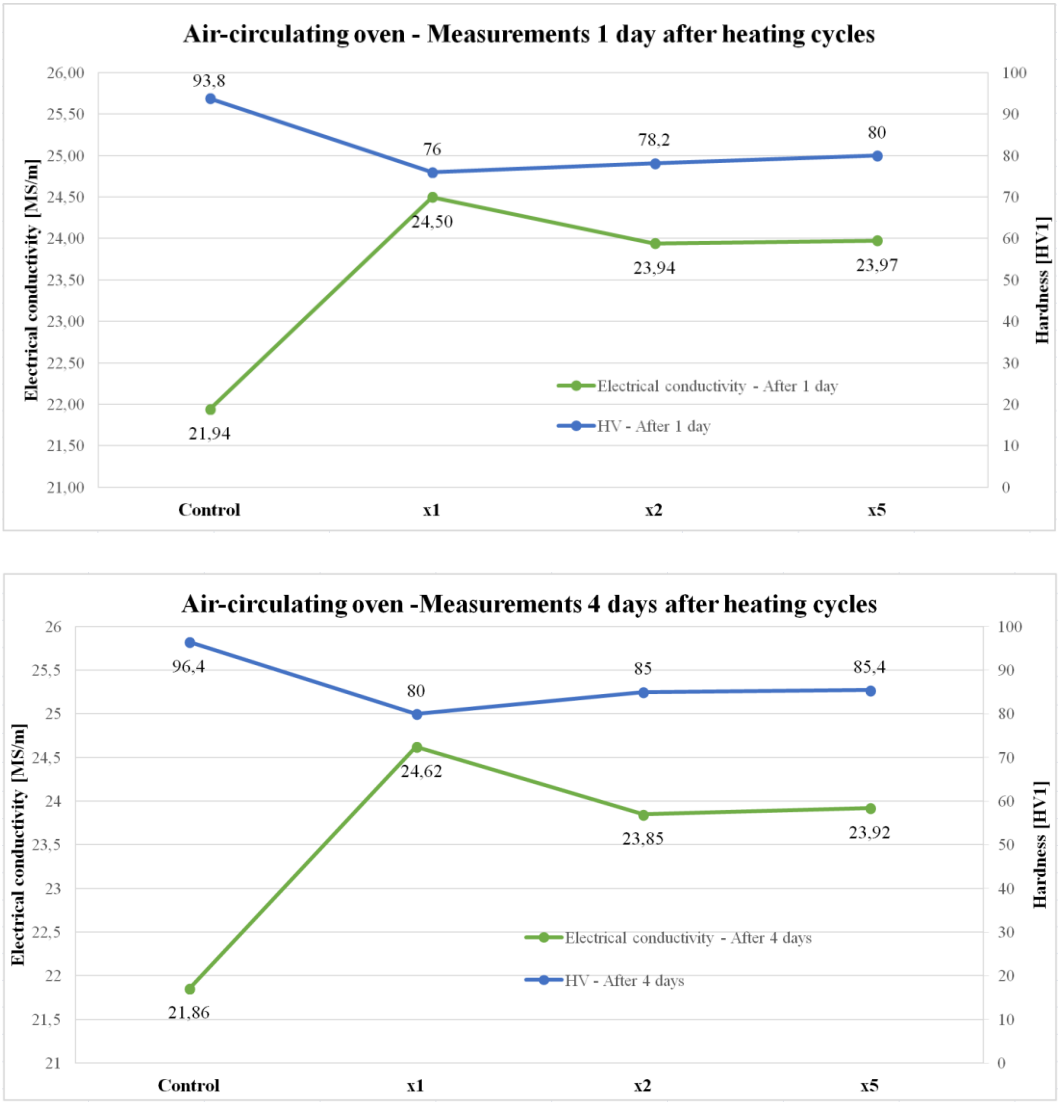

Figure 4.21: Experimental data from hardness and electrical measurements of alloy 4-H2 subjected to subsequent heat treatment (air-circulating oven).

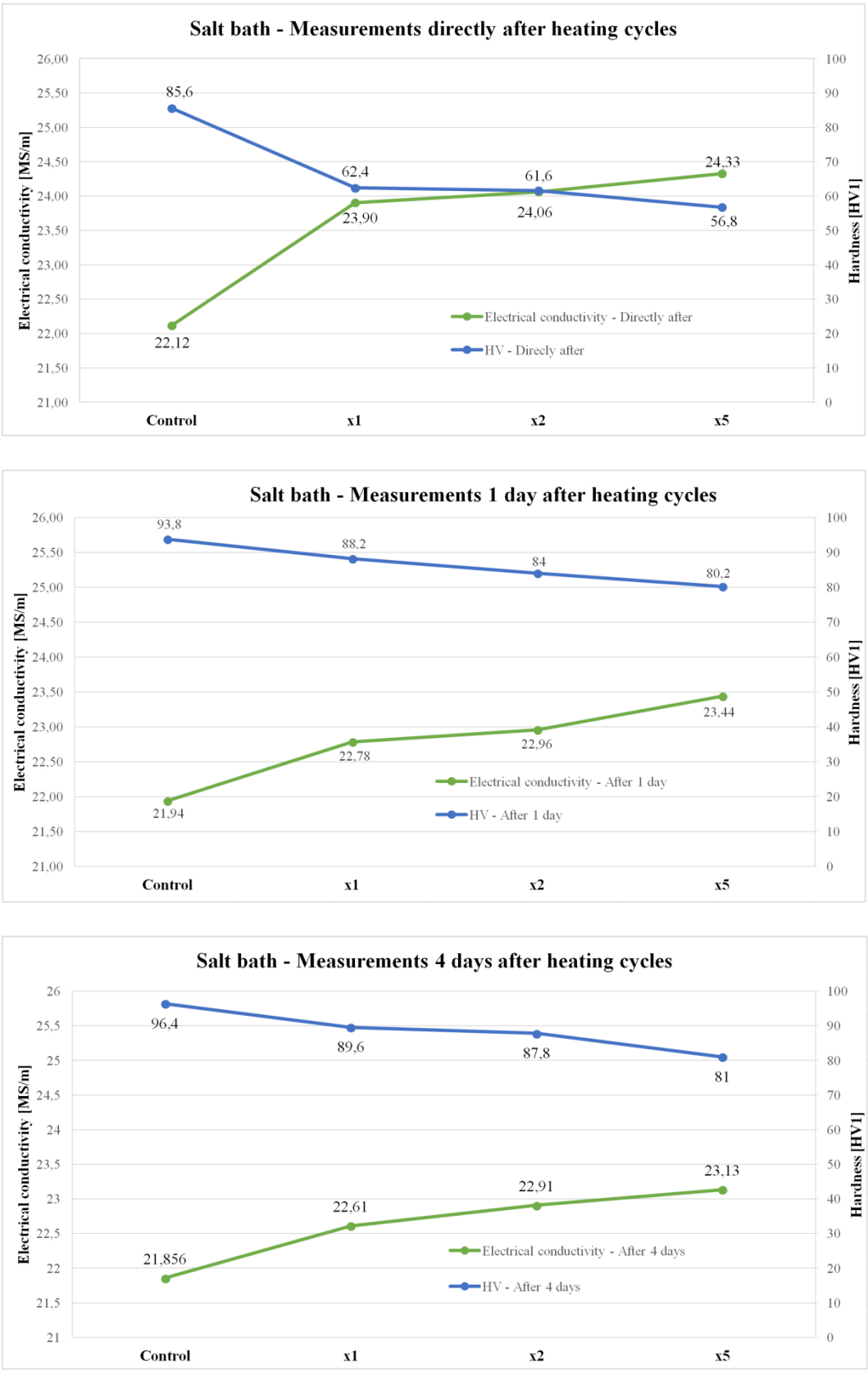

Figure 4.22: Experimental data from hardness and electrical measurements of alloy 4-H2 subjected to subsequent heat treatment (salt bath).

4.5.2 Measurements after number of days (naturally ageing)

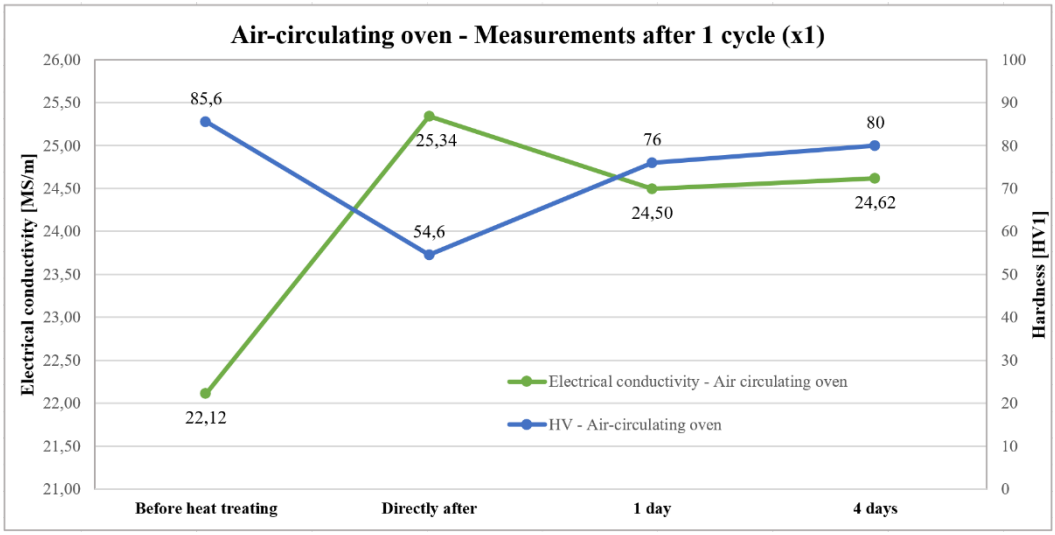

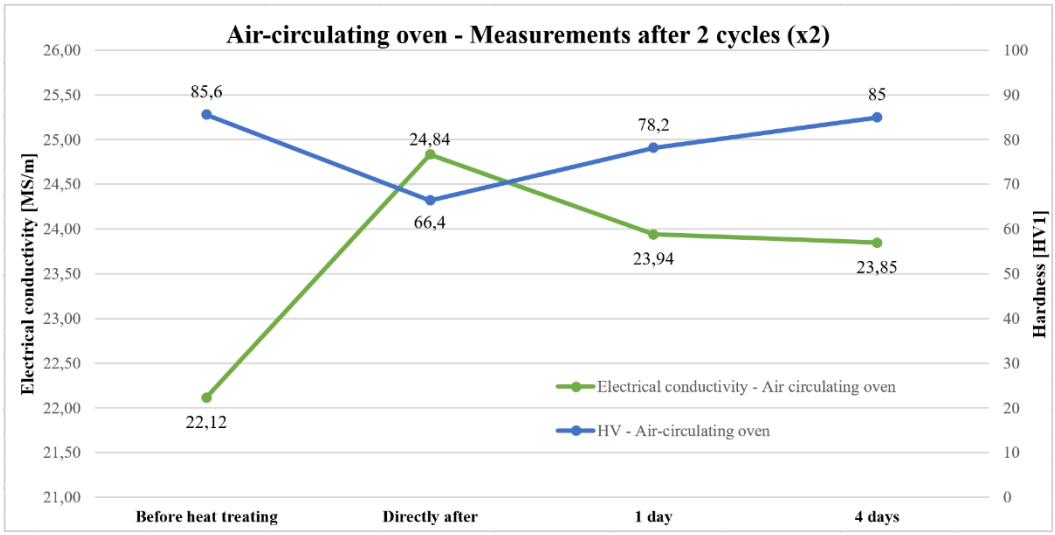

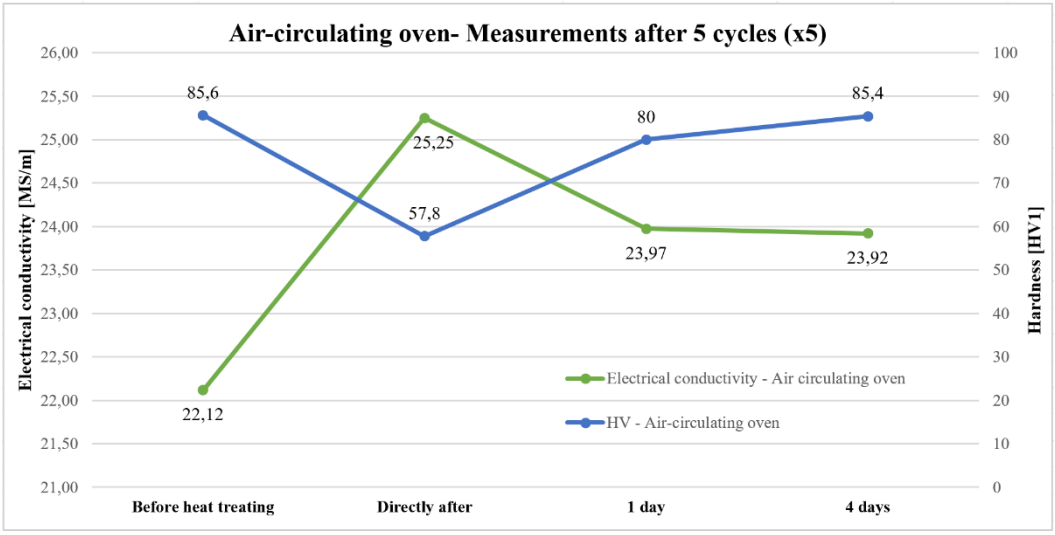

Figure 4.23: Experimental data from hardness and electrical measurements of alloy 4-H2 subjected to subsequent heat treatment (air-circulating oven – cycle x1, x2 and x5).

Figure 4.24: Experimental data from hardness and electrical measurements of alloy 4-H2 subjected to subsequent heat treatment (salt bath – cycle x1, x2 and x5).

4.6 Further investigation after x1 cycle of subsequent heat treatment

Alloy 4-H2 subjected to subsequent heating procedures for 1 cycle (x1) were further investigated considering dispersoid measurements of the sample shown in Figure 4.25. In addition, another hardness- and electrical conductivity- measurement after welding simulation in salt bath (400 °C, 5 seconds) were conducted. The results are presented in Figure 4.26 and Table 4.1.

There is not detected any severe increase in dispersoids compared to before the subsequent heat treatments. The hardness of both samples exposed to the salt bath welding simulation dropped drastically from the x1, subsequent heating stage. As can be seen, there is some hardness gain after a few days in room temperature. Sample x1, subsequent heat treatment in salt bath, weld simulated and cooled in room temperature are the sample that is closest to an industrial procedure.

4.6.1 Dispersoid measurement of alloy 4-H2 (x1, subsequent heat treatment)

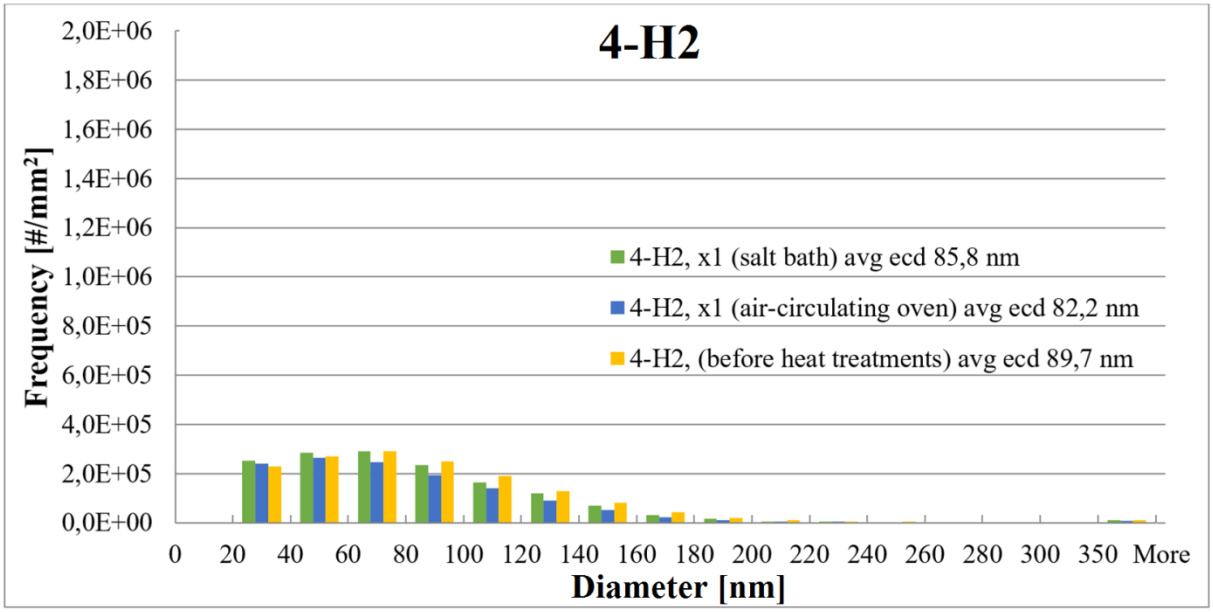

Figure 4.25: Experimental data from dispersoid measurements in SEM and iSolution DT for alloy 4-H2 exposed to both subsequent heat treatments for 1 cycle. Lower detection limit for the dispersoid measurements was set to 20 nm.

4.6.2 Salt bath ``welding simulation´´

Table 4.1:Hardness and electrical conductivity of alloy 4-H2 subjected to both subsequent heat treatment (air and salt bath) for 1 cycle and weld simulated in salt bath (400 °C for 5 seconds).

		Hardness [HV1]			Electrical conductivity [MS/m]		
		Directly after	After 1 day	After 4 days	Directly after	After 1 day	After 4 days
Quenched in water	Air-circulating oven	53,6	63,2	64,8	26,74	26,62	26,56
	Salt bath	61,8	69,4	68,6	25,99	25,60	25,55
Air cooled (RT)	Air-circulating oven	58,0	58,2	59,2	27,96	28,08	28,09
	Salt bath	62,2	63,0	63,4	27,23	27,53	27,56

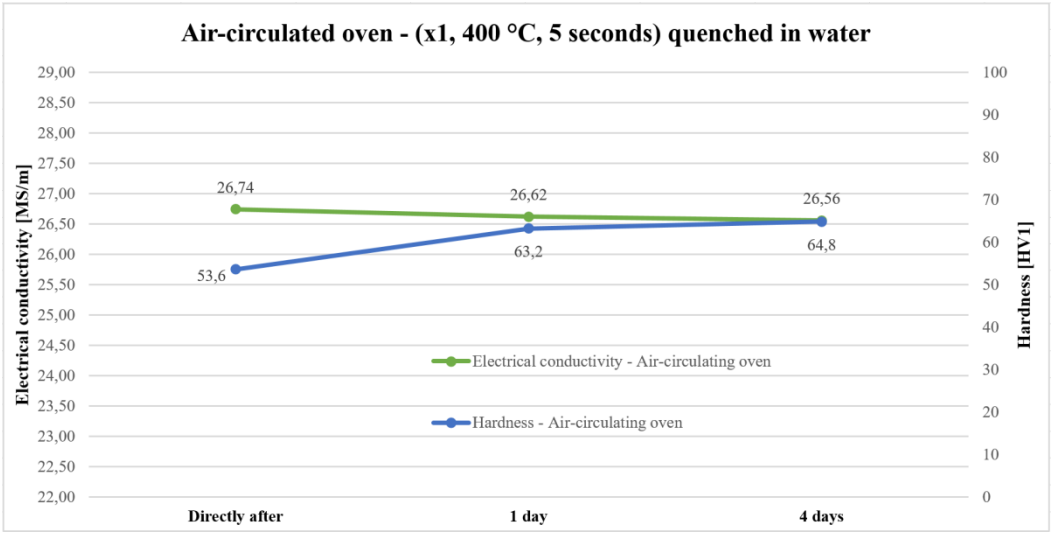

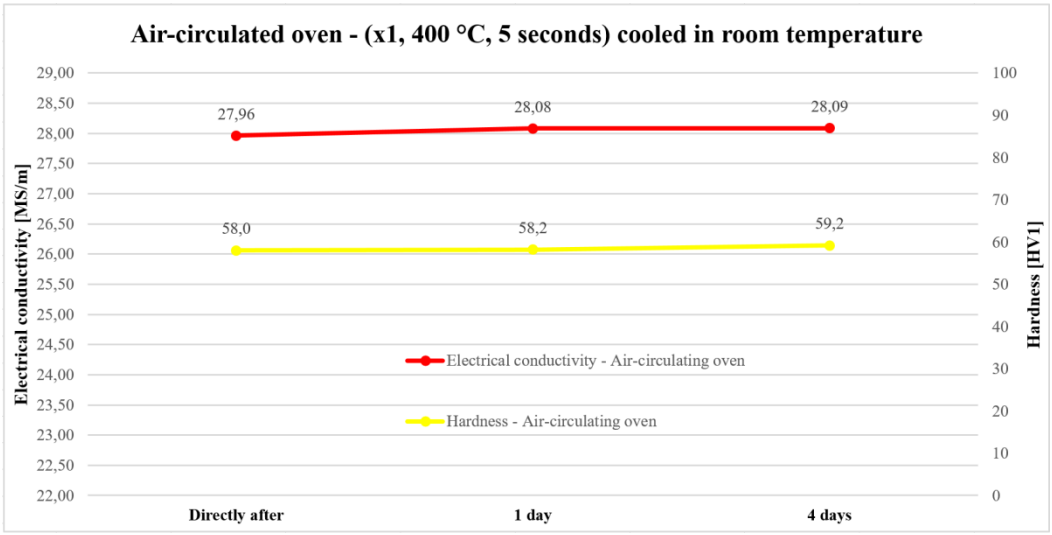

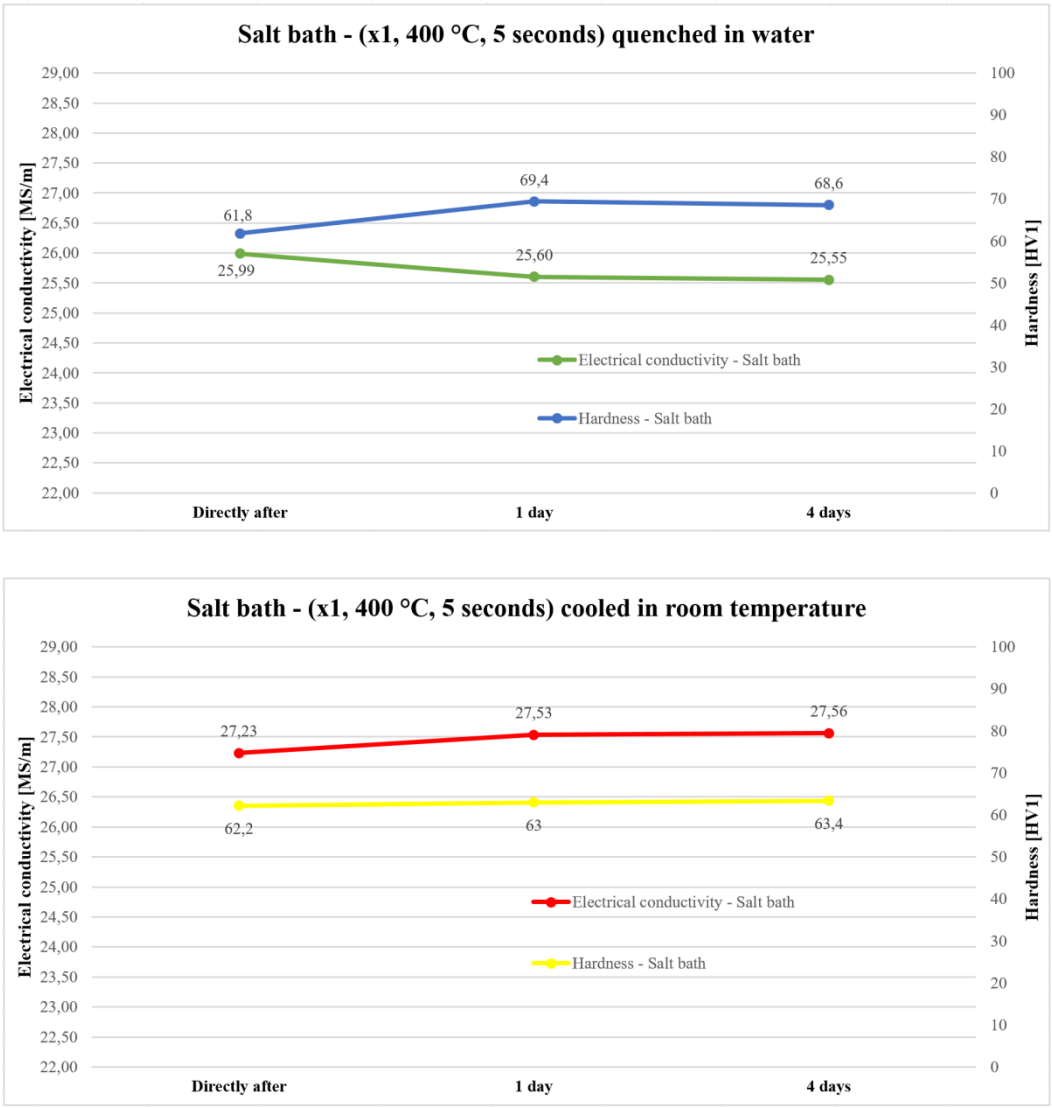

Figure 4.26: Experimental data from hardness and electrical measurements of alloy 4-H2 subjected to both subsequent heat treatment (air and salt bath) for 1 cycle and weld simulated in salt bath (400 °C for 5 seconds) and cooled in two different ways (air and water).

5 Discussion

In this section, the respective results from the various experimental procedures done in this master thesis are punctually analyzed, discussed and explained. This includes effect of homogenization procedure, variation in grain structure as-extruded and after welding, hardness measurements of welded aluminium alloys, measurements of size and density of dispersoids of extruded specimens, the effect of subsequent heat treatment of the extruded alloys with respect to dispersoid density and salt bath welding simulation.

5.1 Microstructure analysis after extrusion

The grain structure and the degree of recrystallization of alloys after extrusion are dependent on several factors including alloy composition, extrusion parameters and homogenization procedure. The microstructure images presented in Figure 4.1 clearly shows that the degree of recrystallization decreases with increasing amount of introduced Mn-, Cr- and Zr-dispersoids. According to the homogenization procedures, it is shown that the H3 variant leads to a more fibrous structure compared to the H1 and H2 variants.

For the samples that have recrystallized, it is seen that the recrystallized layer is concentrated at the surfaces of the extruded profiles. The core for all the samples has not recrystallized. As explained in Section 2.5, the temperature and the experienced force are greater at the surface of the extrusion due to higher friction between the extrusion die and the alloys. The core of the samples is essentially pure elongation compared to the surface of the billet undergoes extensive shear deformation. The higher strain rate creates better condition for recrystallization.

It is stated that the degree of recrystallization decreases with increasing amount of Mn, Cr and Zr. Alloy 5 with the most amount of dispersoids has more or less retarded recrystallization completely for all homogenization variants. The higher density of dispersoids introduced in the alloy, the more pinning points for the moving reaction front is created which retard recrystallization as explained in Section 2.6. Alloy 5 which have the most fibrous structure are the alloy with Zr. From Figure 2.4 it is shown that Zr has higher influence on preventing recrystallization (increase recrystallization temperature of the alloy) compared to Mn and Cr.

The homogenization procedure affects both the size and density of the dispersoids where low homogenization temperature and short holding time promotes higher density of small

dispersoids (Section 2.4). Both the H1 and H2 procedure where homogenized at a temperature of 580 °C while the H3 homogenization temperature was 540 °C. The images shows that the H3 variant has the least recrystallized structure compared to H1 and H2, which indicatesr that the low temperature H3 homogenization has formed a much higher density of small dispersoids and pinning points. It is also interesting to look at the extrusion data shown in Table 3.2. This shows that the breakthrough force (F_{max}) and the die force (F_{min}) is influenced by the nominal values of dispersoids in the alloys. The more dispersoids in the alloy, the more force is needed to press the billet. The effect of homogenization procedure is also interesting represented by a dramatic difference in dispersoid density and diameter for the different homogenization procedure where the H3 procedure has a higher density of small dispersoids. The higher the press force, the more dislocations are generated which increases the stored energy for recrystallization in the material, i.e. increased P_D in Equation 2. At the same time, dispersoids oppose recrystallization through the Zener drag pressure P_Z.[24]

Recrystallization of aluminium alloys are dependent on the balance between the driving pressures for recrystallization resulting from the stored energy generated during thermomechanical processing, and the retarding pressure from obstacles hindering nucleation and growth of new stain-free grains. The variations in the retarding pressure are the main reason for the differences in grain structures, and are caused by the alloying elements in solid solution and dispersoids. The low homogenization procedure is seen to prevent recrystallization effectively.[24]

5.2 Hardness measurements of welded specimens

The hardness in the center of the welding profiles belongs to a different alloy (welding wire AA5183) than the AA6082 alloys. The high temperature has melted the welding wire and the 6082 together and the two types of alloys are expected to be mixed together near the weld line.

In the zone furthest away from the weld line, about 2-2,5 cm from the weld center, the hardness of the alloys after artificial ageing is determined. The heat from the welding procedure has not reached high enough temperature to affect the phases in the alloys at this distance from the weld line. Closer to the weld line in the area denoted the heat affected zone (HAZ), it can be seen that the hardness decreases towards the weld line, indicating that the hardening β’’- precipitates has not withstand the welding temperatures. A slight increase in

hardness between the HAZ and the weld metal center occurs due to fractions of alloying elements in solid solution from the high temperature and cooling rates enabling extensive ageing at room temperature (Section 2.9.4).[45]

Aluminium alloys achieves the highest potential hardness in artificial aged state when aged to T6. The strengthening phases changes when exposed to high enough temperatures and the hardness drops in the HAZ. Dispersoids have usually higher thermal stability than the Mg/Si-phases and contribute to strengthening of alloys. By comparing the mean hardness values of the alloys with respect to the homogenization variants separately, the effect of amount of dispersoids on the artificial aged state as well as the HAZ is determined.

5.2.1 Effect of Mn, Cr and Zr on hardness of welded samples

Table 5.1: Mean hardness values of the unaffected zone and the lowest measured hardness in the HAZ for the different alloy variants (1-5) and the different homogenization procedures (H1, H2 and H3).

Alloy variant	Mean hardness value in unaffected zone [HV1]			Lowest measured hardness in HAZ [HV1]		
	H1	**H2**	**H3**	**H1**	**H2**	**H3**
Alloy 1	99	106	100	56	63	62
Alloy 2	106	110	111	63	67	68
Alloy 3	105	106	107	65	64	67
Alloy 4	110	110	110	65	67	67
Alloy 5	109	109	110	67	65	65

The effect of dispersoids on the hardness of the welded samples for the different homogenization procedures varies as seen from Figure 4.7 - Figure 4.9. Table 5.1 above presents the mean hardness value of the unaffected zone (average of the 10 measurements on each side) and the lowest measured hardness in the HAZ for the different alloys and homogenization extracted from hardenss profiles (Figure 4.2 - Figure 4.6).

For the all the homogenization procedures, the hardness for both the HAZ and the unaffected zone is poorest for alloy 1 (low Si). As can be seen, the alloy 3 (0,6 wt.% Mn + 0,25 wt.% Cr) has lower hardness than alloy 2, 4 and 5.

Precipitation hardening considerably influences the strength of aluminium. After artificial ageing to T6, the β'' (Mg_5Si_6) is the hardest phase that contributes most to strengthen the alloys and thus, the ratio between Mg and Si is essential in formation of these particles. From Equation 6, it is evident that the combined effect of contribution from particles and dispersoids are highly dependent on the contribution from the hardening β''-particles (Mg_5Si_6). To increase the σ_p in the overall macroscopic yield strength σ_y in Equation 3, a dramatic amount of dispersoids are needed for the age-hardened alloys.

As mentioned in Section 2.8.4, the initial Si concentration is affected by Fe-, Mn- and Cr-phases due to consumption of the Si. Less Si in solid solution before artificial ageing, reduces the β''-potential of the alloys which results in a drop in measured hardness in the artificial ageing state with increasing amount of dispersoids. Alloy 1, which has the lowest Si concentration, has the lowest measured hardness for all three homogenization procedures. For the remaining alloys, the Si and Mn concentration are about the same, but is somewhat less for alloy 5.

By looking at the H3 procedures, the hardness is lowest for alloy 3 (apart from alloy 1 with less Si). It seems as this alloy (with most Cr, 0,25 wt%) has the poorest β''-potential and thus formed less hardening β'' (Mg_5Si_6).

The typical hardness in the HAZ for this type of alloys is approximately 65 HV. In order to convert the hardness to yield strength (in MPa), a simple regression formula is used for the various alloys in the HAZ.[47] From this, it is seen that an increase in hardness of 1 HV is equivalent to approximately 3 MPa in yield stress.

$$\boldsymbol{HV = 0,33\sigma_p + 16 \rightarrow \sigma_p = \frac{HV-16}{0,33}} \quad \textbf{(8)}$$

Table 5.2: Hardness values of the lowest point in the HAZ converted to yield stress.

Alloy variant	Lowest measured hardness in the HAZ [HV1]			Converted to yield stress (σ_p) [MPa]		
	H1	H2	H3	H1	H2	H3
Alloy 1	56	63	62	**121**	**142**	**139**
Alloy 2	63	67	68	**142**	**155**	**158**
Alloy 3	65	64	67	**148**	**145**	**155**
Alloy 4	65	67	67	**148**	**155**	**155**
Alloy 5	67	65	65	**155**	**148**	**148**

5.2.2 Effect of homogenization procedure on hardness of welded samples

From the hardness curves presented in Figure 4.2 - Figure 4.9, it is determined that the hardness in the unaffected zone increases with increasing amount of Mn, Cr and Zr. Alloy 1 has the lowest mean hardness with a HV = 99, alloy 2 and 3 have equal hardness with HV = 105 and alloy 4 and 5 are equal with HV = 110. The same trend is determined by looking at the lowest measured hardness in the HAZ.

The hardness trend in the zones is different for the H2 procedure compared to the H1 procedure. Here, alloy 1 and 3 shows the lowest hardness in both the unaffected zone with HV = 106, while alloy 2, 4 and 5 are approximately the same with HV = 110. The same trend is seen for the lowest hardness in the HAZ.

For the H3 procedure, the alloy 1 is by far the weakest alloy in the unaffected zone with HV = 100. Alloy 3 is the second weakest with HV = 107 and alloy 2, 4 and 5 are the hardest with approximately HV = 110. In the HAZ, alloy 1 is the weakest with HV = 62 and the rest of the alloy are approximately the same with HV measurements between 65-68 HV.

As seen from the hardness curves the hardness drops from unaffected zone and towards the weld center. The initial β’’-precipitation structure from the artificial ageing of the aluminium alloys changes due to the temperature exposure from the welding. The typical hardness measurements across the weld appears for all alloys and the alloys that showed best properties in the unaffected zone shows the best properties in the HAZ.

Section 2.9.4 covers the precipitation change from the welding exposure. The fine needle shaped β’’-particles that forms uniformly in the aluminium matrix during the artificial ageing is the dominating hardening phase.

Between the weld metal and the lowest hardness point (± 5 -10 mm) the hardness increases. Here, the alloy has been partially melted and the temperature has been high enough and the cooling fast enough to get some of the reverted structure to reform β’’-particles due to natural ageing for a period of days.

In the point (± 10 mm), it can be seen from the hardness profiles that this has experienced the highest drop in hardness. In this area the small needle shaped β’’-precipitates has dissolved which give poorer strength contribution.

In the area between ± 10 – 25 mm (HAZ) the hardness in the specimen is at its lowest and is increasing towards the unaffected zone. Here, the material have over-aged, i.e. he β''-particles has transferred to β'-particles which are coarse and rod-shaped. In addition, the particles disperses with increasing space between them. At ± 11 mm, the temperature has been higher than at ± 24 mm and the hardness profiles shows that the hardness increases from ± 11 – 24 mm. The closer to the fusion line, the higher is the experienced temperature and the more over-ageing has occurred in the alloy. At ± 24 mm, there has been very little over-ageing compared to point ± 11.

By comparing the hardness curves, it can be seen from the H3 curves, which has prompted the highest density and smallest dispersoids, that the hardness in the HAZ is slightly higher with decreasing amount of dispersoids. Alloy 2 with only Mn has a slightly higher measured hardness in the HAZ when comparing with the alloys that have additions of Cr and Zr. The higher the amount of dispersoids in the alloys, the less β''-particles were originally formed during artificial ageing. In the HAZ, the β''-particles overaged due to the welding. The original hardness of the alloys reduces and there is more coarse β-particles with decreasing amount of dispersoids.

For the H2 curves, alloy 2 (only Mn) and alloy 4 (Mn + 0,15 Cr) shows approximately the same properties. The small Cr addition has not a noticeable effect on the precipitate structure based on hardness measurements. However, the microstructure images of the extruded and the welded samples shows a larger recrystallized area for the alloy 2 indicating that the alloy 4 has formed higher density of dispersoids. With increasing content of Cr (Alloy 3) the hardness drops due to less initial β''-precipitates in the alloy.

The curves from the H1 procedure shows different trend in hardness compared to the other two regarding lowest hardness in the HAZ. The hardness measurements shows increased hardness with increasing amount of dispersoids while for the H2 and H3 procedure shows increased hardness with decreasing amount of dispersoids. The additional heat sequence in the H1 homogenization procedure has given the alloy other properties. The main dispersoids have probably formed during H1-part 1 (rapidly heating to 580 °C and quenched), and H1-part 2 have reprecipitated additional β''-precipitates which maintains in the alloy and/or acted as nucleation sites for more dispersoid formation. Overall, the curves shows none dramatically effect on the hardness of the alloys. The different homogenization procedures has not given substantial impact regarding dispersoid density and not developed increased strength with dispersoids.

In general, the more dispersoids generated in the alloys, the less hardening β''-precipitates is generated which reduces the strength of the alloy in the unaffected zone. A dramatic amount of dispersoids is needed to increase the σ_p explained in Section 2.8.3. The heat from the welding has changed the fine needle shaped β''-precipitates which has coarsened and contribute less to the strengthening of the alloy.

5.3 Microstructure of welded specimens

The welded samples were analyzed in a microscope to see if the temperatures reached in the welding procedure had an effect on the microstructure in the HAZ. All samples in Figure 4.10 - Figure 4.14 showed more or less the same microstructure in the welding zones by comparison to the microstructure as-extruded. This is easier to see from Figure 5.1 below where some of the images are zoomed in.

For the microstructure as-extruded, it was seen that the recrystallization decreased with increasing amount of dispersoids. Homogenization procedure H3 have better microstructure properties than H2 and H1 give poorest resistance to recrystallization. Smaller difference between H2- and H3-procedure is observed for the alloys containing Cr and Zr (alloy 3, 4 and 5).

For all of the pictures, also the most recrystallized, a sharp transition from the alloy used for welding wire and the AA6082 alloys are observed. The sharp transition is a clear indication of that the heat from the welding has not affected the microstructure and none recrystallization are observed in the HAZ. This indicates that the dispersoids has resisted recrystallization of the samples also after the thermal exposure from the welding and the fibrous structure is maintained for the alloys, even near the weld center where the temperature has reached very high temperatures and melting of the welding wire and the samples.

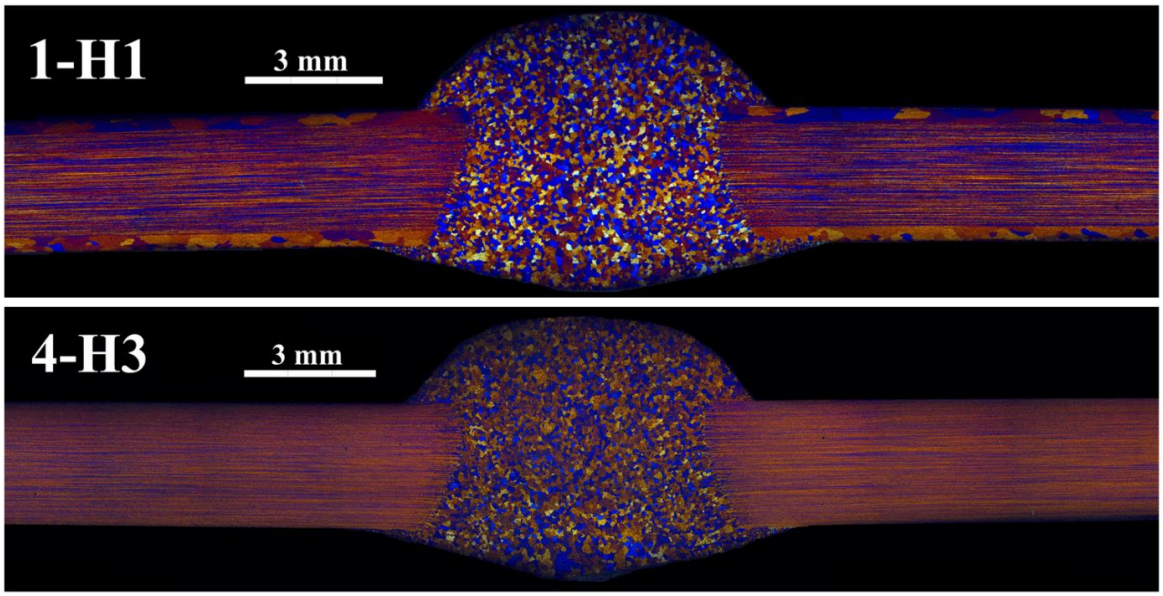

Figure 5.1: Zoomed in images of the microstructure of welded samples. In this case the 1-H1 with large recrystallization and 4-H3 with unrecrystallized structure.

5.4 Dispersoid measurements of extruded alloys

The results in Section 4.4 shows that the dispersoid density increases with increasing amount of Mn, Cr and Zr and with decreasing homogenization temperature. The presence of preferably Mn and Cr may increase the formation of dispersoids as mentioned in Section 2.4. Regardless of homogenization procedure, the alloy 5 with highest levels of dispersoids displayed the highest density of small dispersoids and the alloy 2 with only Mn showed the lowest density of the smallest dispersoids (20-40 nm). It is not found significant difference of dispersoid distribution by comparing homogenization procedure H1 and H2. The 2-H1 and 2-H2 displays much the same distribution and the average ECD are quite similar and has been measured to 92,9 and 91,5 mm respectively. The same is the case for alloy 4 and 5. For all alloys, the H3 procedure displays significant higher distribution of small dispersoid compared to H1 and H2. The average ECD for alloy 2-H3 are 56,8 mm. The average ECD for all samples are shown in Table 5.3.

Table 5.3: Average ECD of alloy 2, 4 and 5 (H1, H2 and H3)

Alloy	Average ECD [nm]		
	H1	H2	H3
2	92,9	91,5	56,8
4	86,3	89,7	49,6
5	74,4	72,8	46,3

The dispersoids containing Mn and/or Cr forms during heating temperatures from 400-580 °C. Small dispersoids are encouraged by low homogenization and short holding time. The H3 homogenization procedure are performed with a lower temperature (540 °C) than the H1 and H2 procedure (580 °C). The H1 procedure had an additional step, which did not make any big difference in dispersoid distribution compared to H2 procedure. This is also seen from the images taken of the grain structure of the alloys after extrusion (Figure 4.1).

By looking at the total count of dispersoids (regardless of size of dispersoids between 20 – 100 nm shown in Figure 5.2, the H1 and H2 procedure share more or less the same pattern. The H3 procedure shows increased density of dispersoids. By looking at the distribution of the smallest dispersoids (range 20 – 40 nm, ECD) shown in Figure 5.3, the same pattern is shown for the variants as for the total dispersoid distribution.

The increase in density for alloy 5 is due to the higher density of dispersoid forming elements.

It is evident that the difference between frequency regarding the smallest particles between H3 procedure compared to H1 and H2 increases due to the lower homogenization temperature. Also the more Mn, Cr and Zr introduced in the alloy, the more dispersoids are formed.

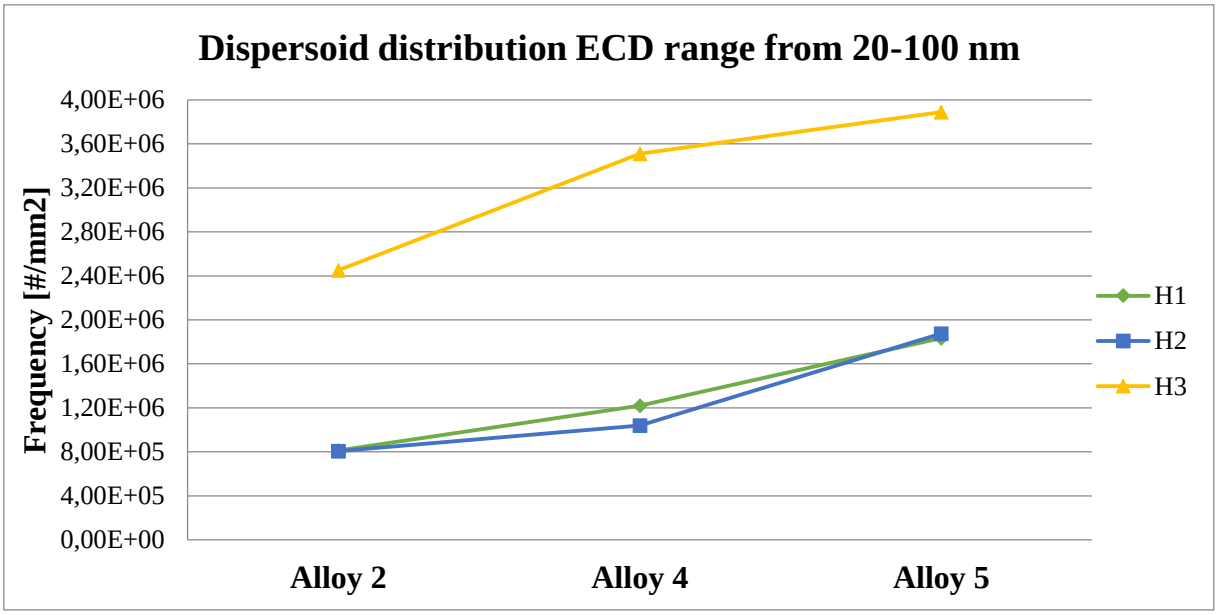

Figure 5.2: Number of dispersoids ranging from 20 – 100 nm.

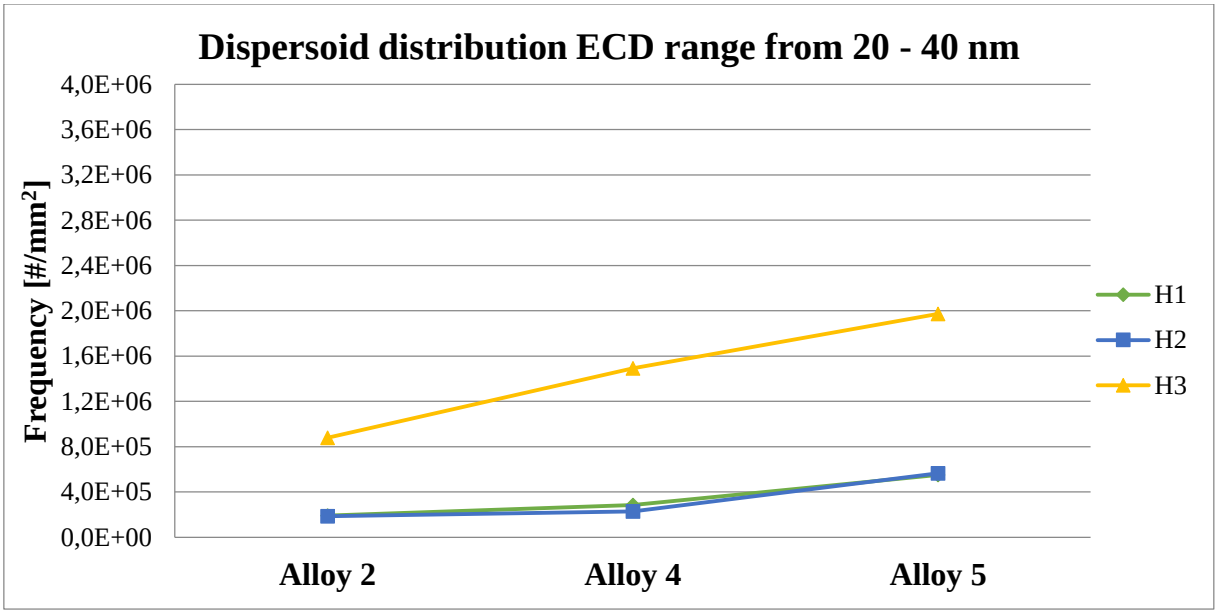

Figure 5.3: Number of dispersoids ranging from 20 – 40 nm.

5.5 Subsequent heat treatment

The thermal cycles for the alloys subjected to subsequent heat treatments as well as salt bath welding simulation are presented in Figure 5.4. Also, the hardness and electrical conductivity measurements from the results in Figure 4.21 - Figure 4.24 are presented in Table 5.4 and Table 5.5.

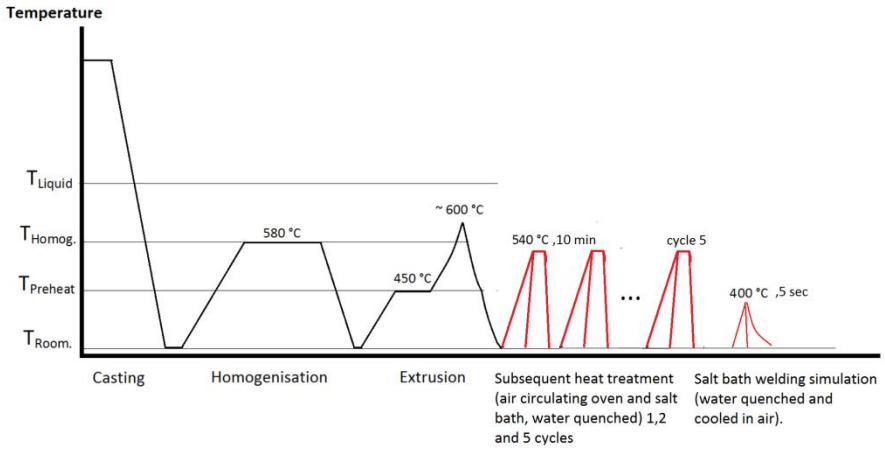

Figure 5.4: Reminder of the thermal heating history of the samples subjected to subsequent heating and salt bath welding simulation.

Table 5.4: Hardness and electrical conductivity of alloy 4-H2 heat treated in air-circulating oven.

Air-circulating oven						
	Hardness [HV1]			Electrical conductivity [MS/m]		
	Directly after	After 1 day	After 4 days	Directly after	After 1 day	After 4 days
Control	85,6	93,8	96,4	22,12	21,94	21,86
x1	54,6	76,0	80,0	25,34	24,5	24,62
x2	66,4	78,2	85,0	24,84	23,94	23,85
x5	57,8	80,0	85,4	25,25	23,97	23,92

Table 5.5: Hardness and electrical conductivity of alloy 4-H2 heat treated in salt bath.

Salt bath						
	Hardness [HV1]			Electrical conductivity [MS/m]		
	Directly after	After 1 day	After 4 days	Directly after	After 1 day	After 4 days
Control	85,6	93,8	96,4	22,12	21,94	21,86
x1	62,4	88,2	89,6	23,90	22,78	22,61
x2	61,6	84,0	87,8	24,06	22,96	22,91
x5	56,8	80,2	81,0	24,33	23,44	23,13

The effect of the subsequent heat treatment is based on measurements of electrical conductivity and hardness. Also, both variants (air-circulating oven and salt bath) heat treated for x1 cycle is further investigated by dispersoid density and size distribution after exposure to 400 °C in salt bath for 5 seconds to simulate the most destructive temperatures experienced in welding. The hardness and electrical conductivity are also measured for these samples.

5.5.1 Air-circulating oven

The results in Figure 4.21 and Figure 4.23 showed that the electrical conductivity measured directly after the respective cycle for the air-circulating oven treatment procedure decreased from 1 cycle to 2 cycles and where increased again when subjected to 5 cycles. The measurements taken 1 and 4 days after the cycles are similar where a decrease in conductivity is observed from 1 – 2 cycles. The conductivity has a slight decrease from measurements taken from 1 – 4 days. As can be seen, the hardness is linked to the conductivity and increases when the conductivity decreases.

5.5.2 Salt bath

The electrical conductivity from salt bath treatment is different from the air-circulating oven where the conductivity increases with number of cycles and decreases with natural ageing (1 – 4 days) as seen from Figure 4.22 and Figure 4.24.

Electrical conductivity is the reciprocal of resistivity and is one of the most sensitive properties of aluminium. The electrical conductivity is particular responsive to variations in composition and is reduced by all known metallic additions. Metallic compounds out of solution depresses the conductivity to a lesser extent compared to in solid solution. Mn is an example of the importance of the condition in which added element appears in aluminium. As the amount of manganese in solid solution increases, the resulting rapid increase in resistivity (decrease in conductivity) is in noticeably contrast to the much slower increase in resistivity as manganese concentration exceeds its solid solubility limit. The effect of two or more addition of elements on the conductivity depends on the relationship between the elements. In general, the effect on the conductivity are additive if the elements is in solid solution individually. If a compound are formed, the solid solubility of one or both elements may be reduced, or the compound may have an internal solubility. Quenching of an alloy after solution heat treatment generally results in the lowest electrical conductivity. This is due to a larger part of the components are retained in solid solution. For alloys that age in room temperature, a subsequent decrease in conductivity may occur during the initial stages of ageing.[48]

Electrical conductivity decreases with increasing density of dispersoids. From the graphs and the electrical conductivity measurements, the salt bath procedure produces higher density of dispersoids compared to the air-circulating procedure. The higher amount of dispersoids and other elements, the lower measure of electrical conductivity. It is also noted that the conductivity for salt bath procedure increases with increasing cycles. This indicates that the majority of the metallic compounds are in solid solution after 1 cycle and that the metallic compounds may have diffused into the matrix.

In Figure 5.6 below the hardness for the subsequent measurements are plotted in the same graph to compare the number of cycles for the two subsequent heating procedures (air oven and salt bath).

For the air-circulating oven cycles, the hardness increases with number of cycles. This indicates that dispersoids have developed in the alloys as explained in Section 2.7.1. During continuous heating, the β'-precipitates nucleate with subsequent growth, coarsening and partial dissolution with increasing temperatures from 100 – 350 °C. By further increase of the temperature, the β'precipitates dissolve completely as the 'u-phase' develops and act as a nucleation site for the dispersoids which will consume the 'u-phase' completely. The final result is a breaking up of the original β' into chains of dispersoids.[15] Based on the hardness and the electrical conductivity measurements, it seems that the attempt to performing the process repeatedly succeeded in forming new nucleation sites for the dispersoids to increase the density of dispersoids.

For the salt bath samples, the hardness behaves different with number of cycles compared to the air-circulating oven samples, which was heated slowly to 540 °C. From the bottom graph in Figure 5.6, it is seen that the hardness for the salt bath samples decreases with number of cycles. In this heating sequence the samples was rapidly heated to 540 °C, hold for 10 minutes and quenched. It appears as the rapid heating fails to develop the phases that act as nucleation sites for the dispersoids and thus fails to increase the dispersoid density. This could be the case if the hardness measurements were stable and not decrease with number of cycles. The several cycles should not decrease the number of dispersoids and thus decrease the hardness. One possibility is that the initial dispersoids coarsens by rapid heating to 540 °C where the smallest dispersoids dissolve and precipitates on larger dispersoids. The increased interparticle spacing and larger dispersoids leads to poorer hardness.

Dispersoid measurements were performed for both air-circulating oven and salt bath after x1 cycle (see Section 5.5.3 below). From these results, it does not seem to occur any dispersoid development after x1 cycle for either of the subsequent heating treatments. It would have been interesting to measure the dispersoids for the samples exposed to more than x1 cycle but due to lack of time, this was not done. However, the decrease in hardness for the salt bath treatment may not be explained by dispersoids. By looking at the electrical conductivity of the samples in Figure 4.23 and Figure 4.24, the salt bath samples shows lower conductivity than the air-circulating samples. This may indicate that the salt bath samples have more Mg and Si elements in solid solution. The rapid heating to 540 °C may have retained the elements in solid solution (based on lower conductivity measurements) and not formed dispersoids. This is sketched in Figure 5.5. It should be pointed out that this is a sketch where the precipitate curve for the dispersoids are roughly drawn to illustrate the explanation.[49] It can be assumed that the rapid heating prevent formation of β' and/or u-phase which act as the nucleation site for dispersoids. The slow heating succeed to form these phases.

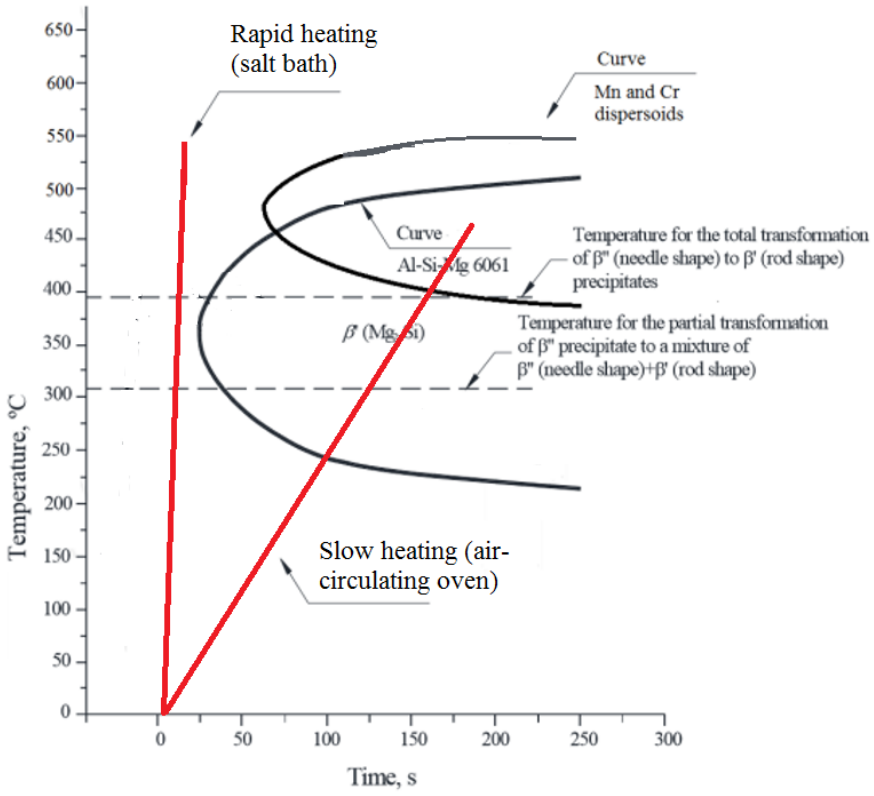

Figure 5.5: TTT-diagram of β'(Mg_2Si)[33] and roughly sketched curve for dispersoids[49]

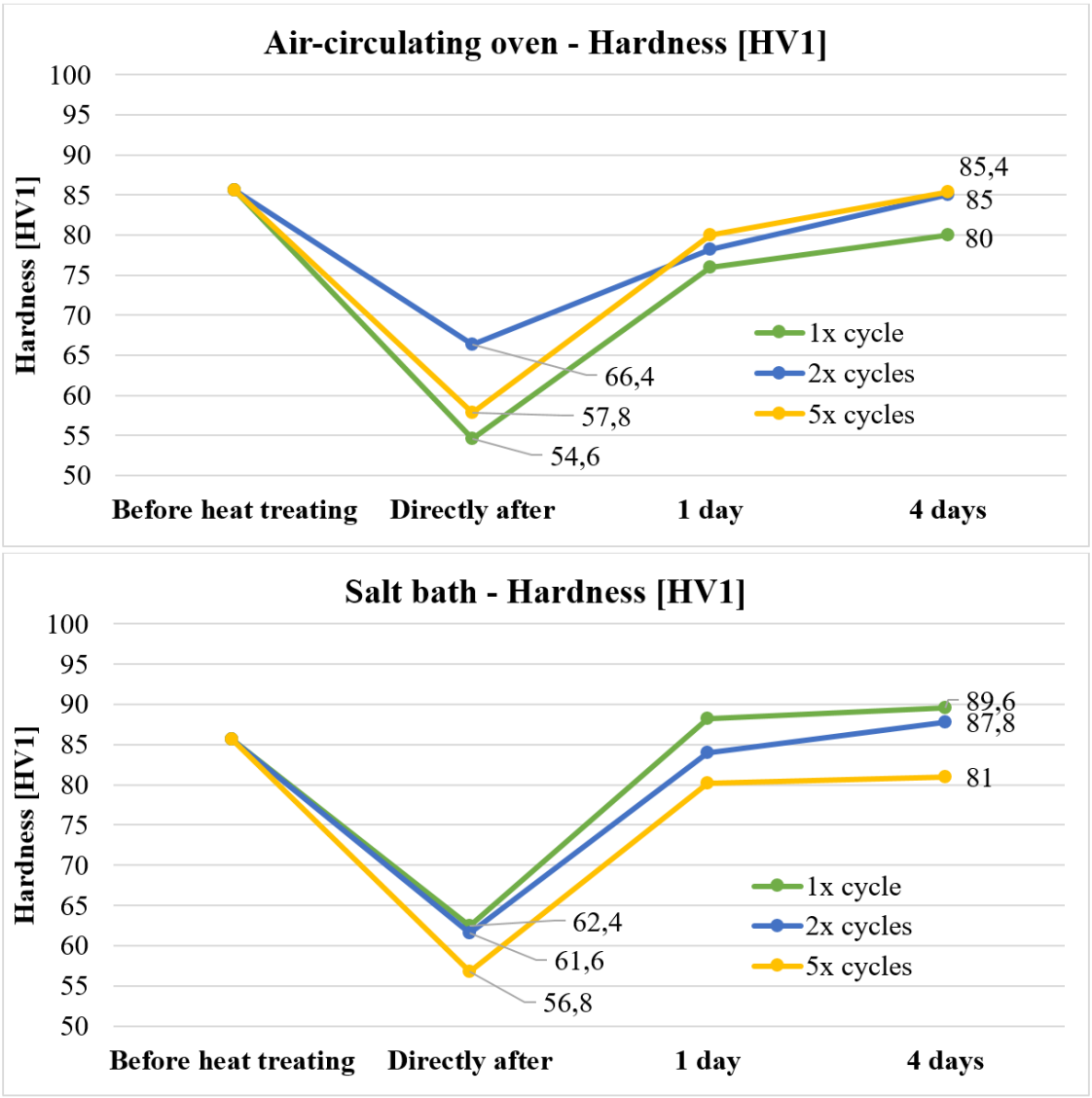

Figure 5.6: Hardness of both subsequent heat treatment variants and cycles.

From the hardness and conductivity results, the salt bath procedure gave a hardness of approximately 90 HV after x1 cycle. By exposing the alloy to more cycles, it seems that the dispersoids coarsens instead of forming more small dispersoids. For the air-circulating subsequent heat treatment, the hardness increases from x1 to x2 cycles. The salt bath procedure has an easier approach in the industry, which was the basis for choosing samples to be measured related to dispersoids.

5.5.3 Dispersoid measurement of alloy 4-H2 (x1, subsequent heat treatment)

The results of the dispersoid measurements taken for the alloys subjected to subsequent heating procedures for 1 cycle (x1, air-circulaating oven and salt bath) has not shown a significant increase regarding dispersoid frequency. The x1 salt bath treatment have a very small increase for the dispersoid sizes up to 80 nm, but the original sample (as-extruded) have a higher frequency of dispersoids from 100 nm. The subsequent heating procedures have not showed a significant increase of dispersoid density.

From the measurements of hardness and electrical conductivity, there seemed to have been developed some levels of dispersoids after x1 cycle for the salt bath version. However, this is not shown from the dispersoid measurements. The Mg and Si phases in solid solution may be the reason for the increase in hardness and low conductivity measurements.

5.5.4 Salt bath welding simulation

After the x1, subsequent heat treatment samples have been exposed to 400 °C for 5 seconds in salt bath (welding simulation), the hardness decreased and the electrical conductivity increased. This is easier to see from the Figure 5.7 below where the results are compared to the measurements before welding simulation (dashed lines).

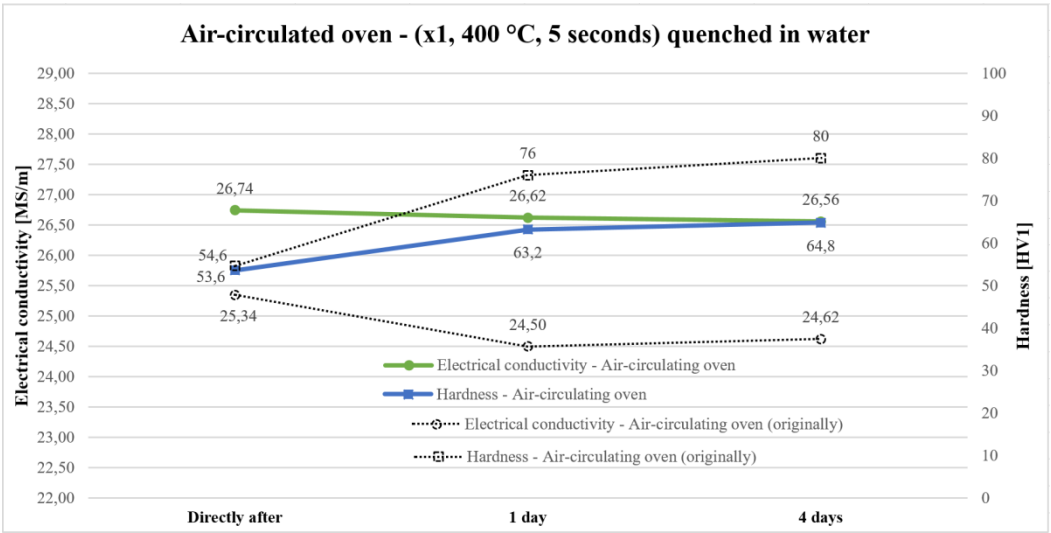

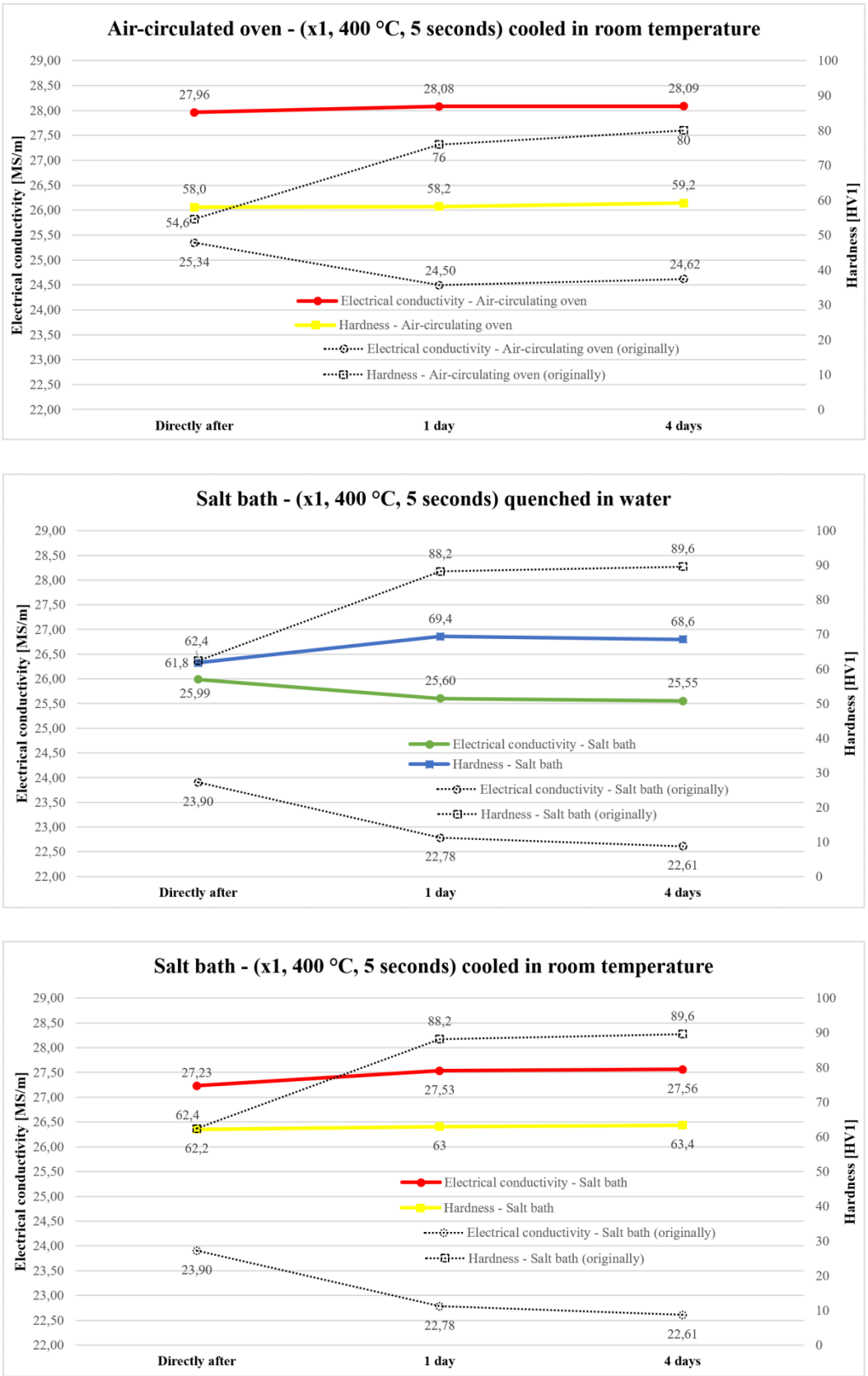

Figure 5.7: Experimental data from hardness and electrical measurements of alloy 4-H2 subjected to both subsequent heat treatment (air and salt bath) for 1 cycle and weld simulated in salt bath (400 °C for 5 seconds) and cooled in two different ways (air and water). Additionally compared to this alloy variant not subjected to salt bath "welding simulation" (dashed lines).

After the subsequent heating procedure, the alloys were hold in room temperature for about a week and there has been naturally ageing. The alloys are considered a T4-alloy (solution treated and natural aged), and the structure before the welding simulation in salt bath consists of many small Mg/Si-clusters. The variant closest to an industrial welding situation in this experiment are the subsequent salt bath variant, weld simulated and cooled in room temperature (the last figure). As can be seen, the hardness has dropped dramatically from before welding (from 89,6 – 63,4 HV). Simultaneously the conductivity increased.

It is evident from the hardness measurements that the alloy have not withstand the thermal cycle of the welding. In Table 5.6 the measured hardness are presented as well as the converted yield stress of the hardness by Equation 8. As can be seen, the measured hardness is approximately the standard hardness in the HAZ of this alloy.

Table 5.6: Hardness of the samples after 1x cycle of subsequent heating and salt bath welding simulation (400 °C, 5 seconds) and converted to yield stress.

Alloy variant	**Measured hardness [HV1]**		**Yield stress σ_y (converted) [MPa]**	
	Air cooled	Water quenched	Air cooled	Water quenched
Air-circulating oven	59,2	64,8	131	148
Salt bath	63,4	68,6	144	160

Figure 5.8 shows an overview of the matrix of alloy AA6056 in T4 (a) and T6 (b) condition. The TEM images shows for the AA6056-T4 coarse precipitates in contrast. For the T6 condition the same coarse particles were found but over a background fully covered with needle type precipitates presenting different orientations along the $[233]_{Al}$ zone axis.[50]

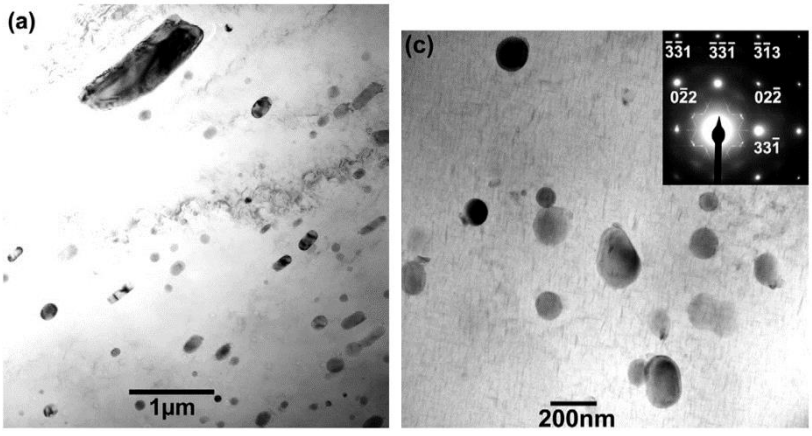

Figure 5.8: TEM images showing (a) coarse round shaped precipitates in AA6056-T4 and (c) coarse round shaped precipitates in AA6056-T6 with high population of needle type β''-precipitates.[50]

It is assumed that the welding of a T6-alloy possible could achieve a higher hardness indicated in Figure 5.9 below. During the welding simulation in salt bath, the small Mg/Si-clusters are believed to transform to coarse β'-precipitates, which affects the conductivity measurements.

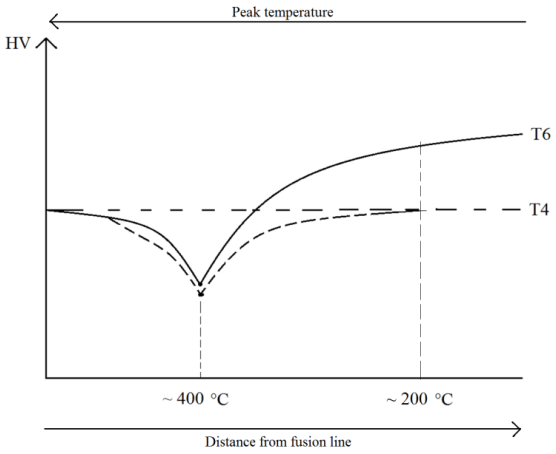

Figure 5.9: Sketch of expected hardness curve of T4 and T6 alloy in conventional welding.

It would have been interesting to see if the samples exposed to more than x1 cycle of the subsequent heating treatments would have shown improved weldability. The air-circulating oven sample showed indications of increased amount of dispersoids with number of cycles. Unfortunately, this were not performed due to lack of time at the end of the Masters' period.

6 Summary

Experiments were performed to study the effect of Mn-, Cr- and Zr-content and homogenization procedures on size distribution of dispersoids, grain structure, mechanical properties and welding of various variants of an AA6082 aluminium alloy. Micro structural-, hardness- and electrical conductivity-analyses were performed. Based on these results the following conclusions can be drawn:

- The typical welding profiles were obtained from all of the welded samples
- Increasing content of Mn, Cr and Zr, short homogenization time and low homogenization temperature forms smaller and higher density of dispersoids.
- High density of dispersoids retard recrystallization effectively after extrusion and welding. Alloys with Zr and homogenization procedure H3 were found to provide the least reccrystallized grain structure.
- The β’’-potential decreases with increasing amount of Mn, Cr and Zr.
- The different levels of dispersoids formed during this work have not been substantial enough to increase the welding properties significantly for the AA6082 alloys.

7 Further work

This study has covered some of the effects of Mn, Cr and Zr and dispersoid density on grain structure and mechanical properties of different variations of welded AA6082-T6-alloys and attempted techniques for increasing the density of dispersoids of a selected AA6082-T4 alloy. Further studies can give more information about the various types of alloys. Suggestions for further work can be:

- The effect of dispersoids on precipitation hardening phases of MgSi
- Exact composition of intermetallic phases
- Dispersoid measurements after all subsequent heating cycles
- Subsequent heating of artificial aged AA6082 alloys and different heat treatment temperature and time procedures.
- Welding and/or salt bath welding simulation of samples after several subsequent heating cycles.
- Measurements of dispersoids smaller than 20 nm by using TEM.
- Different levels of Mn, Cr and Zr. Alloying with Sc or Hf.
- Modeling of the density of dispersoids needed to obtain increase the strength in HAZ (increase of 15-20 MPa is highly desired).
-

8 References

1. Müller, U., *Introduction to Structural Aluminium Design*. 2011, Whittles Publishing.
2. Ruan, Y., Qiu, X. M., Gong, W. B., Sun, D. Q., Li, Y. P., *Mechanical properties and microstructures of 6082-T6 joint welded by twin wire metal inert gas arc welding with the SiO2 flux.* Materials & Design, 2012. 35: p. 20-24.
3. Polmear, I.J., *3 - Wrought aluminium alloys*, in *Light Alloys (Fourth Edition)*, I.J. Polmear, Editor. 2005, Butterworth-Heinemann: Oxford. p. 97-204.
4. HYDRO. *About aluminium - physical properties*. [Web page] [cited 2016 March]; Available from: http://www.hydro.com/en/About-aluminium/Why-aluminium/Physical-properties/.
5. Leader, A. *Aluminium production*. [cited 2016 March]; Available from: http://www.aluminiumleader.com/production/aluminum_production/.
6. AluPro, *Aluminium and the Carbon Economy*. 2015. p. Aluminium life cycle.
7. Design, A. *Aluminium alloys - Alloys for extrusion*. [cited 2016 March]; Available from: http://www.aluminiumdesign.net/design-support/aluminium-alloys-alloys-for-extrusion/.
8. Solberg, J.K., *Teknologiske metaller og legeringer*. 2008, [Trondheim]: Institutt for materialteknologi, Norges teknisk-naturvitenskapelige universitet. III, 316 s.
9. Design, A. *Aluminium Alloys*. [cited 2016 March]; Available from: http://www.aluminiumdesign.net/design-support/aluminium-alloys/.
10. Langkruis, Jørgen van de, *The effect of thermal treatments on the extrusion behaviour of AlMgSi alloys.* 2000.
11. Lodgaard, L., *Precipitation of dispersoids containing Mn and/or Cr in Al-Mg-Si-alloys*. 2000, The Norwegian University of Science and Technoology (NTNU): Trondheim.
12. Rinderer, B., *The metallurgy of homogenisation.* Materials Science Forum, 2011. Vol. 693: p. 264-275.
13. Niels C. W. Kuijpers., F.J.Vermolen., Kees Vuik., Sybrand van der Zwaag., *A Model of the β-AlFeSi to α-Al(FeMn)Si Transformation in Al-Mg-Si Alloys.* Materials Transactions, 2003. Vol. 44(No. 7): p. 1448-1456.
14. Strobel, K., Sweet, E., Easton, M., Nie, J. and Couper, M., *Dispersoid Phases in 6xxx Series Aluminium Alloys.* Materials Science Forum, 2010. 654-656: p. 926-929.

15. Lodgaars, L., Ryum, N., *Precipitation of dispersoids containing Mn and/or Cr in Al–Mg–Si alloys.* Materials Science and Engineering: A, 2000. 283(1–2): p. 144-152.
16. Dieter, G.E., *Mechanical Metallurgy*. 1988, UK: McGraw-Hill Book Company.
17. aluMATTER. *Recrystallization - Effect of strain rate*. [cited 2016 March]; Available from: http://aluminium.matter.org.uk/content/html/eng/default.asp?catid=68&pageid=1935702110.
18. E. D. Sweet, S.K. Charager, N.V. Danilova, Xinquan Zhang, *Effects of Extrusion Parameters on Coarse Grain Surface Layer in 6xxx Series Extrusions.* Proceedings of the Eighth International Aluminum Extrusion Technology Seminar, 2004. Vol. I: p. pp. 115-126.
19. Saha, P.K., *Aluminium Extrusion Technology*. 2000: ASM International.
20. Davydov, V.G., Rostova, T. D., Zakharov, V. V., Filatov, Yu A., Yelagin, V. I., *Scientific principles of making an alloying addition of scandium to aluminium alloys.* Materials Science and Engineering: A, 2000. 280(1): p. 30-36.
21. Bru, M., *The Effect of Mn and Homogenization Procedure on Mechanical Properties and Grain Structure in Extruded AA6082*, in *Department of Materials Science and Engineering*. 2014, Norwegian University of Science and Technology: NTNU Trondheim.
22. Schempp, P., Cross, C. E., Häcker, R., Pittner, A., Rethmeier, M., *Influence of grain size on mechanical properties of aluminium GTA weld metal.* Welding in the World, 2013. 57(3): p. 293-304.
23. aluMATTER. *Recrystallization - Pinning of Grain Boundaries and Zener Drag*. Available from: http://aluminium.matter.org.uk/content/html/eng/default.asp?catid=68&pageid=1042033829.
24. Furu, T., Østhus, R., Telioui, N., Aagård, R., Bru, M., Myhr, O.R.,, *Modeling the Effect of Mn on Extrudability, Mechanical Properties and Grain Structure of AA6082 Alloys. Proceedings of ET'16; the Eleventh International Aluminium Conference of Extrusion Technology Seminar &Exposition, Vol 1, Chicago, US 2016*
25. Averill, B., Eldredge, P., Hassell, C.A., Stasko, D.J., *Chemistry: Principles, Patterns, and Applications, Chapter 23*. 2006: Benjamin Cummings.
26. Murray, J., Peruzzi, A., and Abriata, J.P., *The Al-Zr (aluminum-zirconium) system.* Journal of Phase Equilibria, 1992. 13(3): p. 277-291.

27. Y. Himuro, K. Koyama, Y. Bekki,, *Precipitation Behaviour of Zirconium Compounds in Zr-Bearing Al-Mg-Si Alloy.* Materials science Formum, 2006. 519-521: p. 501-506.
28. Yukichi Umakoshi, Koji Hagihara, Takayoshi Nakano, *Deformation Modes and Anomalous Strengthening of Ni3X -Type Intermetallic Compounds with the Geometrically Close-Packed Structure* Materials science Formum, 2005. 502: p. 145-150.
29. Myhr, O.R., Grong, Ø., Pedersen, K. O., *A Combined Precipitation, Yield Strength, and Work Hardening Model for Al-Mg-Si Alloys.* Metallurgical and Materials Transactions A, 2010. 41(9): p. 2276-2289.
30. ESA, *Hardening Metals*.
31. Foundry Lexicon., *Orowan mechanism*.
32. *Calculated equilibrium phase diagram of Al-Mg2Si*. 2012: Hindawi - International Scholary Reasearch Notices.
33. R.R. Ambriz, D. Jaramillo, *Mechanical Behavior of Precipitation Hardened Aluminum Alloys Welds*. Light Metal Alloys Applications. 2014.
34. Mrówka-Nowotnik, Grazyna., Sieniawski, Jan., *Influence of heat treatment on the microstructure and mechanical properties of 6005 and 6082 aluminium alloys.* Journal of Materials Processing Technology, 2005. 162–163: p. 367-372.
35. Marioara, C.D., Andersen, J., Zandbergen, H. W., *Atomic model for GP-zones in a 6082 Al–Mg–Si system.* Acta Materialia, 2001. 49(2): p. 321-328.
36. Lü, L. and M.O. Lai, *Mechanical alloying*. 1998, Boston: Kluwer Academic Publishers.
37. Friis, J., Holmedal, B., Ryen, Ø., Nes, E., Myhr, O. R., Grong, Ø., Furu, T., and Marthinsen, K., *Work hardening behaviour of heat-treatable Al-Mg-Si-alloys.* Materials science Formum, 2006.
38. Mathers, Gene., *2. Welding Metallurgy*, in *Welding of Aluminium and Its Alloys*. Woodhead Publishing.
39. Halmøy, E., *Sveiseteknikk (Welding technique)*. Vol. Kompendiet (Compendium). 2007, NTNU - Norges teknisk-naturvitenskapelige universitet (Norwegian University of Science and Technology).
40. Missori, S., Sili, A., *Mechanical behaviour of 6082-T6 aluminium alloy welds.* Metallurgical Science and Technology, 2000 Vol. 18(1).

41. Stathers, P.A., Hellier, A. K., Harrison, R. P., Ripley, M. I. & Norrish, J., *Hardness-tensile property relationships for HAZ in 6061-T651 aluminum.* Welding Journal, 2014. **93**(8): p. 301-311.
42. Mathers, Gene., *1. Introduction to the Welding of Aluminium*, in *Welding of Aluminium and Its Alloys*. Woodhead Publishing.
43. Grong, *Ø., Recent Advances in Solid-State Joining of Aluminum.* Welding Journal, 2012. 91(1): p. 26-33.
44. Myhr, O.R., Grong, Ø., Fjær, H. G., Marioara, C. D., *Modelling of the microstructure and strength evolution in Al–Mg–Si alloys during multistage thermal processing.* Acta Materialia, 2004. 52(17): p. 4997-5008.
45. Myhr, O.R. and Grong, *Ø., Process modelling applied to 6082-T6 aluminium weldments—I. Reaction kinetics.* Acta Metallurgica et Materialia, 1991. 39(11): p. 2693-2702.
46. MagmaWeld. *MAL 5183 - MIG Welding Wire - Aluminum Alloys*. Available from: http://www.magmaweld.com/mal_5183_aluminum_mig_mag_welding_wires.html.
47. Holmen, J.K., Børvik, T., Myhr, O. R., Fjær, H. G., Hopperstad, O. S., *Perforation of welded aluminum components: Microstructure-based modeling and experimental validation.* International Journal of Impact Engineering, 2015. 84: p. 96-107.
48. Hatch, J.E., *Aluminium - Properties and Physical Metallurgy*, ed. M. Park. 1984, Ohio, American Society for Metals.
49. Li, Y., *TTT-curve*. 2016, NTNU: Trondheim.
50. Olea, C.A.W., Roldo, L., dos Santos, J. F., Strohaecker, T. R., *A sub-structural analysis of friction stir welded joints in an AA6056 Al-alloy in T4 and T6 temper conditions.* Materials Science and Engineering: A, 2007. 454–455: p. 52-62.